The ORMDL Proteins in Endoplasmic Reticulum Stress-Derived Intestinal Inflammation

Dissertation zur Erlangung des Doktorgrades

der Mathematisch-Naturwissenschaftlichen Fakultät

der Christian-Albrechts-Universität Kiel

Vorgelegt von

Berith Messner

2021

Kiel, Deutschland

"No guts, no story"

– Chris Brady

Erster Gutachter & Betreuer (First Reviewer & Supervisor):	**Prof. Dr. Philip Rosenstiel**
Zweiter Gutachter (Second Reviewer):	**Prof Dr. Thomas Roeder**
Tag der mündlichen Prüfung (Date of oral examination):	01. September 2021
Zum Druck genehmigt (Approved for publication):	01. September 2021

Table of Contents

Table of Figures

List of Tables

1 Introduction

1.1 Inflammatory Bowel Disease

The medical term inflammatory bowel disease (IBD) represents a group of complex chronic inflammatory disorders of the human gastrointestinal tract. Depending on the pathophysiology of the disease, two principal subtypes of IBD are distinct from one another: Ulcerative Colitis (UC, *Online Mendelian Inheritance in Man* OMIM® # 266600) and Crohn's disease (CD, *Online Mendelian Inheritance in Man* OMIM® # 266600). The etiology of IBD is unknown but it is common sense that IBD results from an interplay between dysregulated immune response and environmental factors in a genetically susceptible host. The key feature of IBD's pathogenesis is thereby believed to be an uncontrolled mucosal immune response directed against the host's commensal microbiota [1].

Both disorders, CD and UC, are characterized by chronic relapsing-remitting inflammatory episodes. For the differentiation of CD and UC two main criteria can be applied: the first being the spatial distribution of the inflammation along the gastrointestinal tract and the second being the nature of inflammatory changes in the tissue. While CD can affect the whole digestive tract from mouth to anus, UC is limited to the colon and rectum of patients. Furthermore, CD is characterized by a discontinuous transmural inflammatory phenotype, whereas UC patients display diffuse mucosal inflammation with extensive superficial mucosal and submucosal ulcerations. Despite UC and CD being two different disorders, both may present with any of the following clinical symptoms: abdominal pain, diarrhea, rectal bleeding, and weight loss. These symptoms are often accompanied by malnutrition and inflammatory extraintestinal manifestations, e.g. fatigue and anemia. Apart from the symptoms mentioned above, the risk of developing malignancies (e.g. colorectal carcinoma) and chronic disorders of other body parts (e.g. the skin, liver, joints or bones) is significantly increased in IBD patients [2]. Resulting from these extraintestinal complications patients also show increased mortality.

Despite increasing scientific interest in the topic of IBD, to this day, there is no known cure for the disease. Thus, it is only possible to treat the acute symptoms and to minimize inflammation. The main and long-term aim of treatment is to induce and maintain remission, meaning a state of health in which the patient does not exhibit clinical signs of inflammation. To achieve remission most medications aim at targeting pro-inflammatory molecules, thereby modulating the immune response of patients. Although diagnosis of UC and CD follows very similar patterns, treatment of both disorders differs from patient to patient and is dependent on the severity of the disease.

1.2 Epidemiology of IBD

Since IBD occurs more frequent in populations with Caucasian background than in Europe or North

America it has been characterized as a disease of industrialized Western countries [3]. Currently, in Europe the prevalence for UC and CD are 505 per 100.000 persons for UC and 322 per 100.000 persons for CD [4]. Incidence rates are rising in younger people with peak incidence in the second to fourth decade of life and no obvious gender preference [5].

Of interest, the incidence of IBD has been rising in both the Western world and in developing nations [6-8]. Increasing incidence in countries with former low prevalence like South America, Africa and Asia points towards a correlation between industrialization and Westernization [9, 10].

1.3 Non-genetic, environmental risk factors for IBD

In the past decades, various theories of environmental causes of IBD have been postulated. The most potent theory thereof is the hygiene hypothesis, which proposes that the lack of exposure to enteric pathogens in childhood increases the likelihood of developing immunologic disorders [11, 12]. The hygiene hypothesis is supported by studies conducted in Canada and Sweden. Research shows that immigrants have lower IBD incidence which is further associated with decreasing risk for increasing age at immigration [7, 13]. In support of these findings, studies conducted in monozygotic twins show low concordance rates (27-56 % for CD, 15-19 % for UC) for IBD within the pairs. This suggests that genetic predisposition alone is not sufficient for developing the disease but rather that environmental factors (e.g. upbringing of children in urban rather than rural environment or infection with *Helicobacter pylori*) are playing a major role [14].

Numerous studies on environmental, lifestyle-associated risk factors (e.g. smoking, oral contraceptive pills and diet) could show an influence of these factors on the etiology of IBD; however, none of the risk factors completely explains the environmental component of IBD's development. A meta-analysis on smoking showed that active smokers were less likely to develop UC in comparison to non-smokers while exhibiting an increased risk for acquiring CD [15]. The highest incidence of smoking is found in countries with the lowest incidence of IBD [16, 17], highlighting the importance of further research in this field.

Dietary factors have been extensively studied in IBD, but results have offered only inconsistent conclusions. Various studies report high consumption of dietary fiber to protect from IBD [18-21]. However, other studies have failed to recapitulate this interaction [19, 22, 23]. Long-chain omega-3 fatty acids have been shown contribute to the development of IBD. Nevertheless, these fatty acids were linked to both protective and risk associations [19, 20, 24].

Taken together, these data point towards a critical role for non-genetic, environmental factors in the development and manifestation of IBD in genetically predisposed patients.

1.4 Genetic risk factors

The importance of genetic susceptibility has been confirmed by genetic studies like linkage analysis and genome-wide association studies (GWAS), which have identified more than 160 different IBD genetic susceptibility loci [25]. While linkage analysis is a well-established method to map heritable trait genes to their respective chromosome locations, GWAS are used to find common risk alleles occurring significantly more frequent in patients compared to healthy controls. However, since most of the susceptibility loci only contribute to disease development with low odds ratios (1-1.5), genetic predisposition cannot be the only cause for disease aetiology. The genetic attributions of 13,6 % for CD and 7,5 % for UC also underline the complexity of IBD [26-30]. Even though genetics cannot fully explain the development of the disease, the identified risk loci and their respective genes contributed significantly to the understanding of IBD and its underlying signaling pathways.

Since the first published GWAS studies in 2002 [31], many risk loci for CD or UC only, or both disorders, have been identified. To this day, 242 IBD susceptibility loci are identified with only 45 of them being mapped to known variants [32, 33]. Interestingly, in CD alone 170 susceptibility loci have been confirmed [34]. These loci include genes involved in mucosal barrier function, autophagy, ER stress, bacterial recognition, and immune regulation. *NOD2* (Nucleotide-binding oligomerization domain-containing protein 2), which was the first gene to be associated with CD aetiology [35, 36], until today remains the risk locus conferring the highest risk for disease development. *NOD2* is located on chromosome 16q12 and harbours three distinct single nucleotide polymorphisms (SNPs), which were found to be directly associated with CD [36-38]. Heterozygosity at the *NOD2* locus leads to a two- to fourfold risk increase in Caucasian CD patients, while homozygosity is associated with a 20- to 40-fold increase in genotype-relative risk [35, 39, 40]. Loss of *NOD2* function is associated with inadequate bacterial sensing, which can lead to inefficient control of microbial infections by the immune system.

However, NOD2 is not only linked to bacterial sensing but also to autophagy, where it recruits ATG16L1 (autophagy related 16 like 1) to the plasma membrane, thus initiating formation of autophagosomes and finally bacterial clearance. Of note, a SNP in the coding region of *ATG16L1* (T300) has been linked to CD, thus providing further proof for autophagy as an important cellular pathway contributing to disease development [41-43].

Apart from autophagy also dysfunction in endoplasmic reticulum (ER) stress, meaning the accumulation of unfolded or misfolded proteins in the ER, has been linked to the pathophysiology of IBD. ER stress directly induces autophagy, which, in turn, serves a compensatory function to limit ER stress [44]. Another cell biological pathway to resolve ongoing ER stress is the unfolded protein response (UPR). Genes involved in the UPR have been characterized as IBD risk genes, meaning that these genes are associated with increased risk to develop the disease. These UPR-associated IBD risk genes comprise *AGR2* (anterior gradient protein 2) [45], *XBP1* (X-box binding protein 1) [46], and *ORMDL3*

(orosomucoid 1 like 3) [47, 48]. Interestingly, genetic deletion of *Xbp1* specifically in intestinal epithelial cells (IEC) of mice results in spontaneous enteritis (for more detailed information see chapter 1.8.5.3). While polymorphisms in the *ORMDL3* gene have first been associated with asthma [49], this gene is now also recognized as IBD risk gene [47] (for details see chapter 1.9).

Further risk loci discovered within candidate genes for both CD and UC include proteins involved in immunological pathways like T cell signaling (interleukin 23 receptor, *IL23R*) [50, 51]. Risk loci within candidate genes for UC comprise the anti-inflammatory cytokine interleukin 10 *(IL10*) [52-54] and human leukocyte antigen (*HLA*) [55, 56].

1.5 The intestinal epithelium

The intestinal epithelium consists of a single cell layer that differs both in architectural structure and cellular composition between the small intestine and colon. While the small intestine exhibits protruding structures, termed villi, for better nutrient absorption and increase of the mucosal surface area, the colon consists of a comparatively flat mucosal surface. However, both the small and large bowel exhibit invaginations termed crypts of Lieberkühn [57]. These crypts harbor various differentiated intestinal epithelial cell (IEC) populations, namely intestinal stem cells (ISCs), Goblet cells, enterocytes, enteroendocrine cells and tuft cells. Of interest, the small intestine harbors two additional cell types which, under homeostatic conditions cannot be found in the colon: Paneth cells and Microfold cells (M cells). Goblet cells and M cells, which are located overlaying Peyer's patches, are needed for intestinal tolerance and the induction of mucosal immune responses. Enterocytes are responsible for nutrient and water absorption, tuft cells protect against helminth infection, whereas enteroendocrine cells secrete hormones. Paneth cells and ISCs are located at the base of the crypt where they intercalate, thereby forming the ISC niche. This niche's function is to restore and support the ISCs the best way possible, e.g. by secretion of Wnt2b (Family Member 2 beta), a member of the canonical Wnt signaling pathway. Two different types of ISCs can be distinguished by one another by their respective markers: Lgr5 (Leucin rich repeat containing G protein-coupled receptor 5) and Olfm4 (Olfactomedin-4) are established markers for crypt base columnar cells (CBCs), whereas +4 cells are characterized by the expression of Bmi1 (BMI1 proto-oncogene, polycomb ring finger) and Lrig1 (Leucine rich repeats and immunoglobulin like domains 1) [58-61]. While ISCs give rise to transit-amplifying cells, Paneth cells release antimicrobial peptides (e.g. lysozyme (Lyz)) to protect their surrounding ISCs. Intestinal crypts undergo constant replenishment and renewal with a complete replacement of crypt IECs within 4-5 days [62].

1.6 The role of the immune system in IBD

The mammalian immune system comprises two distinct responses termed innate immunity and adaptive

immunity. While the innate immune response represents the first, non-specific line of defense against any pathogens, the adaptive immune response acts in a specific manner and provides the host with long-lasting immunity. Cells belonging to the innate immune response, like macrophages or dendritic cells (DCs), but also non-immune cells like IECs have the potential to recognize the intestinal microbiota via their specific pathogen associated molecular patterns (PAMPs) and thus can quickly initiate inflammatory responses to pathogen invasion. Moreover, DCs function as professional antigen presenting cells (APCs), which mediate T cell activation and the consequent activation of adaptive immune responses. A key player of the adaptive immune response are T cells, which can be divided into Th1, Th2 and Th17 subsets. While Th1 cells produce mainly IFNγ, Th2 cells initiate the production of IL-4, IL-5 and IL-13 cytokines. Of interest, various studies have suggested CD to be a Th1-mediated disease due to high IFNγ levels, while UC is considered to be a Th2-mediated disease as indicated by high amounts of IL-13 [63-67]. However, there is also evidence that the Th1/Th2 paradigm in IBD may be misleading as different studies have shown that patient biopsies indeed rather exhibit mixed cytokine profiles [68-70]. Th17 cells represent a T cell subset characterized by cytokine production of IL-17A, IL-21 and IL-22. High IL-17A transcript levels have been described for CD and UC mucosa and lamina propria [71]. Furthermore, the LP fraction of IBD patients exhibits higher numbers of Th17 and Th1/Th17, characterized by IFNγ and IL-17A production, underscoring their importance in the disease [70].

Studies in animal models have drawn the attention to the role of CD4 positive (CD4+) T cells in the pathogenesis of IBD. Adoptive transfer of CD4+ T cells in an immunocompromised animal leads to induction of intestinal inflammation, which is strongly dependent on the host's microbiota [72-74]. Since CD4+ T cell responses are associated with MHCII processing and presentation on APCs, the data strongly suggests an important role for MHCII positive APCs in IBD pathogenesis. Of note, IECs express MHCI and MHCII similarly to professional APCs like DCs or macrophages. For IECs to function as non-professional APCs, they must be capable of internalizing and processing antigens. This antigen presentation by IECs depends on inflammatory stimuli: Under constitutive conditions, IECs mediate induction of CD4+ T cells with a regulatory phenotype while inflammatory stimuli cause IECs to activate CD4+ T cells with the capacity to secrete proinflammatory cytokines [75, 76]. Elevated levels of MHCII have been observed in the context of mucosal inflammation as occurring in CD [77].

1.7 The gut microbiota in IBD

The human body contains about 3 x 10^{13} cells. The overall number of bacteria colonizing the human host, both inside and outside the body, is about the same with approx. 3,8 x 10^{13} [78]. Microbes colonizing the colon represent about 0.3 % of the total body weight [79]. Consequently, the intestinal homeostasis highly depends on a functioning interplay between gut microbiota, intestinal epithelium and the host immune response [80].

Dysbiosis, an alteration of the normal gut microbiota composition, is known to be an important feature of intestinal inflammation [81, 82]. Under homeostatic conditions the resident intestinal microbiota interacts with colonocytes to prevent dysbiosis. Inflammation in IBD is characterized by a reduced diversity of microbiota, which leaves the host more susceptible to infection with pathogens [83, 84]. Studies in pediatric patients with Crohn's disease treated with or without antibiotics state that exposure to antibiotics during childhood can result in microbial dysbiosis, which, in turn, is associated with the development of IBD [83]. This finding indicates the importance of perturbations of the infant intestinal microbiota on the etiology of IBD.

1.8 Endoplasmic reticulum stress (ER Stress) and the unfolded protein response (UPR)

In eukaryotic cells, the endoplasmic reticulum (ER) presents as a membrane system with tubules and a single lumen. The ER is crucial for the proper folding and secretion of secretory and membrane proteins. Furthermore, the it is involved in processes like lipid biosynthesis and the regulation of calcium (Ca^{2+}) signaling. Under homeostatic conditions, the protein load of the ER and its protein folding capacity are well balanced. However, the process of protein folding and maturation is highly sensitive and can be disturbed by numerous factors including oxidative stress, ER Ca^{2+} depletion, increased mRNA translation or inflammation. Only properly folded proteins are transported from the ER to the Golgi apparatus, where they are further modified. Proteins, which are not properly folded, either remain inside the ER or undergo ER-associated protein degradation (ERAD). The accumulation of unfolded or misfolded proteins in the ER is termed ER stress. ER stress can be resolved by activation of an evolutionary conserved mechanism termed unfolded protein response (UPR). The UPR enables the eukaryotic cell to cope with ER stress and aims at restoring cellular homeostasis. However, irremediable ER stress induces an UPR response that is directed towards the engagement of apoptosis, meaning programed cell death, rather than restoring homeostasis [85].

The protein-folding capacity of the ER is highly dependent on the respective cell type. Secretory cells like β-cells of the pancreas or IECs contain a large, well-developed ER. Resulting from the larger ER and the increased protein-folding capacity, these specialized cell types are more prone to ER stress.

Under homeostatic conditions, 78 KDa glucose-regulated protein (Grp78, also termed Hspa5 and BiP), a key chaperone, binds to the luminal domains of three stress sensors: activating transcription factor 6 (ATF6), inositol-requiring enzyme 1 (IRE1) and PRKR-like endoplasmic reticulum kinase (PERK). Upon accumulation of unfolded or misfolded proteins in the ER, Grp78 binds to these proteins' exposed hydrophobic domains, and releases the three UPR sensors. As a consequence, Grp78 release reveals an ER export motif in ATF6, while IRE1α and PERK oligomerize and auto-phosphorylate [86] (Fig. 1.1).

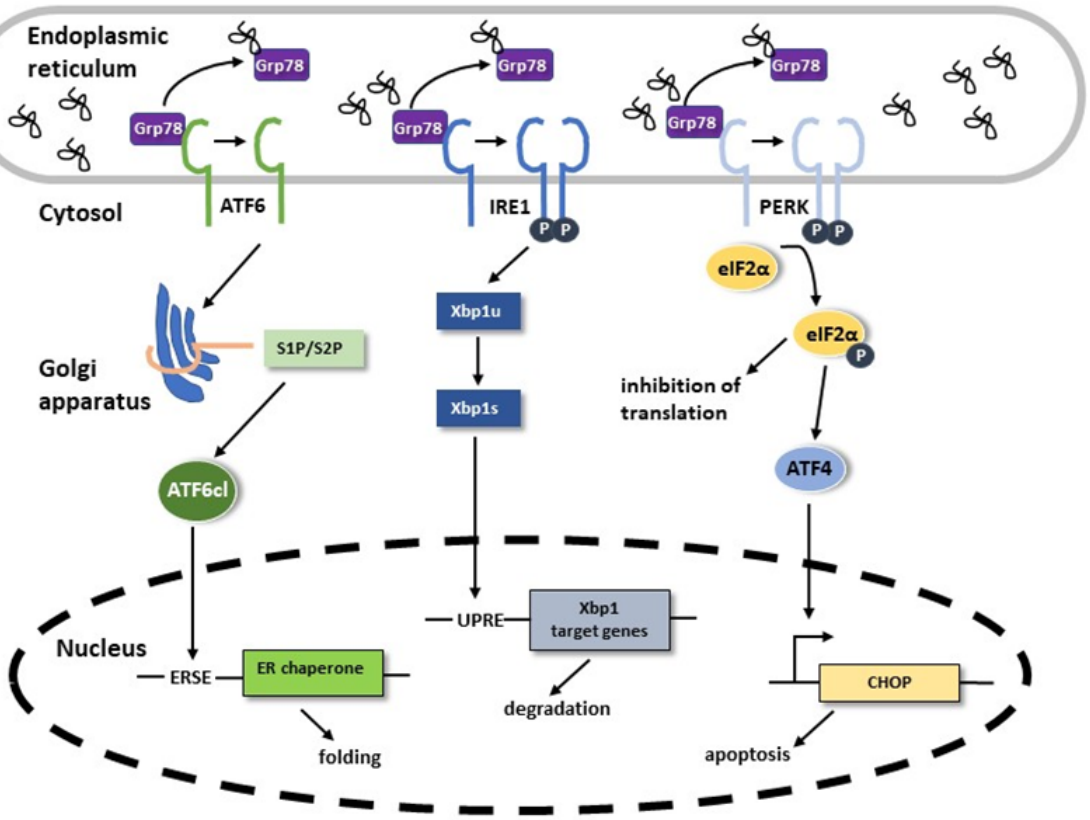

Figure 1.1: The unfolded protein response resolves endoplasmic reticulum stress.
Endoplasmic reticulum (ER) stress activates the unfolded protein response (UPR) in eukaryotic cells. Accumulation of unfolded proteins in the ER leads to release of the chaperone 78 kDa glucose-regulated protein (Grp78) from its binding partners, the three transmembrane proteins activating transcription factor 6 (ATF6), inositol-requiring enzyme 1 (IRE1) and PRKR-like endoplasmic reticulum kinase (PERK). Release of Grp78 activates the three stress sensors and induces their specific pathways. ATF6 translocates from the ER to the Golgi complex where it is cleaved by the site 1 (S1P) and site 2 proteases (S2P) releasing ATF6's cytosolic domain. Cleaved ATF6 (ATF6 cl) then induces transcription of chaperones via the ER stress element (ERSE). Upon ER stress, IRE1 autophosphorylates and oligomerizes. IRE1 initiates downstream signaling through unconventional splicing of the transcription factor X-box binding protein 1 (Xbp1; Xbp1 unspliced = Xbp1u). Spliced Xbp1 (Xbp1s) induces transcription of chaperones and components of ER associated degradation (ERAD). Activation of PERK results in phosphorylation of eukaryotic translation initiation factor 2A (eIF2α). eIF2α either induces inhibition of translation or selectively induces translation of activating transcription factor 4 (ATF4), which, in turn controls expression of the pro-apoptotic C/EBP homologous protein (CHOP). P = phosphorylation, UPRE = unfolded protein response element.

1.8.1 ATF6 signaling

The mammalian genome consists of two *ATF6* genes (*ATF6A* and *ATF6B*, respectively), of which only *ATF6A* is associated with UPR activation [87]. ATF6 functions as a transcription factor (TF), however, it is synthesized as a type II transmembrane protein. Upon ER stress, ATF6 is transported from the ER [88] to the Golgi apparatus for following activation through cleavage by the site 1 and site 2 protease (S1P and S2P, respectively) [89]. The cytosolic domain of cleaved ATF6 (ATF6 cl) translocates to the nucleus and initiates adaptation e.g. by upregulation of factors important for ERAD [90].

1.8.2 PERK signaling

Dissociation of Grp78 from the ER luminal domain of PERK allows for PERK to homodimerize and autophosphorylate, resulting in activation of its cytoplasmic kinase domain. However, it has been shown

that not only dissociation of Grp78 but also changes in lipid composition of the ER membrane can induce PERK signaling, thus pointing towards an important role of lipid metabolism for the UPR activation in general [91, 92]. Following activation of PERK's kinase domain, the now activated PERK phosphorylates eukaryotic translation initiation factor 2 subunit alpha (eIF2α). Finally, this phosphorylation results in inhibition of the assembly of eIF2−GTP–Met-tRNA ternary complex (eIF2-TC), thus blocking translation and thereby enabling the cell to cope with temporary, acute ER stress. However, not all mRNAs are translationally inhibited. Indeed, some mRNAs can not only bypass the inhibition of translation but are upregulated during ER stress conditions. One important example of such a favoured mRNA is the important UPR mediator activating transcription factor 4 (ATF4), which contains an internal ribosome entry site sequence in its 5' untranslated region (UTR) [93]. ATF4, in turn, initiates transcription of CHOP (C/EBP homologous protein) [94, 95], which is associated with ER stress-mediated apoptosis in the case of chronic, excessive ER stress [96, 97].

Interestingly, the PERK signaling pathway can additionally be activated completely independently of ER stress. Cellular stressors such as amino acid deprivation, oxidative stress and double-stranded RNA, which is part of the interferon antiviral response can lead to ER stress-independent PERK activation via different kinases [98, 99].

1.8.3 IRE1 signaling

The IRE1 signaling pathway is conserved throughout the eukaryotic kingdom. IRE1 is the only identified ER stress sensor in yeast and its homologue is still present in mammals and plants, where it activates the UPR [100-103]. The mammalian genome encodes two isoforms of IRE1, IRE1α and IRE1β, respectively. Notably, IRE1α is ubiquitously expressed, whereas the expression of IRE1β is limited to the intestinal epithelium.

IRE1 is a transmembrane protein with kinase and endoribonuclease (RNase) properties. In case of ER stress, IRE1 dimerizes and trans-autophosphorylates, thus inducing RNase activity by conformational change. IRE1's RNase catalyzes alternative splicing of a 26-nucleotide intron within the Xbp1 mRNA, thus inducing a shift of the reading frame. The resulting transcription factor is termed Xbp1s (spliced Xbp1). It controls genes involved in cellular processes like protein folding, secretion, ERAD and lipid synthesis [101, 104, 105]. Conversely, kinase activity of IRE1 is needed for activation of Jun-related kinase (JNK) and nuclear factor kappa B (NF_KB).

1.8.4 Interactions between the three UPR signaling pathways

The UPR is a flexible, adaptive network that is based on interactions between its three signaling pathways. These crosstalk events are especially important because they allow for finetuning of the ER stress re-

sponse e.g. depending on the affected cell type. Depending on the kind and duration of ER stress interactions between the three signaling pathways can either result in restoration of cellular homeostasis or in controlled cell death.

Studies have identified interactions between all three UPR signaling pathways. Especially for the IRE1 and the ATF6 signaling pathway several interaction mechanisms have been described. The ATF6 pathway can influence the IRE/XBP1 pathway via cleaved ATF6-dependent transcriptional activation of XBP1. This mechanism allows for the ATF6 signaling pathway to directly interact with the IRE pathway, and not via the XBP1 target sequence Unfolded protein response element (UPRE) [106, 107]. Of interest, the spliced form of XBP1 can also directly influence the ATF6 signaling pathway by binding to the ATF6 target ERSE [108]. This mechanism results in increased transcription of ER chaperones. However, upon short exposure to ER stress ER chaperone activation via cleaved ATF6 is favored in comparison to XBP1 signal transduction since XBP1 first needs to be translated to then induce the target genes. In a second mechanism that arises in late stages of ER stress, ATF6α heterodimerizes with XBP1s to control ERAD gene expression via the UPRE [90]. This fusion of cleaved ATF6 and spliced XBP1 leads to degradation of both proteins and finally restores cell homeostasis [109].

Both ATF6 and IRE signaling pathways also interact with the PERK pathway of the UPR. The PERK pathway ligand CHOP gets activated not only by ATF4 but also by ATF6α and XBP1 [110, 111]. A recent study also provides a link between the PERK and IRE pathways. In conditions of terminal UPR PERK attenuates IRE via induction of dephosphorylation of the phosphatase RNA polymerase II associated protein 2 (RPAP2). The dephosphorylated RPAP2 then inhibits the endoribonuclease activity of IRE1 and causes death receptor 5 (DR5)-mediated apoptosis [112].

1.8.5 ER Stress and the UPR in intestinal epithelial cells under inflammatory conditions

In eukaryotes, induction of the UPR enables cells to survive ER stress. It is known that especially those cell types with a high secretory burden, e.g. Paneth cells and goblet cells in the mammalian small intestine, are highly dependent on a functioning UPR. Paneth cells also play an important role in the pathogenesis of IBD because of their role as mediators of both the stem cells niche and commensal microbiota composition, which is the major source for a dysfunctional immune response in IBD [113-115]. In humans, GWAS studies provided a first link between disturbances in the UPR and the development of intestinal inflammation. GWAS found several disease susceptibility loci within or close to genes, which have been associated with ER or UPR function. These genes include, among others, *AGR2, ATF6, XBP1,* and *ORMDL3*. Moreover, IBD patients also exhibit increased expression levels of the ER chaperone GRP78 [116] indicating the importance of ER stress on IBD development. To study the link between ER stress/UPR and intestinal inflammation *in vivo* several studies used mouse models with genetic deletion

of ER stress related genes. Of interest, all studies show that genetic deletion of ER stress related genes either causes spontaneous intestinal inflammation or enhances susceptibility to induced colitis models.
The IBD risk gene *AGR2* encodes a protein disulfide isomerase (PDI), which is localized in the ER. *AGR2* is expressed in IEC, namely goblet and Paneth cells, as well as in enteroendocrine cells of the small intestine [117]. Decreased expression levels of this ER stress related gene have been associated with both forms of IBD, CD and UC [45]. Deletion of *Agr2* in a mouse model ($Agr2^{-/-}$) caused spontaneous ileocolitis characterized by increased mRNA expression levels of the ER stress markers Grp78, CHOP and Xbp1. Furthermore, *Agr2* deletion resulted in decreased Mucin 2 (*Muc2*) expression in goblet cells and changes in localization and expansion of Paneth cells within the small intestine [118].

1.8.5.1 The ATF6 signaling pathway in intestinal inflammation

Deficiency for the UPR stress sensor *Atf6a* in mice ($Atf6a^{-/-}$) led to increased susceptibility to dextran sodium sulfate (DSS)-induced colitis, which was characterized by increased disease activity as presented by severe body weight loss, rectal bleeding, and mucosal damage. Furthermore, *Atf6a* deficiency caused reduced mRNA expression of ER chaperones such as Grp78, Grp94 (also termed Endoplasmin or Hsp90b1) and $p58^{IPK}$ in comparison to their littermates, suggesting that the absence of *Atf6a* impairs UPR signaling in IECs under conditions of intestinal inflammation [119].
In the same study, mice deficient for the ATF6-dependent ER-based chaperone $p58^{IPK}$ ($p58^{IPK-/-}$) were subjected to DSS colitis. Of interest, $p58^{IPK-/-}$ mice were more susceptible to DSS colitis than their littermates and showed increased protein levels of the ER chaperone Grp78 and the pro-apoptotic chaperone CHOP [119]. Another study used a tamoxifen-inducible mouse model to target Grp94, an Atf6α target gene. Mice deficient for *Grp94* showed severe impairment of intestinal homeostasis characterized by rapid and severe body weight loss, loss of intestinal villus morphology and, finally, lethality about 2 weeks post-tamoxifen [120]. The previously described studies are complemented by findings in a mouse model with a hypomorphic allele of *Mbtps1* (Membrane-bound transcription factor site-1 protease). This gene encodes for the membrane-bound transcription factor S1P, which is important for cleavage and thus generation of the transcriptionally active form of ATF6. The *Mbtps1* missense mutation exhibited an increased susceptibility to DSS-induced colitis as well as reduced levels of the ER chaperones GRP78 and GRP94 in the colon [121]. Taken together, all these studies highlight the importance of the ATF6 signaling pathway of the UPR in intestinal inflammation and maintenance of homeostasis.

1.8.5.2 The PERK signaling pathway in intestinal inflammation

Another UPR pathway that has been the aim of several *in vivo* studies is the PERK signaling pathway. To identify the importance of this pathway on the pathogenesis of intestinal inflammation *in vivo*, mice with a non-phosphorylatable form of eIF2α in IECs ($eIF2a^{A/A\_IEC}$) were used. Under physiological conditions,

the small intestines of these animals revealed dysregulated UPR signaling pathways in IECs as well as disturbances in Paneth cell protein secretion. Loss of phosphorylated eIF2α (p-eIF2α) resulted in increased sensitivity to both DSS-induced colitis and oral infection with *Salmonella enterica* subsp. enterica serovar Typhimurium [2]. Another study investigated the role of the pro-apoptotic factor Chop, a downstream target of PERK and peIF2α via ATF4. In contrast to other components of the UPR, deletion of *Chop in vivo* caused amelioration of the disease in the course of DSS-induced and TNBS (trinitrobenzene sulfonic acid)-induced colitis models [122]. These findings demonstrate an important role of epithelial p-eIF2α in mucosal homeostasis.

1.8.5.3 The IRE1α/XBP1 signaling pathway in intestinal inflammation

Evidence for an interaction between the IRE1 signaling pathway of the UPR and the development of intestinal inflammation was gained from studies in mice. IRE1α, which is encoded by *Ern1*, IRE1β, encoded by *Ern2*, and Xbp1 as a downstream target of IRE1 have been subject of extensive investigation. Interestingly, mice deficient for IRE1α (*IRE1a*$^{-/-}$) or Xbp1 (*Xbp1*$^{-/-}$) exhibit embryonic lethality, suggesting that both UPR targets are indispensable for embryonic development *in vivo* [123, 124]. Upon genetic deletion of the IEC-specific isoform *IRE1β* mice showed enhanced susceptibility to DSS-induced colitis and also exhibited increased protein levels of the ER stress marker GRP78 [125].

To further emphasize the impact of the IRE1/XBP1 signaling pathway on intestinal inflammation, a study by Kaser *et al.* focussed on the effect of *Xbp1* deletion specifically in IECs (*Xbp1*$^{\Delta IEC}$) of mice [46]. The investigators found that in comparison to their littermates, which carried only the floxed alleles but not the VillinCre enzyme responsible for gene deletion (*Xbp1*$^{fl/fl}$), *Xbp1*$^{\Delta IEC}$ mice developed spontaneous small intestinal inflammation characterized by a discontinuous, patchy distribution. Clinical features of this inflammation comprised crypt abscesses, ulcerations and infiltration of immune cells in the lamina propria, which are known features of human IBD. Furthermore, intestinal epithelia of *Xbp1*$^{\Delta IEC}$ mice showed increased Grp78 and CHOP levels, indicating increased ER stress upon *Xbp1* deficiency. Moreover, *Xbp1*$^{\Delta IEC}$ intestine exhibited both a complete depletion of Paneth cells, which secrete antimicrobial peptides (e.g. lysozyme and defensins), and a reduction of mucin-producing goblet cells. Since Paneth cells are the most highly secretory cells within the IEC pool, Kaser *et al.* hypothesized that *Xbp1* deficiency causes these cells to undergo programmed cell death to cope with increased ER stress. An experiment in mice with tamoxifen inducible *Xbp1* deletion in the IECs indeed showed more apoptotic Paneth and goblet cells. Additionally, 5-bromo-2'-deoxyuridine (BrdU) staining for proliferative cells indicated that 24 h after injection, *Xbp1*$^{\Delta IEC}$ epithelium showed an increased cell migration rate. Furthermore, the intestinal epithelium exhibited increased mRNA levels of Tnfα, an inflammatory mediator that is secreted by Paneth cells, and CHOP as a marker of ER stress. Interestingly, the study provides evidence that the colon is not affected by *Xbp1* deletion under basal conditions. However, when subjected to a DSS colitis,

Xbp1$^{\Delta IEC}$ mice showed increased susceptibility. Also, *Xbp1*$^{\Delta IEC}$ animals proved to be more prone to oral infection with *Listeria monocytogenes* when compared to *Xbp1*$^{fl/fl}$ [46].

A follow-up study by Niederreiter *et al.* [126] aimed at further characterizing the *Xbp1*$^{\Delta IEC}$ mouse model by focussing especially on the previously described phenotype of increased cell proliferation. The authors found that deficiency for *Xbp1* leads to an increase in Lgr5^{+} and Olfm4^{+} ISCs in both ileal and colonic tissue, which is accompanied by increased expression of *Wnt11* (Wnt family member 11) by the surrounding Paneth cell remnants in the ileum. This result is of special interest because it highlights the impact of Paneth cells, and even morphologically condensed remnants thereof, on maintenance of the ISC niche. Furthermore, reduced or absent function of Xbp1 in IECs has been described to result in increased splicing of *Xbp1* [46]. This finding indicated unresolved ER stress in the tissue and pointed towards increased IRE1α activation [101]. Thus, the authors sought to investigate the impact of the ER stress sensor IRE1 in *Xbp1* deficient ISCs. Their study describes that while *Xbp1* deficient mice display increased ISC numbers, all other IEC populations as well as an observed hyperproliferation of the epithelium remain unaffected by IRE1α hyperactivation. To find a reason for the epithelial hyperproliferation the authors focused on the JAK1/STAT3 pathways. Indeed, the study confirms elevated phosphorylation of both proteins in *Xbp1*$^{-IEC}$ epithelium. However, chemical inhibition of Stat3 transcription indicated reduced turnover of the intestinal epithelium of *Xbp1*$^{-IEC}$ mice but not *Xbp1*$^{fl/fl}$ mice. The authors concluded that Stat3 activation in the transit-amplifying zone of *Xbp1* deficient epithelium mediates ER stress-dependent IEC hyperproliferation. When investigating Stat3 phosphorylation in Xbp1-silenced ModeK cells, an IE cell line, the authors found elevated levels of phosphorylation both under basal conditions and upon ER stress induction by tunicamycin. Furthermore, *Xbp1* silenced ModeK cells exhibited induced mRNA expression and protein secretion of IL-6 (interleukin-6) and IL-11 (interleukin-11), two generic Stat3-activating cytokines [127]. Investigation of NF-$_{K}$B, a transactivator of IL-6 and characteristic by-product of ER stress [128], furthermore revealed elevated total protein levels of NF-$_{K}$B p65 and phosphorylated p65 in IECs of *Xbp1*$^{-IEC}$ mice. Consequently, the authors concluded that hypomorphic Xbp1 function causes increased NF-$_{K}$B-dependent activation of Stat3 in IECs. To test the hypothesis that Jnk may be associated with both ISC expansion and hyperproliferation in *Xbp1*-deficient animals, Niederreiter and colleagues administered a pharmacological inhibitor of Jnk phosphorylation to the mice, which affected neither Olfm4^{+} ISC numbers nor IEC turnover. Also, Jnk phosphorylation levels in IECs of both *Xbp1*$^{-IEc}$*;Ern1*$^{-IEC}$ and *Xbp1*$^{-IEC}$ mice were not altered, hence not under the control of IRE1α [126]. Thus, Jnk is thought not to have an impact on the *Xbp1*-deficient hyper regenerative phenotype.

Table 1: Phenotypes of the *Xbp1*$^{\Delta IEC}$ mouse model as described by Kaser *et al.* [48] and Niederreiter *et al.* [126].

Phenotype	Condition	Reference
spontaneous enteritis	basal	[46]
depletion of Paneth cells due to apoptosis	basal	[46]
reduced Goblet cell numbers	basal	[46]
increased cell migration	basal	[46]
increased NF-κB-dependent activation of Stat3	basal	[126]
IRE1 hyperactivation	basal	[126]
IRE1-dependent JNK phosphorylation	basal	[46]
increased ISC numbers	basal	[126]
increased susceptibility to colitis	DSS colitis	[46]
increased susceptibility to *Listeria* infection	*L. monocytogenes* (oral infection)	[46]

1.9 ORMDL Proteins

In 2002, Hjelmquist *et al.* [129] first described the identification of *ORMDL1* (ORM1 (S. Cerevisiae)-like 1), located within the retinitis pigmentosa locus at chromosome 2q32.2. ORMDL1 is one member of a gene family in *Mus musculus* and *Homo sapiens* comprising the three genes *ORMDL1*, *ORMDL2* (ORM1 (S. Cerevisiae)-like 2) and *ORMDL3* (ORM1 (S. Cerevisiae)-like 3). While the three genes are localized on human chromosomes 2q32, 12q13.2, and 17q21, in mice *Ormdl1*, *Ormdl2* and *Ormdl3* can be found on chromosomes 1, 10, and 11, respectively. Human ORMDL proteins comprise 153 amino acids and possess an atomic mass of approx. 17 kilodalton (kDa). Comparison of the three human ORMDL proteins revealed conservation of 116 out of the 153 amino-acid residues (approx. 76 %) and about 95 % identity between human and murine orthologues [129]. Cantero-Recasens *et al.* suggest that ORMDL proteins function as ER transmembrane proteins with both N- and C-terminus facing the cytoplasm and a large loop facing the ER lumen [130]. Of interest, the ORMDL gene family is highly phylogenetically conserved with homologues in, among others, yeast, plants, *Drosophil*a melanogaster and vertebrates. Furthermore, ORMDL genes are ubiquitously expressed in both embryonic and adult tissue [129].

1.9.1 Association of ORMDL proteins with human inflammatory diseases

Of all three members of the ORMDL gene family *ORMDL3* is not only the most studied gene but also the only locus to be associated with IBD. In 2007, ORMDL3 was first identified as susceptibility gene for asthma and its role has been confirmed in several follow-up studies [49, 131-135]. Using GWAS and replication studies ORMDL3 could also be linked to other inflammatory diseases. In 2010, Mc Govern *et al.* showed association with ORMDL3 with UC [47]. In 2013, however, Hoefkens *et al.* proposed a link between several SNPs in the *ORMDL3* genetic region and CD rather than UC [136]. Of interest, *ORMDL3* expression levels in both asthma and IBD are elevated in patients compared to controls [137,

138]. Besides asthma and IBD, polymorphisms within *ORMDL3* region could also successfully be linked to type I diabetes [139], primary biliary cholangitis [140, 141], rheumatoid arthritis [142], atherosclerosis [143] and ankylosing spondylitis [144].

1.9.2 Functions of ORMDL proteins

Several studies on the functions of ORMDL proteins have shed light on their involvement in mediation of the ER homeostasis. Among others, ORMDL proteins are involved in cellular processes such as UPR as a response to ER stress conditions, Ca^{2+} homeostasis, and sphingolipid synthesis. The known functions of ORMDL proteins within the ER are outlined below.

1.9.2.1 ORMDL3 and the immune system

As ORMDL3 is associated with several proinflammatory autoimmune diseases like asthma and IBD, various studies suggested that the protein may play an important role in mediating the immune system. This hypothesis is supported by the finding that *ORMDL3* is expressed in immune cells, among others [49, 129]. Of interest, UPR induction in immune cells dramatically elevates production of type I interferon (IFN), which is essential for anti-viral responses, and pro-inflammatory cytokines like IL-23 [145, 146]. Murine studies have provided insight into the association of ORMDL3 with the type I IFN-regulated chemokine CXCL10 (C-X-C motif chemokine 10) [147, 148]. A study by Liu *et al.*, which was conducted in ORMDL3 overexpressing THP-1 monocytes demonstrated that upon rhinovirus infection these immune cells exhibited increased mRNA expression levels of the ER stress marker *HSPA5* and type I IFN marker *IFNB1* (interferon b1) [149]. Moreover, the authors showed that RV stimulation of the Bjab B cell line induced *IFNB1* and *CXCL10* mRNA, and also upregulated *ORMDL3* and *HSPA5* expression [149] In order to further specify the function of ORMDL3 in lymphocytes, Carreras-Sureda and colleagues performed a study in Jurkat T cells, thereby showing that ORMDL3 modulates both store-operated calcium entry (SOCE) and T cell activation [150].

1.9.2.2 ORMDL3 in ER Stress/UPR

In yeast, absence of Orm1 and Orm2 impairs ER quality control and constitutively activates the UPR [151]. Similarly, human ORMDL proteins have also been associated with modulation of UPR signaling in mammalian cells. However, these data are not consistent between different studies as will be discussed below.

A study by Cantero-Recasens in human embryonic kidney cells (HEK-293) suggested a role of ORMDL3 in modulation of the PERK pathway, as displayed in increased levels of phosphorylated eIF2α upon ORMDL3 overexpression [130]. Surprisingly, no changes in IRE1 signaling (e.g. *XBP1* splicing) have been observed. This is of special interest because upregulation of the PERK-ATF4 pathway has been

described to induce *XBP1* splicing by upregulation of *IRE1a* expression [152]. In contrast to this data, another study showed that overexpression of ORMDL3 in Cos-7 fibroblast-like cells reduced UPRE promoter activity, thus indicating less *XBP1* splicing [47]. Furthermore, a study by Miller *et al.* demonstrated increased ERSE promoter activities in ORMDL3 overexpressing A549 lung epithelial cells, suggesting an influence of ORMDL3 on the ATF6 signaling pathway of the UPR. Both other UPR signaling pathways, IRE1 and PERK, however, showed no alteration by ORMDL3 overexpression [148]. Finally, a study in human airway epithelial cells (1HAE) found no differences in UPR activation upon small interfering RNA (siRNA) knockdown of ORMDL3 [138]. Taken together, the described inconsistencies in study outcomes indicate a complex role of ORMDL3 in modulating the UPR. It can be assumed that function of ORMDL3 is not only dependent on the cell type but also depends on the scope and duration of ER stress.

To further characterize the role of ORMDL3 on the three UPR pathways *in vitro*, our group performed a study in HEK-293 cells. The results of this study show that silencing of ORMDL3 reduced ATF6α cleavage upon ER stress induction, whereas overexpression of ORMDL3 promoted ATF6α processing by induction of ERSE target genes [153]. This finding is consistent with a study from Miller *et al.* [148] who demonstrated *SERCA2B*, a target gene of ATF6α, induction upon ORMDL3 overexpression. Furthermore, in our group ORMDL3 overexpression induced the PERK UPR signaling pathway by enhancing ATF4 promoter activity, while inhibiting the IRE1 pathway as presented by both reduced XBP1 splicing and UPRE promoter activity [153] (unpublished data).

1.9.2.3 ORMDL1 and ORMDL2 in the context of disease

When searching for information on the role of ORMDL1 and ORMDL2 in the context of disease, the researcher finds only very few results. Despite their high amino acid identity to ORMDL3, ORMDL1 and ORMDL2 seem to be less associated with known diseases. There are, however, some studies providing an insight into the role of the two proteins in disease onset: A study by Toncheva *et al.* links polymorphisms not only in ORMDL3 but also in ORMDL1 and ORMDL2 to asthma [154]. Additionally, Zhu and colleagues suggest a role for the ORMDL protein family in human clear cell renal cell carcinoma (ccRCC) development [155]. A study in mice further highlights the importance of ORMDL1 for proper myelination of the ischiadic nerve [156]. To our knowledge, no association between ORMDL1 and ORMDL2 and IBD have been described.

1.9.2.4 ORMDL3 and autophagy

ORMDL3 is involved in cellular processes like the mediation of ER stress by the UPR, calcium homeostasis, sphingolipid synthesis, and inflammatory disorders. Interestingly, several of these processes have been linked to autophagy induction [157-159], thus suggesting a possible link between ORMDL3

and the autophagic pathway.

In 2015, Ma *et al.* published their study of the impact of ORMDL3 on artherosclerosis in Chinese Han population [143]. Since autophagy is activated upon modification of lipid synthesis, inflammation and ER stress, the authors postulated an association of ORMDL3 with autophagy. Indeed, the group found that knockdown of ORMDL3 in endothelial cells suppressed both oxidized low-density lipoprotein-induced and basal autophagy via Beclin-1 (BECN1). Another study conducted by Dang *et al.* in splenic B cells of *Ormdl3* deficient mice demonstrated a mediating role of ORMDL3 on autophagy via the ATF6-BCN1 autophagy pathway [160]. Moreover, the authors claim that ORMDL3 ensured splenic B cell survival by autophagy induction and, consequently, suppression of apoptosis. Additionally to these two studies, a recent study by Kiefer *et al.* [161] postulates a reduction in toll-like receptor 4 (TLR-4)-dependent autophagy in ORMDL3-overexpressing macrophages. These findings are supplemented by a study from Stengel, which shows that not only *Ormdl3* but also *Ormdl1/3* deficiency impaired autophagy in murine IECs and iMEFs (immortalized mouse embryonic fibroblasts) [162].

1.9.2.5 Regulation of calcium (Ca^{2+}) homeostasis

The ER functions as an intracellular Ca^{2+} store. Tightly controlled Ca^{2+} levels are needed to guarantee proper secretion and folding of proteins in the ER. Thus, disturbances in the Ca^{2+} homeostasis cause ER stress, which, in turn, activates the UPR signaling pathways [163]. Ca^{2+} homeostasis in the ER is maintained by Ca^{2+} release channels and pumps that ensure the exit of Ca^{2+} from the ER to the cytoplasm or back to the ER [164]. One of the protein groups responsible for the import of Ca^{2+} into the ER lumen is the sarco/endoplasmic-reticulum Ca^{2+} ATPase (SERCA), a downstream target of the ATF6 signaling pathway [165]. Different studies have linked ORMDL3 to SERCA proteins, thus providing a link between ORMDL3 and Ca^{2+} homeostasis. However, results obtained from these studies are inconsistent. On the one hand, Miller and colleagues demonstrated increased mRNA levels of *SERCA2b* upon ORMDL3 overexpression in lung epithelial cells (A549) [148]. This finding was supported by another study from the same group that was conducted *in vivo* in transgenic mice overexpressing human ORMDL3. Miller *et al.* could show that ORMDL3 overexpression caused increased mRNA levels of *Serca2b* [147]. On the other hand, ORMDL3 has been found to act as negative regulator of SERCA proteins. Overexpression of ORMDL3 in human HEK-293 cells resulted in elevated cytosolic Ca^{2+} levels and reduced ER-mediated Ca^{2+} signaling [130]. Of interest, a study in the immune cell line Jurkat supported the findings from those experiments with HEK-293 cells. It has been found that ORMDL3 modified lymphocyte activation by impeding entry of cytosolic Ca^{2+} into the ER lumen, which suggests a strong connection between ORMDL3 and inflammatory processes [150].

1.9.2.6 Sphingolipid synthesis

Sphingolipids comprise a family of lipids exerting different functions in both intra- and intercellular signaling and structure of cellular membranes. Sphingolipids are composed of a N-acetylated sphingoid backbone with various fatty acids resulting in the production of ceramide species, all of which exhibit a distinct head group. The synthesis of sphingolipids starts in the ER and is completed in the Golgi apparatus. This *de novo* synthesis pathway begins with the condensation of an amino acid, e.g. serine and palmitoyl coenzyme A (CoA) by serine palmitoyltransferase (SPT) resulting in the formation of 3-ketodihydrosphingosine. Several reaction steps finally generate the products ceramide, sphingomyelins and glycosphingolipids. Interestingly, sphingolipid metabolites like ceramide, sphingosine-1-phosphate or ceramide-1-phosphate (C1P) have been shown to play important roles in the modulation of cellular immune and inflammatory processes [157].

Immunoprecipitation and mass spectrometry studies in yeast could show a direct interaction between Orm1/2 and Lcb1 (serine C-palmitoyltransferase long chain base LCB1), Lcb2 (serine C-palmitoyltransferase LCB2) and Tsc3, the subunits of yeast SPT [166]. This finding already indicated a first connection between ORMDL proteins and sphingolipid synthesis. Additionally, Orm proteins were shown to act directly on Lcb1 and Lcb2, thus negatively regulating sphingolipid synthesis. Loss of *Orm1/2* in yeast cells caused increased levels of long chain bases (sphingolipids), whereas inhibition of SPT in the same cells resulted in normal cell growth [151, 166].

In yeast, Orm-1 and Orm-2 have been shown to inhibit SPT, the rate-limiting enzyme in *de novo* ceramide synthesis. Since it was thought that the three human orthologues ORMDL1-3 may perform similar functions in mammalian cells, Cai *et al.* used a mass spectrometry approach to determine the effect of siRNA-induced downregulation of single ORMDLs in HepG2 liver cells [167]. The group found that siRNA-mediated downregulation of ORMDL3, but not ORMDL1 or ORMDL2, caused elevation of dihydroceramide levels, which represent a group of ceramide precursors. Like their lack of effect on dihydroceramides, siORMDL1 and siORMDL2 also did not have a reproducible effect on ceramides. However, when investigating sphingoid bases, the authors found that siORMDL1 increased sphingosine, a degradation product of ceramide, levels.

1.9.3 Characterization of intestinal inflammation in *Ormdl* deficient mouse models

Previous studies from our group aimed at characterizing the impact of ORMDL proteins on the development of intestinal inflammation *in vivo*. Consequently, several mouse lines were generated to investigate whole-body or IEC specific knockout of the different *Ormdl g*enes during homeostasis and under inflammatory conditions e.g. in a DSS colitis model. The following chapter aims at providing an overview about the different mouse strains and all studies that have been conducted therein.

1.9.3.1 The *Ormdl1* deficient mouse model

Whole-body deletion of *Ormdl1* was achieved by deleting exon two containing the start codon of this gene [153]. No compensatory upregulation of *Ormdl2* or *Ormdl3* both on mRNA expression and protein level was observed. *Ormdl1* deficient mice did not exhibit alterations in lifespan or fertility. Under basal conditions, ileum and colon tissue showed no abnormality in comparison to those from wild type (WT) mice. An acute DSS colitis also revealed no significant differences between *Ormdl1* deficient and wild type mice neither in body weight loss nor histological scoring of colon tissue [153], suggesting that deletion of *Ormdl1* alone does not cause alteration of intestinal homeostasis *in vivo*.

1.9.3.2 *Ormdl3* deficient mouse models

In a first study, the phenotype of $Ormdl3^{\Delta IEC}$ and $Ormdl3^{-/-}$ mice was assessed under physiological conditions [153]. Of note, none of the two strains exhibited any obvious morphological abnormalities in comparison to their wild type littermates as indicated by inconspicuous histological scores of ileum and colon tissues. Consequently, in a next step both strains, $Ormdl3^{\Delta IEC}$ and $Ormdl3^{-/-}$, were subjected to acute DSS colitis, which induces inflammatory responses in the intestine and therefore resembles human IBD [168]. When being subjected to DSS, mice of both genotypes exhibited higher body weight loss and increased disease activity than the control mice ($Ormdl3^{fl/fl}$ and $Ormdl3^{+/+}$, respectively). However, while whole-body deficiency of *Ormdl3* caused increased susceptibility to acute DSS colitis, IEC-specific deletion of *Ormdl3* was found to rather delay post-DSS recovery. These contrasting findings may be due to tissue-specific functions of ORMDL proteins. Of note, $Ormdl3^{-/-}$ animals showed significantly elevated serum levels of the cytokine IL-1β, which is among the main drivers of inflammation in human IBD [169, 170], and reduced liver weight. The latter is of special interest because IBD patients show extra-intestinal manifestations in the hepatobiliary system, thus highlighting the importance of this organ for disease development and progression [171].

To also study the effects of long-term inflammation, $Ormdl3^{\Delta IEC}$ mice were subjected to chronic DSS colitis. Interestingly, it was found that $Ormdl3^{\Delta IEC}$ animals were less susceptible to chronic DSS treatment than their wild type littermates as indicated by decreased body weight loss, faster recovery as well as lower histological scores at the end of the experiment. To study mechanistic effects of ORMDL3 during colitis development, $Ormdl3^{-/-}$ animals were subjected to DSS for two to four days. Inspection of colonic tissues revealed elevated and prolonged levels of p-eIF2α, indicative of unresolved ER stress in $Ormdl3^{-/-}$ mice. Of interest, elevated colonic p-eIF2α levels tissue have also been linked to human IBD pathogenesis, supporting the hypothesis that upregulation of p-eIF2α in the colon causes increased sensitivity to intestinal inflammation. Furthermore, inspection of liver tissue showed increased protein levels of p-eIF2α and the pro-apoptotic factor CHOP, which might be the cause of liver weight reduction in $Ormdl3^{-/-}$ mice at the end of the acute DSS colitis.

To further investigate the role of ORMDL3 during ER stress *in vivo*, *Ormdl3*$^{-/-}$ mice received an intraperitoneal injection with tunicamycin, an ER stress-inducing chemical. All animals survived the injection, indicating that ORMDL3 is dispensable for survival of persistent ER stress. However, *Ormdl3*$^{-/-}$ mice showed higher susceptibility to tunicamycin treatment as presented in acute fatty liver degeneration and elevated levels of the cytosolic protein marker ADRP, among others [153]. Moreover, tunicamycin-treated *Ormdl3*$^{-/-}$ mice exhibited dysregulated UPR signaling as presented in upregulation of UPR mediators like CHOP, p-eIF2α and Xbp1s in both liver and kidney tissue.

A second study from our group [162] not only confirmed that *Ormdl3*$^{-/-}$ mice were born at Mendelian ratios and showed normal life expectancies but also underlined the impact of ORMDL proteins on body growth. The latter became visible in a decrease in body size in comparison to wild type littermates. When inspecting small intestine and colon of *Ormdl3*$^{-/-}$ mice, no histological differences between the genotypes and no signs of spontaneous intestinal inflammation could be observed. To investigate the effect of the microbiota on the *Ormdl3* deficient phenotype, mice were infected with *E. coli* LF82 and exhibited decreased *Ormdl3* mRNA expression as well as reduced ORMDL protein levels. Furthermore, *Ormdl3* deficient mice were more susceptible to adherent-invasive *E. coli* (AIEC) colonization, thus underscoring the importance of this gene on IBD development as AIEC is linked to the pathogenesis of the disease. When investigating IECs within the SI, the data showed that *Ormdl3* deficient mice exhibited both reduced Paneth cell and goblet cell numbers when compared to WT controls. Of interest, the ER of Paneth cells exhibited expansion of the ER compartment, suggesting an abnormal Paneth cell function and induction of an ER stress response. However, *Ormdl3* deficient mice did not exhibit higher UPR activation levels neither on mRNA nor protein level.

Table 2: Phenotypes of the *Ormdl3*$^{\Delta IEC}$ and *Ormdl3*$^{-/-}$ mouse models as described by Jentzsch [153] and Stengel [162].

Phenotype	Condition	Reference
decrease in body growth	basal	[153, 162]
reduced IFNγ expression levels in serum and colon	basal	[153]
no spontaneous intestinal inflammation	basal	[153, 162]
decrease in Paneth cell and Goblet cell numbers	basal	[162]
expansion of ER in Paneth cells	basal	[162]
increased susceptibility to acute DSS	DSS colitis	[153]
elevated IL-1β serum levels	DSS colitis	[153]
increased susceptibility to AIEC colonization	AIEC colonization (oral infection)	[162]

1.9.3.3 *Ormdl1/3* and *Ormdl1/2/3* deficient mouse models

A follow-up study by Stengel [162] aimed at characterizing the impact of ORMDL proteins on intestinal inflammation. To explore this impact *in vivo*, mice deficient for *Ormdl1/3* and *Ormdl1/2/3* in the whole

body were generated. Of interest, while *Ormdl1/3* double deficient mice were born at sub-Mendalian ratios and exhibited a reduction in lifespan, Ormdl*1/2/3* triple deficient mice suffered from embryonic lethality altogether, suggesting an important role for ORMDL proteins during embryogenesis. When assessing adult *Ormdl1/3* mice, the author found that these mice not only exhibited decreased overall body size but also a decrease in body weight in comparison to wild type mice. In line with the findings from *Ormdl1* and *Ormdl3* single deficient mice [153], *Ormdl1/3* deficient mice up to 25 weeks of age also did not exhibit any signs of spontaneous intestinal inflammation [162]. However, when investigating Paneth cells as the source of defense against bacterial invasion of these mice, it was found that the ER of *Ormdl1/3* deficient Paneth cells was significantly dilated compared to those of *Ormdl3* deficient and wild type Paneth cells [162]. Furthermore, *Ormdl1/3* deficient mice exhibited a significant decrease in Paneth cell numbers as indicated by decreased lysozyme positive cells in histology. To test the idea of disturbed Paneth cell function, small intestinal crypts from these mice were isolated, infected with the Crohn's disease-associated invasive bacterial strain *E. coli* LF82 [172] and bacterial numbers were quantified two hours post infection. The results showed reduced bacterial killing capacities for *Ormdl1/3* deficient crypts indicating reduced levels or secretion of antimicrobial peptides [162]. Of interest, *Ormdl1/3* deficient mice infected with *E. coli* LF82 also revealed both a decrease in PAS+ Goblet cells in the colon and corresponding decreased *Muc2* expression in the ileum and colon. Moreover, untreated *Ormdl1/3* deficient mice showed a dilated ER lumen in Goblet cells and enterocytes, which resembled the phenotype observed in Paneth cells [162]. Since a dilated ER lumen is often linked to an initiation of ER stress responses, the author next examined mRNA expression and protein levels of ER stress markers such as GRP78 and GRP94. Neither in young mice up to 20 weeks of age or freshly isolated crypts of *E. coli* LF82 infected mice any UPR activation upon *Ormdl1/3* deficiency was observed. However, 1-year-old *Ormdl1/3* deficient mice exhibited reduced expression of some ER stress markers in ileal tissue, while GRP94 protein levels remained unchanged compared to wild type mice [162].

Noteworthy, *Ormdl1/3* deficient mice of both sexes displayed signs of severe neurological defects, such as abnormal limb-clasping reflexes and impaired motor coordination ability. Pathohistological analysis of brain sections characterized a progressive degeneration of the basal ganglia and progressive astrogliosis, which was postulated to be caused by impaired autophagy. *Ormdl1/3* deficient iMEFs showed a strong reduction in LC3 turnover and elevated p62 levels, among others, which was also confirmed upon siRNA mediated ORMDL1 and ORMDL3 knockdown in IECs. These results again suggest an association of ORMDL proteins with autophagy.

Another study on *Ormdl1/3* deficient mice was published by Clarke *et al.* just recently [156]. Since the ORMDL protein family has been associated with sphingolipid and ceramide synthesis, the group focused on the characterization of sphingolipids and their corresponding phenotype. The authors found that *Ormdl1/3* deficient mice not only showed significant lower body weight compared to WT mice but also

confirmed the finding that *Ormdl1/3* deficient mice exhibit severe neurological defects like abnormal hindlimb clasping. This phenotype was complemented by the finding that brains from *Ormdl1/3* deficient mice showed substantially higher levels of dihydrosphingosine, dihydroceramide, ceramide and sphingosine compared to *Ormdl3* single deficient mice. Since sphingolipids are key components of the myelin membrane surrounding axons in the nervous system, the authors hypothesized that the ORMDL family may be crucial during the formation of myelin membranes after birth. This hypothesis was further underscored by the fact that breedings to obtain *Ormdl1/2/3* triple deficient mice was not successful due to embryonic or neonatal lethality. Noteworthy, the group found that the sciatic nerve of *Ormdl1/3* deficient mice exhibited a highly abnormal morphology accompanied by significantly lower myelinated axons. The authors claimed that tight regulation of shingolipid synthesis by the ORMDL proteins is essential for preventing nervous system damage during spingolipid-dependent myelination [156].

1.10 Objectives of this study

IBDs with their two major subtypes CD and UC are chronic conditions of the human gastrointestinal tract. To characterize the genetics underlying IBD development, GWA studies have been conducted. These studies suggest that genes involved in cellular pathways such as autophagy and the UPR, which resolves ER stress, play an important role in IBD pathogenesis. IBD risk genes not only comprise ATG16L1, an autophagy-related gene, but also Xbp1 and Ormdl3, which are both associated with the UPR. Since, to this day, the impact of Ormdl3 on IBD development and progression has been the subject of only few studies, our group set out to characterize the role of Ormdl3, and its two homologues Ormdl1 and Ormdl2, on intestinal inflammatory conditions *in vitro* and *in vivo*.

Previous *in vitro* studies from our group performed in human cell lines demonstrated that ORMDL3, ORMDL1 and ORMDL2, influence both *Xbp1* splicing and UPRE promoter activity. Thus, these studies gave us a first hint towards a connection between ORMDL proteins, especially ORMDL3, and the IRE1 signaling pathway of the UPR. Further studies from our group indicated that a deficiency for *Ormdl3* in mice is associated with increased susceptibility to acute DSS-induced colitis. This finding is of special interest because mice deficient for *Xbp1*, another UPR-related gene, also show increased susceptibility to DSS-induced colitis [46]. Consequently, in this study we aimed at characterizing the impact of double deficiency of both *Ormdl3* and *Xbp1* on the intestinal phenotype in a mouse model under homeostatic and inflammatory conditions. Therefore, we used mice deficient for both genes, *Ormdl3* and *Xbp1* (termed $Ormdl3^{-/-}/Xbp1^{\Delta IEC}$ or *Ormdl3/Xbp1* double deficient mice; see Table 8 for further explanation), and compared them to mice deficient only for *Xbp1* (termed $Ormdl3^{+/+}/Xbp1^{\Delta IEC}$ or *Xbp1* deficient mice; see Table 8 for further explanation).

To further characterize a possible interaction between the three ORMDL homologues *in vivo*, we also studied the impact of *Ormdl2* deficiency on susceptibility to acute DSS-induced colitis.

The aims of this thesis were divided into three different categories, based on the genotypes of the cells and mouse models used in the experiments. These categories comprise the characterization of intestinal inflammation and its phenotype in

1) *Ormdl3* deficiency,
2) *Ormdl3*/*Xbp1* double deficiency, and
3) *Ormdl2* deficiency.

To specify our aims, we further subdivided the three categories mentioned above into different research questions, which are shown below. Within this study we aimed at answering the following questions:

1) *Ormdl3* deficiency
   - Is *Ormdl3* deficiency associated with ER stress and the activation of the UPR, and especially the IRE1α/XBP1 pathway, in murine intestinal epithelial cells?
2) *Ormdl3*/*Xbp1* double deficiency
   - When compared to *Xbp1* single deficiency, does *Ormdl3*/*Xbp1* double deficiency cause more ER stress in the intestine?
   - Do *Ormdl3*/*Xbp1* double deficient mice exhibit spontaneous intestinal inflammation?
   - Does ageing of *Ormdl3*/*Xbp1* double deficient mice affect their intestinal phenotype?
   - What are possible candidate genes driving a phenotypic difference between *Ormdl3*/*Xbp1* double deficient mice and *Xbp1* deficient animals?
   - What is the role of ORMDL3 in *Xbp1* deficiency in experimental colitis?
3) *Ormdl2* deficiency
   - What is the role of ORMDL2 in experimental colitis?

2 Materials and Methods

2.1 Cell Biological Methods

2.1.1 Cell Lines

ModeK iXPB1 cells with XBP1 knockdown by stable overexpression of siRNA and ModeK iCtrl cells used for *in vitro* investigations were received as a gift from A. Kaser (University of Cambridge, United Kingdom) [46]. ModeK cells were cultured in their respective media (Gibco/Life Technologies, Darmstadt, Germany) and incubated at 37 °C with 5 % (v/v) carbon dioxide. All cell culture steps were carried out in a laminar flow hood (Thermo Scientific, Bremen, Germany) under sterile conditions.

Table 3: Cell line used for *in vitro* investigations.

Cell line	Received from	Species	Tissue	Nutrition medium
ModeK iXbp1/iCtrl	A. Kaser (Cambridge, UK)	murine	duodenal epithelium	DMEM GlutaMAX + 10 % FCS + NEAA + HEPAS + Pen/Strep

For cell line maintenance, cells were split twice a week. For splitting, cells were washed with PBS and treated with a trypsin/EDTA solution (Life Technologies, Darmstadt, Germany) for 5 minutes at 37°C. To ensure inactivation of trypsin after complete detachment of cells, full culture media was added. Cell suspensions were centrifuged at 300 g for 5 min, resuspended in fresh media and re-plated at the desired concentrations (Table 4).

Table 4: Overview of cell culture dishes and cell numbers used for experiments.

Experiment	Cell culture dish	Cell number/well	Volume medium [ml]
Protein lysates	6-well plate	2×10^5	2
RNA isolation	6-well plate	2×10^5	2
Fluorescence microscopy	6-well plate	2×10^5	2
FACS measurement	6-well plate	2×10^5	2
Luciferase assay	96-well plate	1×10^4	0.1

2.1.2 Transfection of cells with small interfering RNA

ModeK cells were transfected using Viromer® Blue transfection reagent (Lipocalyx GmbH, Halle, Germany). Viromer® Blue reagent contains medium sized and neutrally charged branch polymer that bind siRNA. The resulting transfection complexes enter the cell via endocytosis. Following endocytosis, the transfection complexes escape the endosome and release their cargo, the siRNA.

For transfection of ModeK cells, siRNA was diluted in a 1.5 ml reaction tube to 2.8 µM using Buffer Blue, a buffer provided by the company. In a next step, the appropriate amount of Viromer® Blue was pipetted to the wall of a second 1.5 ml reaction tube and diluted in Buffer Blue. Afterwards, the solution containing Viromer® Blue was pipetted to the siRNA solution and mixed swiftly. After a 15 min

incubation at RT, the transfection complex was added to the cells. The transfection reagent was distributed within the wells by gently shaking the cell culture plate horizontally. Cells were placed into the incubator for a 24 h incubation. All steps described for siRNA transfection were performed under sterile conditions.

Table 5: Overview of volumes used for Viromer Blue transfection of cells.

Cell culture plate	Viromer® Blue + Buffer Blue + siRNA [µl/well]
6-well plate	100
96-well plate	5

2.1.3 Promoter-mediated luciferase reporter assay

The dual-luciferase reporter assay system (Promega, Mannheim, Germany) was used to measure activation of UPR-activated intracellular response elements. The response element investigated was UPRE as a target of the IRE/XBP1 signaling pathway. The promoter regions of UPRE were cloned upstream of the firefly (*Photinus pyralis*) luciferase. A second luciferase from *Renilla reniformis* (pRL-TK; Clontech) was used as internal transfection and cell viability control. Normalization of the data was performed by dividing the firefly luciferase bioluminescence by the *Renilla* bioluminescence.

ModeK cells were seeded on 96-well plates at a density of 2 x 10^5 cells per well. After a 24 h incubation at 37°C, cells were transfected with siRNA against ORMDL3 or scrambled siRNA as control. Following another 24 h incubation, ModeK cells were transfected with 20 ng of the UPRE firefly luciferase reporter construct, and 3 ng of the *Renilla* luciferase plasmid pRL-TK. 24 h later, cells were stimulated with tunicamycin (2 µg/ml) to induce ER stress. For quantification of luciferase activity 24 h after stimulation, cells were lysed using 25 µl passive lysis buffer and subjected to a freeze-thaw cycle before analysis. Cell lysates were analysed using a 96-well microplate reader (Tecan, Männedorf, Switzerland) and dual-luciferase activity was assessed as relative light units.

2.1.4 Flow cytometric analysis

Cell surface expression of major histocompatibility complex 2 (MHCII) on isolated IECs and lamina propria (LP), SI organoids or ModeK cells was assessed by flow cytometry. Briefly, 2.5 x 10^5 cells were treated with anti-CD16/32 to block Fc receptors and to prevent unspecific antibody binding, washed with FACS buffer and incubated with the indicated antibody conjugates for 30 min at 4 °C in a final volume of 10 µl FACS buffer. After the staining, cells were washed three times with FACS buffer and either fixed using 1 % paraformaldehyde solution or incubated in FACS buffer. The appropriate isotype-matched control antibodies were included in the experiment to determine the level of background staining. Flow cytometric analyses were performed using a FACSCalibur fluorescence-activated cell sorting system (BD Biosciences, Heidelberg, Germany) with BD CellQuest ProTM software (BD

Biosciences, Heidelberg, Germany). All applied antibodies are listed in the supplementary information (Table 22).

2.2 Molecular biological methods

2.2.1 Isolation of RNA from small intestinal tissue, organoids or cell lines

RNA extraction from murine tissue, organoids and cell lines was performed using RNeasy Mini Kit (Qiagen, Hilden, Germany) according to manufacturer's protocol. Tissue samples were disrupted and homogenized using the TissueLyserII (Qiagen, Hilden, Germany) within 350 µl RLT buffer and 1 % β-mercaptoethanol. Organoids and secondary cells were lysed directly in their respective plates and transferred into a microcentrifuge tube. Cell lysates were loaded onto QIAshredder spin columns for sample homogenization. To prevent contaminations by genomic DNA, an on-column DNase digestion was performed. The purified RNA was eluted in 20-50 µl RNase-free water and RNA concentration was determined using a NanoDrop ND-1000 spectrophotometer (PeqLab Biotechnologie GmbH, Erlangen, Germany). RNA samples were stored at -80 °C until further processing.

2.2.2 cDNA synthesis

Complementary DNA (cDNA) from RNA templates was synthesized using the Maxima H Minus First Strand cDNA Synthesis Kit (Thermo Scientific, Bremen, Germany). According to manufacturer's protocol, 0.1 – 1 µg total, purified RNA was used as a template for cDNA synthesis. Briefly, RNA was incubated with Oligo(dt) oligonucleotides, dNTP mix and water at 65 °C for 5 min (Table 6). In the next step, 5X RT buffer and Maxima H Minus reverse transcriptase were added and incubated as indicated in the manufacturer's protocol. The newly synthesized cDNA was diluted in a ratio of 1:10 with nuclease-free water and stored at -20 °C.

Table 6: Reverse transcription components and incubation times.

Step	Reagents	Quantity	Incubation temperature and time
1	RNA	500 ng	
	$Oligo(dt)_{18}$ oligonucleotide	0.125 µl	
	dNTP mix (10 mM each)	0.5 µl	5 min at 65 °C
	nuclease-free water	fill up to 7.5 µl	
2	5x RT buffer	2 µl	10 min at 25 °C
	Maxima H Minus RT	0.5 µl	15 min at 50 °C 5 min at 85 °C

2.2.3 Quantitative real-time polymerase chain reaction (TaqMan/SYBR Green Assay)

Today, quantitative real-time PCRs (qPCRs) are widely used to quantify mRNA levels by usage of target-specific oligonucleotides. qPCRs are based on the PCR method, but in contrast to the latter, qPCRs are

characterized by an additional DNA quantification step at the end of each amplification cycle. For quantification of mRNA levels DNA-intercalating fluorescent dyes like SYBR Green or fluorophore-coupled hybridization probes called TaqMan probes are used.

In this work, both oligonucleotides and predesigned TaqMan probes were used. The latter were purchased from Applied Biosystems (Carlsbad, USA). TaqMan probes and oligonucleotides used for SYBR Green Assay are listed in the supplemental material (Tables 25 and 26). All qPCR experiments were performed in sample duplicates on a 384-well plate on a 7900HT Fast Real Time PCR System (Applied Biosystems, Darmstadt, Germany). For one PCR mixture 5-10 ng cDNA and 0.5 µl of the respective, specific TaqMan® gene expression assay was used. Every PCR program was run according to the TaqMan Gene Expression Master Mix protocol (Applied Biosystems, Darmstadt, Germany). For quantification of mRNA levels cycle threshold (Ct) values of the target genes were normalized to the respective mRNA levels of housekeeping genes *Gapdh* or *β-Actin*.

2.3 Protein biochemical methods

2.3.1 Preparation of total protein lysate

Total protein lysates were extracted from ModeK cells or murine crypts to determine the protein content of IECs. Protein content was analyzed using gel electrophoresis. Isolated ModeK cells or crypts in 1.5 ml tubes were lysed using RIPA buffer with 1x Halt™ combined protease and phosphatase inhibitor (Thermo Scientific, Bremen, Germany). Lysates were stored on ice for 5 min and resuspended using a pipette to ensure complete cell lysis. Protein lysates were stored at -20°C short-term.

2.3.2 Determination of protein concentration

Following overnight incubation, lysates were centrifuged for 10 min at 4°C and 10.000 rpm to remove cell debris and genomic DNA. The supernatant was transferred to 1.5 ml reaction tubes and used for determination of protein concentrations. Determination of protein concentrations was performed using the Bio-Rad CD protein assay (Bio-Rad, Munich, Germany) according to manufacturer's protocol. This colorimetric method is based on the Lowry assay [173], a biochemical method for the quantitative determination of total level of proteins in a solution. The Lowry protein assay comprises two steps: First, the reaction of copper ions with peptide bonds under alkaline conditions and second, the oxidation of aromatic protein residues, which results in a characteristic blue color. For the determination of total proteins 5 µl of protein lysate were diluted in 5 µl of *aqua bidest.* and the assay reagents were added in the respective amounts indicated by manufacturer. Samples on a 96-well plate were incubated under dark conditions on a shaker for 15 min at RT followed by measurement of absorbance of protein samples. For determination of protein concentration, absorbance of protein samples was correlated with a bovine serum albumin (BSA) standard.

2.3.3 Gel electrophoresis of proteins

Protein separation by molecular weight was performed using precast gradient polyacrylamide gels. These gels ensure an improved separation of proteins under denaturing conditions. For separation of proteins with a molecular weight between 12 and 260 kDa, precast NuPAGE® 4-12 % Bis-Tris gels (Life Technologies, Darmstadt, Germany) were used. Contrasting to the usually used SDS-PAGE gels, these gels contain Bis-Tris/HCl buffer instead of SDS. Protein lysates were supplemented with NuPAGE® LDS Sample Buffer (Thermo Scientific, Bremen, Germany) and incubated at 70 °C for 10 min before electrophoresis. SDS-PAGE was performed at 160 V with a maximum current of 300 mA for 2 h at RT in a XCell SureLock Mini Cell system (Life Technologies, Darmstadt, Germany). For gel runs, NuPAGE MOPS SDS Running Buffer was used, while protein size was estimated using pre-stained PageRuler plus protein ladder 10-250 K (Thermo Scientific, Bremen, Germany).

2.3.4 Immunodetection of proteins by Western blotting

For further identification of proteins, separated peptides were transferred from the Bis-Tris polyacrylamide gel onto a polyvinylidene difluoride membrane (PVDF; Bio-Rad, Munich, Germany) using the semi-dry blotting system Trans-Blot Turbo™ Transfer System (Bio-Rad, Munich, Germany). This transfer system uses a discontinuous buffer system of two anode buffers and one cathode buffer, which are used to equilibrate PDVF membranes and blot papers for subsequent blotting. Blotting was achieved using a constant current of 0.1 A and a maximum voltage of 25 V for 30-45 min. To prevent unspecific binding of the antibodies, PDVF membranes were blocked for 1 h at RT with 5 % (w/v) blotting grade blocker (non-fat dry milk) in Tris-buffered saline (TBS) supplemented with 0.1 % Tween 20 (TBST). Next, membranes were treated with the desired primary and secondary antibody combinations (see Table 22 and 23) to achieve detection of the desired antigens. Therefore, primary antibodies were diluted in TBST according to manufacturer's recommendations and incubated either for 1 h at RT or ON at 4°C under mild agitation. To remove any non-bound primary antibody from the membrane, three washing steps with TBST were performed for 15 min each. Afterwards, a horseradish peroxidase (HRP) conjugated secondary antibody recognizing the Fc region of the primary antibody was diluted in TBST according to manufacturer's instructions, transferred to the membrane and incubated for 1 h at RT. Proteins were detected using a chemiluminescent substrate kit (Thermo Scientific) recognizing the HRP-coupled secondary antibody and results were recorded with an automated developer machine (Agfa, Mortsel, Belgium).

2.4 Generation, handling and treatment of mice

Weight- and gender-matched mice backcrossed for at least 6 generations were used at an age of 12 to 20 weeks or 1 year, respectively. For experiments, including DSS treatment, equal numbers of male and

female animals (at least n = 4 per genotype) were employed wherever possible. Procedures involving animal care were conducted in accordance with national and international laws and appropriate permission. *In vivo* experiments were performed in accordance with the German guidelines for animal care and protection. Animal research as part of this study was carried out in accordance with the guidelines of animal care of the Christian Albrechts University (CAU) Kiel and the University Medical Center Schleswig-Holstein (UKSH) (Table 7).

Table 7: License numbers for animal experiments.

License number	Designated use
V 312-7224-121-33 (77-6/13)	Sacrifice for tissue harvesting
V 242-17696/2016(32-3/16)	Acute and chronic DSS colitis

2.4.1 Mouse strain nomenclature

Due to the number of mouse strains discussed in this study the following table is meant to provide an overview of the nomenclature of these strains.

Table 8: Mouse strain nomenclature.
KO = (whole-body) knockout, VilCre = Villin Cre recombinase, IEC = intestinal epithelial cell.

Ormdl2KO		
$Ormdl2^{+/+}$ *Ormdl2* wild type allele	$Ormdl2^{+/-}$ *Ormdl2* heterozygous	$Ormdl2^{-/-}$ deficiency for *Ormdl2* (whole-body)
Ormdl3KO		
$Ormdl3^{+/+}$ *Ormdl3* wild type allele	$Ormdl3^{+/-}$ *Ormdl3* heterozygous	$Ormdl3^{-/-}$ deficiency for *Ormdl3* (whole body)
***Ormdl3KO Xbp1VilCre* (*Ormdl3KO Xbp1*$^{\Delta IEC}$)**		
$Ormdl3^{+/+}/Xbp1VilCre$ ($Ormdl3^{+/+}/Xbp1^{\Delta IEC}$) *Ormdl3* wild type allele, deletion of *Xbp1* in IECs	$Ormdl3^{+/-}/Xbp1VilCre$ ($Ormdl3^{+/-}/Xbp1^{\Delta IEC}$) *Ormdl3* heterozygous, deletion of *Xbp1* in IECs	$Ormdl3^{-/-}/Xbp1VilCre$ ($Ormdl3^{-/-}/Xbp1^{\Delta IEC}$) double deficiency for *Ormdl3* (whole body) and *Xbp1* (specifically in IECs)

2.4.2 Animal husbandry

Animals were housed under specific pathogen-free (SPF) conditions in individually ventilated cages (IVC) either at the Central Animal Facility of the University Hospital Schleswig-Holstein (Kiel, Germany) or in the Victor Hensen Facility of Kiel University (Kiel, Germany). Mice were kept in a 12 h light-dark cycle under barrier conditions at 21°C ± 2°C and 60 % ± 5 % humidity and were provided with food and tap water *ad libitum*.

2.4.3 Generation of *Ormdl2* constitutive knockout (*Ormdl2KO/Ormdl2*$^{-/-}$) mice

The murine *Ormdl2* gene (ensemble gene ID: ENSMUSG00000025353) localizes on chromosome 10 and comprises four exons. *Ormdl2* deficient (*Ormdl2*$^{-/-}$) mice were purchased from the UC Davis Mouse Biology Program (California, USA). Deficiency for *Ormdl2* was induced by deletion of exon 2 and 3 (Fig. 2.1). To achieve this deletion, the targeting vector designed with two *loxP* sites flanking both exon 2 and 3 was electroporated into C57BL/6N embryonic stem cells. Upon successful recombination, embryonic stem cells were microinjected into C57BL/6 blastocysts and resulting chimeras were bred with C57BL/6N-A^{tmBrd}.

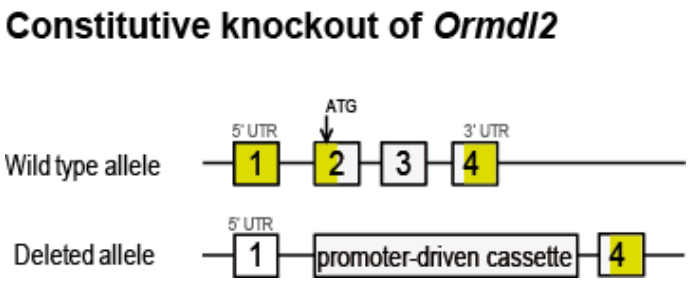

Figure 2.1: Targeting strategy for the generation of *Ormdl2* constitutive knockout alleles.
The translation initiation codon (ATG) of *Ormdl2* is located on exon 2. The coding region comprises exon 2 to 4. To generate constitutive whole-body knockout of *Ormdl2*, exon 2 and 3 were flanked by *loxP* sites. UTR = untranslated region

2.4.4 Generation of mice with constitutive knockout of *Ormdl3* and conditional knockout of *Xbp1* specifically in IECs (*Ormdl3KO Xbp1VilCre/Ormdl3*$^{-/-}$*/Xbp1*$^{\Delta IEC}$)

To study the interaction between the two IBD risk genes *Ormdl3* and *Xbp1* in the intestinal epithelium *in vivo*, mice with a double deficiency for the two genes were generated. *Ormdl3* constitutive knockout mice were generated and bred with *Xbp1* conditional knockout mice, which have been described previously [46, 126]. Briefly, *Ormdl3* deficient (*Ormdl3*$^{-/-}$) mice were generated in collaboration with TaconicArtemis GmbH (Cologne, Germany). Deficiency for *Ormdl3* was induced by deletion of exon 2 to 4 (Fig. 2.4). The targeting vector, comprising exons 2 to 4 flanked by *loxP* sites, was electroporated into C57BL6/N Tac embryonic stem cells. Positive embryonic stem cells with the incorporated modified sequence were identified by double positive selection using puromycin and neomycin. Resulting chimeras were bred with Flp deleter mice (C57BL/6-Tg(CAG-Flpe)2Arte) to ensure both germline transmission and removal of

selection markers. Consequently, *Ormdl3*$^{-/-}$ mice were generated by breeding *Ormdl3* conditional mice to Cre deleter mice (C57BL/6-*Gt(ROSA)26Sortm9(Cre/ESR1)Arte)*. Importantly, mice with constitutive knockout alleles were bred with C57BL6/N wild type mice to remove the Cre recombinase and thus prevent from unspecific genetic side effects.

The murine *Xbp1* gene (ensemble gene ID: ENSMUSG00000020484) localizes on chromosome 11 and comprises five exons. Consequently, the murine *Xbp1* gene was isolated to create a targeting vector comprising intron 2 (Fig. 2.4). Additionally, the targeting vector contained a loxP site flanking exon 2 and a floxed neomycin resistance gene cassette in intron 1 of the *Xbp1* gene. The vector was electroporated into W4/129 embryonic stem cells and its sequence was incorporated into the genome by homologous recombination. Positive embryonic stem cells with the incorporated modified sequence were identified by Southern Blot and injected into C57BL/6 blastocysts to obtain chimeras. The latter were bred to establish a *Xbp1*^{floxneo} strain, whose mice were bred with EIIacre mice to induce partial Cre-mediated recombination. To obtain *Xbp1*$^{fl/fl}$ animals, male mice with deletion of the neo cassette were mated with wild type females. Consequently, mice exhibiting *loxP* sites (*Xbp1*$^{fl/fl}$) were bred with *VillinCre* (B6.SJL-Tg(Vil-cre)997Gum/J) purchased from Jackson Laboratory (Bar Harbor, USA) to generate mice with an *Xbp1* deficiency specifically in the intestinal epithelium (*Xbp1*$^{\Delta IEC}$).

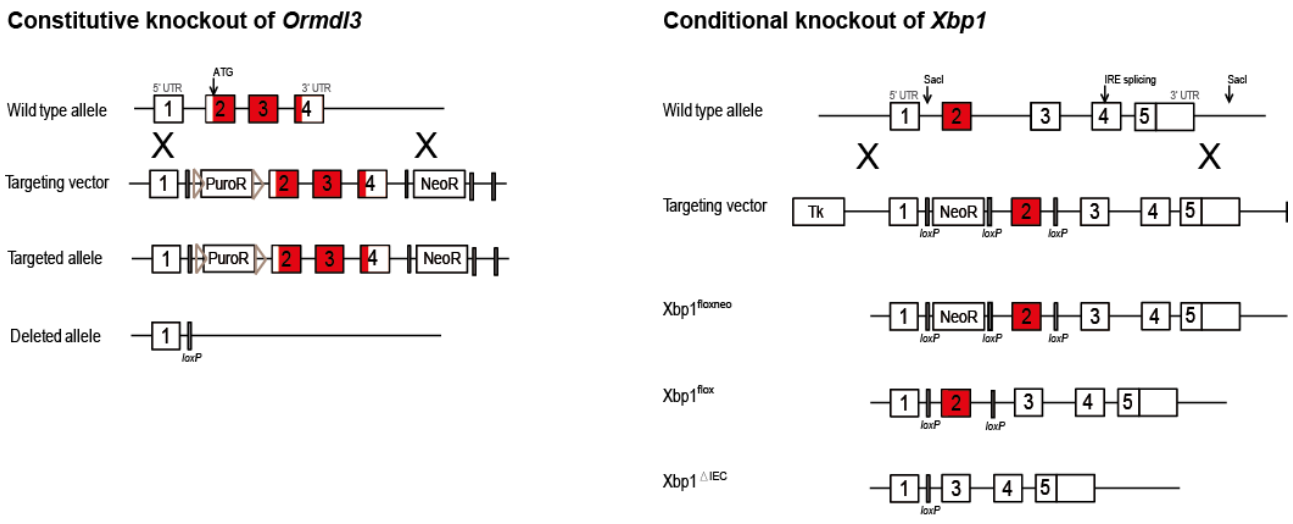

Figure 2.2: Targeting strategy for the generation of *Ormdl3* constitutive and *Xbp1* conditional knockout alleles.
The targeting strategy for the generation of *Ormdl3*$^{-/-}$ (left) and *Xbp1*$^{\Delta IEC}$ (right) mice is depicted schematically. UTR = un-translated region, PuroR = puromycin resistance, NeoR = neomycin resistance, loxP = locus of X-over P1

2.4.5 Genotyping

Genotyping of murine genomic DNA was performed by polymerase chain reaction (PCR). Genomic DNA was isolated from tail biopsies of two- to three-weeks-old mice. Briefly, the tissue was boiled in 100 µl of 50 mM sodium hydroxide (NaOH) for 1 h and centrifuged. The supernatant containing DNA was collected and subjected to different touch-down PCRs using GoTaq DNA polymerase (Promega,

Mannheim, Germany). All oligonucleotides and conditions used for PCR reactions are listed in Tables 9, 10 and 11.

Table 9: Oligonucleotides for genotyping PCR.

Target gene	Species	Forward primer	Reverse primer
Ormdl2 (WT 407 bp, KO 872 bp)	*M. musculus*	5'-ACACCTCCCCCTGAACCTGAAA	5'-AATACCATGGAACCAG CAAGGAATGC
Ormdl3 WT (194 bp)	*M. musculus*	5'-CTTCATCCGTTGTTGCTTGC	5'-TCCCCTACAGATCTCCTGAGG
Ormdl3 KO (277 bp)	*M. musculus*	5'-CTTCATCCGTTGTTGCTTGC	5'-TCACAGTGCCAGTAGGAAACC
Xbp1 (WT 170 bp, floxed 251 bp)	*M. musculus*	5'-CCTGTGGGACAGAATGG ACCCAG	5'-CGCATACACAGCTGCTTT TATCC
VillinCre	*M. musculus*	5'-CAAGACCCCCATAGGAAGCC	5'-ACATCTTCAGGTTCTGCGGG
VillinCre (internal control)	*M. musculus*	5'-TCATGGAAATCCTACAGCAGGGACC	5'-GTCATGCTGGAGAATGAG AAGC

Table 10: Components of genotyping PCR.

Component	Volume per reaction [µl]
DNA	1
5x GoTaq Green Buffer	4
dNTPs (10 mM each)	0.5
forward primer (10 µM)	0.25
reverse primer (10 µM)	0.25
GoTaq polymerase	0.5
nuclease-free water	13.5

Table 11: Temperature profile of genotyping PCR.

Temperature [°C]	Time	Cycles
95	3 min	1
95	30 sec	28-33
T_{anneal}	30 sec	
72	30 sec	
72	7 min	1
4	hold	1

2.4.6 Agarose gel electrophoresis

For the separation of DNA fragments and subsequent verification of PCR product size agarose gel electrophoresis was used. 0.5 % TAE gel containing 1 % (w/v) agarose were run at a constant voltage of 120 V and a maximum current of 300 mA for 30-60 min using a Bio-Rad Power Pac 300 power supply

(Bio-Rad, Munich, Germany). For visualization of nucleic acids by UV excitation a SYBR Safe DNA gel stain was added to the liquid agarose-TAE mixture. SmartLadder Mw-1700-10 (Eurogentec, Cologne, Germany) was used as molecular weight standard to characterize bands between 200 and 10.000 bp. After electrophoresis, images were taken using Molecular Imager ChemiDoc XRS Imaging System (Bio-Rad, Munich, Germany).

2.4.7 Histology

2.4.7.1 Immunofluorescence of cells

Immunofluorescence (IF) is a technique used to visualize the distribution of a target molecule within a sample. IF uses the specificity of antibodies to their target to initiate a fluorescent signal, where an antigen is located within the cell.

ModeK cells were seeded on cover slips overnight. Following a washing step with PBS, cells were fixed in 4 % (w/v) paraformaldehyde for 30 min at room temperature. Afterwards, cells were washed three times with PBS and permeabilized for 3 min at room temperature using 1 % (v/v) Triton X-100 in PBS supplemented with 5 % (w/v) BSA. Unspecific binding sites were blocked with 5 % (v/v) goat serum for at least 60 min at room temperature. Incubation with the primary antibody (see Table 22) was performed using a dilution of 1:500 overnight at 4 °C. Following three washing steps with PBS, cells were incubated with the second antibody for 45 min at room temperature. Cells were washed for three times with PBS following a washing step with *aqua dest.* and subsequently embedded in mounting medium (Roth, Karlsruhe, Germany). Stainings were analyzed using a Zeiss AxioImager.Z1 apotome fluorescence microscope and AxioVision Rel 4.9 software (ZEISS, Oberkochen, Germany).

2.4.7.2 Immunofluorescence of tissue

For IF staining of tissue, 3.5-4.5 µm sections of paraffin-embedded ileum swiss rolls were deparaffinized with Xylol substitute (Roth, Karlsruhe, Germany) and incubated in citric buffer for 3 minutes. Next, sections were blocked in PBS containing 5 % BSA and 0.2 % Triton-X for 30 minutes after removal of citric buffer and before incubation of a primary antibody overnight at 4°C (see Table 22, supplement). Secondary antibodies conjugated with fluorophores were added after washing steps with PBS for 45 minutes. Last, tissue was counterstained with DAPI and mounted with fluorescence mounting medium (DAKO). Stained sections were then air-dried and left at 4°C for further storage. Stained tissue was examined using a Zeiss AxioImager.Z1 apotome fluorescence microscope and AxioVision Rel 4.9 software (ZEISS, Oberkochen, Germany).

2.4.7.3 Immunohistochemistry

Immunohistochemistry (IHC) is a technique used to detect the location of proteins and other antigens

in tissue sections. The antibody-antigen interaction is then visualized by chromogenic detection with a colored enzyme substrate.

2.4.7.3.1 Tissue Processing

Murine tissue was fixed in 10 % (w/v) formalin for 24 h at 4 °C. For complete dehydration, tissue was immersed in a series of ethanol solutions of increasing concentrations up to 100 %. Afterwards, the ethanol was gradually replaced with xylene and finally paraffin. The paraffin-embedded tissue was dissected into 3.5 - 4.5 µm sections using a RM2255 microtome (Leica, Wetzlar, Germany).

2.4.7.3.2 Hematoxylin and Eosin (H/E) Staining

Samples on slides were rehydrated in decreasing xylene and ethanol solutions followed by washing steps with distilled water. Slides were stained for 2-5 min in hematoxylin. Haematoxylin in complex with aluminum salts is positively charged and reacts with negatively charged, basophilic cell components including nucleic acids which are stained blue. Counterstaining of the cytoplasm of cells was achieved with 1 % (v/v) eosin solution for 2 min. Eosin is negatively charged and therefore reacts with positively charged, acidophilic components such as amino groups in proteins in the cytoplasm, which are stained pink. Slides were dehydrated and embedded in Roti-Histo-Kit mounting medium (Roth, Karlsruhe, Germany). Slides were examined with a Zeiss AxioImager.Z1 apotome fluorescence microscope and the AxioVision Rel 4.9 software (ZEISS, Oberkochen, Germany).

2.4.7.3.3 3,3'-Diaminobenzidine (DAB) Staining

After rehydration, slides were boiled for 20 min in citrate buffer (pH 6.0) for antigen retrieval. Blocking of unspecific binding sites was achieved by incubation with 5 % (v/v) goat serum in PBS. Naturally occurring peroxidases were inactivated by treating slides with 3 % hydrogen peroxide. Antibody incubation and 3,3'-diaminobenzidine (DAB) staining was performed according to the manufacturer´s instructions of the Vectastain Elite ABC Kit (Vector Labs, Peterborough, United Kingdom). Briefly, a primary antibody was amplified by incubation with a biotinylated secondary antibody. Colorimetric reaction of DAB was achieved by oxidation using a horseradish peroxidase-conjugated streptavidin antibody in the presence of hydrogen peroxide. Oxidation of DAB finally results in the deposition of a brown precipitate. Antibodies are listed in Table 22.

2.4.7.4 Histological scoring of small intestinal and colonic tissue

Mice were sacrificed using cervical dislocation followed by heart puncture. The small intestine and colon were removed from the abdominal cavity. Afterwards, the intestine was cut open longitudinally, and about ten centimeters of the most distal small intestine or colon were taken for swiss rolls. For these swill rolls

the intestine was rolled up, starting with the distal part, thereby having the distal ileum, or the distal colon, at the very inner layer and the proximal intestine (jejunum or proximal colon) at the very outer layer. Formalin-fixed and paraffin-embedded intestinal tissue was sectioned and stained with hematoxylin and eosin (H&E).

The following semi-quantitative scoring system was used for the assessment of spontaneous intestinal inflammation. Histological subscores (for each parameter: 0, absent; 1, mild; 2, moderate; 3, severe) include mononuclear cell infiltrates, crypt hyperplasia, epithelial injury/erosion, polymorphonuclear cell infiltrates and transmural inflammation. Extent factor was derived according to the fraction of bowel length involved by inflammation: 1, < 10 %, 2, 10-25 %, 3, 25-50 % and 4, >50 %. Ileal and colonic inflammation was assessed blindly to the genotype and experimental conditions of the samples.

2.4.8 Dextran sodium sulfate-induced colitis

DSS-induced colitis is a widely used experimental measure to study intestinal inflammation *in vivo*. Administration of DSS for several days leads to colitis development characterized primarily by weight loss and bloody diarrhea, followed by ulcerations and immune cell infiltrations into the mucosa [174]. In this study DSS colitis was used to characterize the impact of *Ormdl3/Xbp1* double deficiency and *Ormdl2* single deficiency on the course and development of the disease.

2.4.8.1 Acute and chronic DSS colitis in *Ormdl3/Xbp1* double deficient mice

Experimental acute colitis in *Ormdl3/Xbp1* double deficient mice was induced in 8-15 weeks old male and female mice (n = 7 for $Ormdl3^{+/+}/Xbp1^{\Delta IEC}$, n = 6 for $Ormdl3^{-/-}/Xbp1^{\Delta IEC}$). Acute colitis was induced by administration of 2 % (w/v) DSS dissolved in autoclaved drinking water for five consecutive days, followed by five days of regular drinking water. Mice were exposed to drinking water *ad libitum*. Weight loss and wellbeing of the animals was monitored closely every day. Mice were sacrificed on day 10 of the experiment unless otherwise stated.

Experimental chronic DSS colitis in *Ormdl3/Xbp1* double deficient mice was induced in 8-15 weeks old male and female mice (n = 4 for $Ormdl3^{+/+}/Xbp1^{\Delta IEC}$, n = 4 for $Ormdl3^{-/-}/Xbp1^{\Delta IEC}$). Chronic colitis was induced over 30 days by administration of 2 % (w/v) DSS dissolved in autoclaved drinking water in three cycles of five consecutive days with each DSS cycle followed by five days of regular drinking water. Mice were exposed to drinking water *ad libitum*. Weight loss and wellbeing of the animals was monitored closely every day. Mice were sacrificed on day 30 of the experiment unless otherwise stated.

2.4.8.2 Acute DSS colitis in *Ormdl2* deficient mice

Experimental acute colitis in *Ormdl2* deficient mice was induced in 9-11 weeks old male mice (n = 5 for $Ormdl2^{+/+}$ and n = 5 for $Ormdl2^{-/-}$). Acute colitis was induced by administration of 2 % (w/v) DSS

dissolved in autoclaved drinking water for six consecutive days, followed by four days of regular drinking water. Mice were exposed to drinking water *ad libitum*. Weight loss and wellbeing of the animals was monitored closely every day. Mice were sacrificed on day 10 of the experiment unless otherwise stated.

2.4.8.3 Disease activity index

The course of the disease was monitored during DSS experiments and scored using the disease activity index (DAI), a combined score of stool blood, stool consistency and body weight loss. Scores were determined as indicated in Table 12.

Table 12: Disease activity score (DAI).

Points	Weight loss [%]	Stool consistency	Fecal blood
0	0	Formed	Hemoccult negative
1	1-5	Formed but soft	HC slightly positive
2	6-10	Unformed/smeary	HC strongly positive
3	11-20	-	Blood visible by eye
4	>20	Diarrhea	Rectal bleeding

2.4.9 Primary cell isolation

Isolation of primary cells comprised the isolation of both small intestinal crypts and small intestinal organoids from mice under homeostatic or DSS colitis conditions.

2.4.9.1 Isolation of small intestinal crypts

Mice were sacrificed using cervical dislocation followed by heart puncture. The small intestine was removed from the abdominal cavity. Afterwards, the intestine was cut open longitudinally, cleaned in ice-cold PBS in a cell culture dish and cut into small pieces of approx. 5 mm length. For bulk-processing of several small intestinal samples, the pieces were transferred to 50 ml centrifuge tubes containing ice-cold PBS. In case of just few samples, pieces were transferred directly to 50 ml centrifuge tubes containing 20 ml ice-cold PBS plus 5 mM ethylenediaminetetraacetic acid (EDTA) and incubated on ice for 10 min. This EDTA chelation is necessary for isolation of crypts from the surrounding tissue. Subsequently, tubes were inverted carefully for 5 times at 0, 5, and 10 minutes of incubation time and the PBS/EDTA was replaced at each timepoint mentioned. Following incubation time, the PBS/EDTA was replaced by 20 ml of ice-cold PBS. For dissociation of the crypts from the tissue tubes were shaken vigorously twice for 15 sec each, interjected by a 15 sec break. After shaking, the tubes were incubated on ice for 5 min before repeating the shaking steps. Next, the solution containing tissue pieces was strained through a 100 nm cell strainer to obtain small intestinal crypts only. To freeze the small intestinal crypts for later experiments, 500 µl of the crypt-containing PBS solution was transferred to 1.5 ml centrifuge tubes and

centrifuged at 4°C and 1200 rpm for 10 min. Following centrifugation, the supernatant was removed, and the crypt-containing pellet was transferred immediately to -80°C for long-term storage.

2.4.10 Establishment of small intestinal organoid cultures

Small intestinal organoids were isolated according to the protocol for crypt isolation. To ensure both a suitable density for optimal growing conditions and equal numbers of organoids per sample, crypts were counted following isolation. In order to assess crypt numbers, 5 µl of the crypt-containing PBS solution were pipetted onto a cell culture dish. Crypt numbers within this droplet were counted manually using a light microscope (Zeiss, Jena, Germany). The required volume of PBS-crypt solution was calculated using the following formula:

$$x = \frac{w*d*v*5}{n}$$

with n = counted number of crypts, w = desired number of wells, d = desired density of crypts (number/µl Matrigel), v = desired volume of Matrigel per well (in µl)

Thus, for 4 wells with 10 crypts/µl in 100 µl Matrigel the following formula applies: $x = \frac{20.000}{n}$

Consequently, the required volume was transferred to 1.5 ml centrifuge tubes and centrifuged at 4°C and 1200 rpm for 10 min. The supernatant was removed and, depending on the experiment, the pellet was resuspended in 50-100 µl ice-cold Matrigel per well on a pre-warmed 24-well plate. To ensure polymerization and, subsequently, hardening of the Matrigel the plate was incubated at 37°C in a humidified 5 % CO_2 atmosphere for 10-15 min. Depending on the volume of Matrigel used, 300-500 µl IntestiCult Organoid Growth Medium (STEMCELL, Köln, Germany) were added per well. For maintenance, medium was changed every 3-4 days and organoids were passaged approx. every 7 days. Stimulation of organoids for experiments was performed on day 5 after the last passage.

2.4.10.1 Stimulation of small intestinal organoids

Stimulation of small intestinal organoids was performed by transfer of the chemicals tunicamycin or DSS directly into the medium. The respective concentrations and incubation times used for stimulation experiments are indicated within the figures.

2.4.10.2 Quantification of cell death in small intestinal organoid cultures using PI staining

Organoids derived from mice of indicated genotypes were seeded out into 24-well plates. After reaching a stage with multiple crypt-like buds (usually after three to five days), organoids were treated with indicated stimulants for indicated time.

To evaluate epithelial cell death, Intesticult medium was discarded and the Matrigel containing organoids was dissolved in PBS. Next, the gel was collected in 1.5 ml collection tubes, suspended in 1 ml of ice-

cold PBS and centrifugated at 4°C for 5 minutes at 400 x g. Following centrifugation, the supernatant was removed. The gel pellet containing organoids was incubated in TrypLE Express (ThermoFisher Scientific, Steineich, Germany) for 5 min at 37°C to dissociate organoids into single cells, followed by washing steps using ice-cold PBS. 250.000 single cells were incubated in staining solution containing 2 µl PI in 100 µl PBS each and then subjected to flow cytometry analysis using BD FACSCalibur™ (San Jose, United States) and BD CellQuest™ Pro Software. The gating strategy involved plotting PI fluorescence intensity against forward scatter to distinguish PI^{high} vs. PI^{low} populations which are assumed to be dead versus living cells. These gates ensured exclusion of any cellular clumps. Dead (PI^{high}) cells were quantified as fraction of dead cells (= dead cells/total single cells).

To further visualize dead cells in organoids, 1 µl of PI was added to SI organoids in 500 µl Intesticult medium for 4 hours. Afterwards, medium was removed and replaced by PBS. Dead cells were imaged using Zeiss Axio Vert.A1 observer (Jena, Germany) and Zeiss AxioVision LE software. Merged images with a bright-field image overlaid by RFP-filtered fluorescence channel capture showing dead (PI^{high}) cells were generated. Magnification is indicated in the respective figures.

2.4.10.3 Colony Formation Assay

Colony formation assay is an *in vitro* cell survival assay, which is based on a single cell's ability to proliferate into a colony [175]. For colony formation assays, 1-2 wells containing $Ormdl3^{+/+}/Xbp1^{\dashv IEC}$ and $Ormdl3^{+/+}/Xbp1^{\dashv IEC}$ SI organoids were used to obtain the desired number of cells. In a first step, the medium was aspirated and 500 µl TrypLE Express plus the anoikis-preventing agent Y-27632 (concentration 1:1000) were added to each well. Next, the cell suspension was collected in 15 ml collection tubes and incubated for 10 min at 37°C in a water bath followed by a centrifugation step for 3 min at 400 xG. Following centrifugation, the supernatant was discarded and the pellet containing single cells was resuspended in 1 ml advanced DMEM/F12 medium. The number of single cells was specified using an automated cell counter. After counting the number of cells per ml, the appropriate volume containing 5.000 cells/well was transferred to 1.5 ml tubes and spun down for 3 min at 400 xG. Following this centrifugation step, the supernatant was aspirated, and the pellet resuspended in a 50 µl PBS-Matrigel mixture. Single cells were seeded out as 5 wells per genotype with 5.000 cells/well and 100 µl of Intesticult medium. Medium was changed every second day and colonies were counted on day 5 and day 10 of the assay. Furthermore, the size of colonies was determined on day 10 of the experiment and images were taken using a Zeiss Axio Vert.A1 observer (Zeiss, Jena, Germany) and Zeiss AxioVision LE software.

2.4.10.4 Isolation of intestinal epithelial cells and cells from lamina propria

IECs and cells from the lamina propria were isolated from small intestine and colon tissues using the Lamina Propria Dissociation Kit (Miltenyi Biotec, Bergisch Gladbach, Germany). 12- to 20-weeks-old

mice were sacrificed and the intestine removed, flushed with PBS, and cut longitudinally into pieces of approximately 0.5 cm length. Isolation and purification of intraepithelial lymphocytes and lamina propria cells was performed according to manufacturer's protocol.

2.5 RNA sequencing and analysis

Total RNA was extracted from SI organoids seeded from *Ormdl3*$^{+/+}$, *Ormdl3*$^{+/+}$/*Xbp1*$^{-IIEC}$ and *Ormdl3*$^{-/-}$/*Xbp1*$^{-IIEC}$ mice using the RNeasy mini kit from Qiagen standard protocol. Paired-end sequencing libraries were constructed for three replicates of each genotype from the total RNA isolated using TruSeq Stranded mRNA kit (Illumina Inc.). Sequencing was performed on the Illumina HiSeq3000 (2 x 75 bp) using standard protocols. Adapters and low-quality bases from the RNA-seq reads were removed using Trim Galore (version 0.4.4) [176], a wrapper tool for Cutadapt [177] and FastQC [178]. The filtered reads were mapped to the mouse genome (GRCm38) using STAR aligner (version 2.5.2b) [179]. Estimation of expression counts of mouse genes was performed by featureCounts (version 1.5.2) [180]. Differential expressed genes were identified using the Bioconductor package DESeq2 (version 1.20.0) [181]. This statistical tool is based on a negative binomial distribution model with dispersion trend smoothing. Genes with FDR adjusted p-value of 0.1 were considered to be differentially expressed. Moreover, the normalized reads counts per sample were determined by estimating size factors to control for library size, followed by a log2 transformation of the raw count data using DESeq2. The normalized counts for the top 50 differential expressed genes were used to draw a heatmap based on using R package stats (version 3.6.3 [182]) and Venn diagrams were drawn to highlight genes of interest using VennDiagram package in R (version 1.6.20) [183].

2.6 Statistical analysis

Statistical analysis was performed using the GraphPad Prism 5 software package (GraphPad Software Inc., La Jolla, USA). Student's unpaired *t* test was performed unless otherwise stated. Data are shown as mean, standard error of the mean (SEM or s.e.m) or standard deviation (SD or s.d.). A p-value of $p \leq 0.05$ was considered as statistically significant (*). P-values of $p \leq 0.01$ (**) were considered as strongly significant, $p \leq 0.001$ (***) and **** $p < 0.0001$ as highly significant.

3 Results

3.1 ORMDL3 is associated with ER stress and the UPR in the murine intestinal epithelium.

Cantero-Recasens *et al.* [130] were the first to provide a link between ORMDL3, ER stress and the UPR, respectively. The authors showed that overexpression of ORMDL3 in human HEK293 cells not only led to a SERCA-dependent reduction in Ca^{2+} release from the ER but also affected phosphorylation of eIF2α, a downstream target of the PERK pathway of the UPR. Studies from our group confirmed these findings in different human cell lines and provided evidence for a modulating role of ORMDL3 in all three UPR pathways. However, *in vivo* experiments, which were performed on small intestinal or colonic tissue of mice showed no significant differences between *Ormdl3*$^{+/+}$ and *Ormdl3*$^{-/-}$. We hypothesize that this discrepancy between human and murine cells arises from the heterogenous nature of our murine samples. The tissues used for *in vivo* experiments in this study thus included both intestinal epithelium and lamina propria separated from one another.

To investigate the impact of ORMDL3 on ER stress and the UPR specifically in the murine intestinal epithelium we used small intestinal organoids. In this 3D culture system, isolated small intestinal crypts containing stem cells form "mini guts" termed organoids. These organoids exhibit a histological hierarchy, which resembles the *in vivo* state of the small intestinal epithelium.

We used small intestinal organoids of *Ormdl3*$^{+/+}$ and *Ormdl3*$^{-/-}$ mice for subsequent qPCR analysis of *Ormdl1*, *Ormdl2* and *Ormdl3* mRNA expression on the one hand, and different ER stress target genes on the other hand. To examine possible differences between short- and long-term ER stress, organoids were treated with different durations and concentrations of tunicamycin (TM), a potent inducer of ER stress *in vitro*, which blocks the formation of protein N-glycosidic linkages. Acute, short-term ER stress led to a significant increase in *Ormdl1* expression in *Ormdl3* deficient organoids and a strong, though not significant increase in *Ormdl2* (Fig. 3.1A). In chronic ER stress conditions, however, this compensatory upregulation could not be observed (Fig. 3.1C). Strikingly, deficiency in *Ormdl3* also caused significant upregulation of four (*Hsp90b1*, *ATF4*, *ATF6*, *Dnajc3*) out of seven ER stress related genes upon acute ER stress (Fig. 3.1B). Upregulation of *ATF4* and *ATF6* thereby point towards a role of ORMDL3 in the PERK and ATF6 pathways of the UPR. Expression of *Xbp1*, which is a downstream target of IRE1, was not affected by *Ormdl3* deficiency upon acute ER stress induction. Under chronic ER stress conditions, however, mRNA expression of all seven UPR-related genes remained unaltered between *Ormdl3*$^{+/+}$ and *Ormdl3*$^{-/-}$ (Fig. 3.1D). It should also be noted that all differences mentioned above only occur under ER stress conditions. Under homeostasis, no differences in gene expression neither in the three *Ormdl* genes nor in UPR-related genes could be observed. This finding is consistent with and supported by unpublished results from our group, which show that under basal conditions *Ormdl3* deficiency does not cause activation of the UPR in the murine small intestine [162].

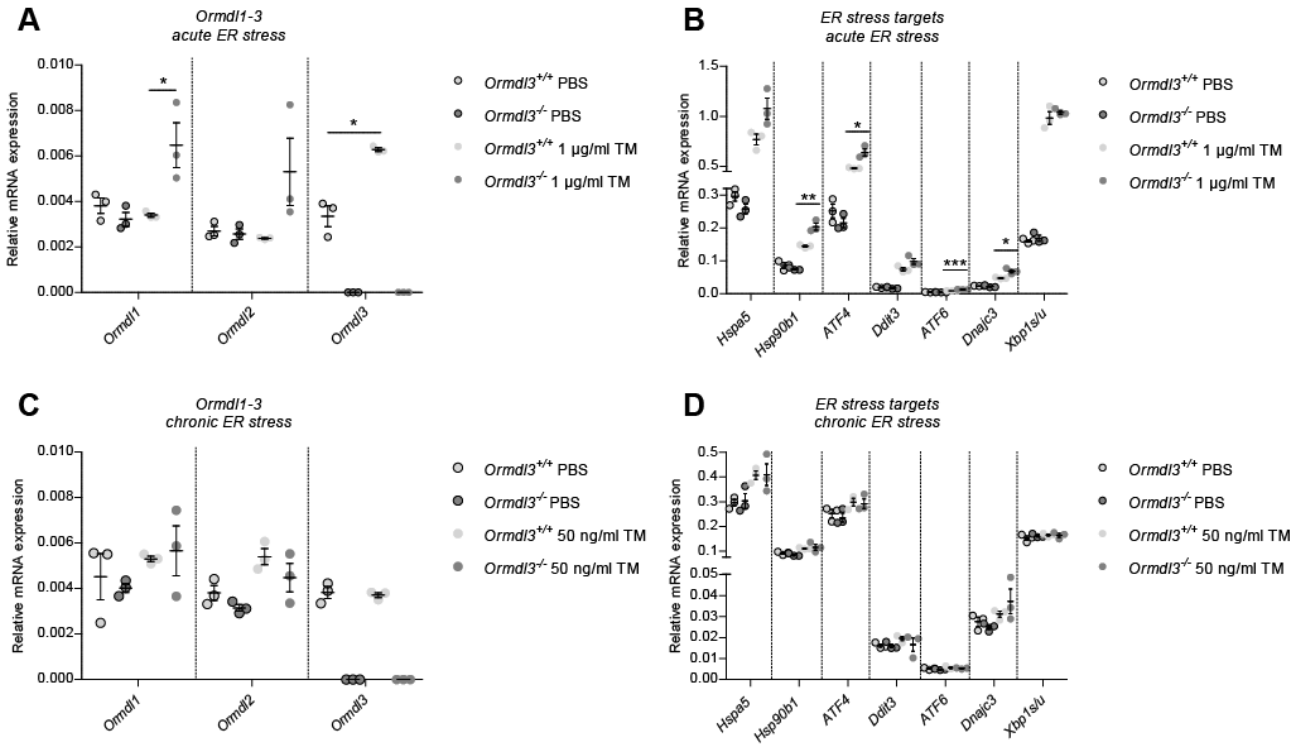

Figure 3.1: Induction of acute ER stress in *Ormdl3* deficient organoids leads to both compensatory upregulation of *Ormdl* genes and upregulation of UPR-related genes, while chronic ER stress does not alter gene expression. **(A)** Small intestinal organoids from *Ormdl3*$^{+/+}$ and *Ormdl3*$^{-/-}$ mice (n = 3 technical replicates per group) were analyzed for mRNA expression of *Ormdl1*, *Ormdl2* and *Ormdl3* both under homeostasis (PBS) or under acute ER stress conditions (TM). Organoids were treated with 1 µg/ml Tunicamycin for 6 h, respectively. Data are normalized to *β-actin*, mean ± s.e.m. **(B)** Small intestinal organoids from *Ormdl3*$^{+/+}$ and *Ormdl3*$^{-/-}$ mice (n = 3 technical replicates per group) were analyzed for mRNA expression of the ER stress markers Heat Shock Protein Family A Member 5 *(Hspa5*), Heat Shock Protein 90kDa Beta member 1 (*Hsp90b1*), Activating Transcription Factor 4 (*ATF4*), DNA Damage Inducible Transcript 3 (*Ddit3*), Activating Transcription Factor 6 (*ATF6*), DnaJ Heat Shock Protein Family (Hsp40) Member C3 (*Dnajc3*) and X box-binding protein 1 (*Xbp1*) under homeostasis (PBS) or under acute ER stress conditions (TM). Organoids were treated with 1 µg/ml Tunicamycin for 6 h, respectively. Data are normalized to *β-actin*, mean ± s.e.m. **(C)** Small intestinal organoids from *Ormdl3*$^{+/+}$ and *Ormdl3*$^{-/-}$ mice (n = 3 technical replicates per group) were analyzed for mRNA expression of *Ormdl1*, *Ormdl2* and *Ormdl3* both under homeostasis (PBS) or under chronic ER stress conditions (TM). Organoids were treated with 50 ng/ml Tunicamycin for 24 h, respectively. Data are normalized to *β-actin*, mean ± s.e.m. **(D)** Small intestinal organoids from *Ormdl3*$^{+/+}$ and *Ormdl3*$^{-/-}$ mice (n = 3 technical replicates per group) were analyzed for mRNA expression of the ER stress markers *Hspa5*, *Hsp90b1*, *ATF4*, *Ddit3*, *ATF6*, *Dnajc3* and *Xbp1* under homeostasis (PBS) or under chronic ER stress conditions (TM). Organoids were treated with 50 ng/ml tunicamycin for 24 h, respectively. Data are normalized to *β-actin*, mean ± s.e.m. Statistical analysis: Two-tailed Students *t* test with * $p < 0.05$, ** $p < 0.01$, *** $p < 0.001$. Xbp1s/u = Xbp1 spliced/unspliced.

3.2 DSS stimulation of *Ormdl3* deficient organoids causes activation of the UPR.

We next sought to investigate the effect of the chemical DSS on the *Ormdl3* deficient intestinal epithelium *in vitro*. DSS is commonly used to induce colitis in mice. Even though DSS colitis is a widely established model, the mechanism by which this chemical induces intestinal inflammation is still unclear. It is assumed that DSS damages the epithelial monolayer, thus allowing the dissemination of proinflammatory intestinal contents (e.g. bacteria) into underlying tissue. Since the organoid model is an established model to study the intestine *in vitro*, we wondered if it would be possible to induce a colitis-like response in small intestinal organoids. To mimic both acute and chronic colitis conditions, we varied duration and concentration of DSS treatment in *in vitro* experiments. Following DSS stimulation, organoids of *Ormdl3*$^{+/+}$ and *Ormdl3*$^{-/-}$ mice were used for subsequent qPCR analysis of *Ormdl1*, *Ormdl2* and *Ormdl3* mRNA expression on the one hand, and different ER stress target genes on the other hand. All target genes were chosen because of their association with ER stress, which is a known feature of DSS colitis *in vivo* [119].

When analysing the results of this experiment, we found that both acute and chronic DSS stimulation (5 % for 3 h or 2 % DSS for 24 h) of small intestinal organoids caused a strong upregulation of the *Ormdl* mRNAs in comparison to homeostasis (PBS; Fig. 3.2A, C). Interestingly, upon chronic DSS treatment *Ormdl1* and *Ormdl2* are significantly downregulated in *Ormdl3* deficiency under control conditions (PBS), which is an observation contrasting with the results of tunicamycin treatment (see Fig. 3.1 for comparison).

Moreover, we found that DSS stimulation of both *Ormdl3*$^{+/+}$ and *Ormdl3*$^{-/-}$ led to upregulation of all ER stress related genes but one when compared with unstimulated organoids. Of note, the one gene being downregulated upon acute and chronic DSS treatment in *Ormdl3*$^{+/+}$ and *Ormdl3*$^{-/-}$ organoids was *Xbp1*, the downstream target of IRE1 (Fig. 3.2B, D). When comparing *Ormdl3*$^{+/+}$ and *Ormdl3*$^{-/-}$ organoids we identified *Xbp1* mRNA expression to be dependent on the type of DSS treatment: While under acute DSS treatment *Xbp1* is upregulated in *Ormdl3* deficient organoids in comparison to *Ormdl3* wild type organoids, we find the same mRNA to be downregulated in *Ormdl3* deficient organoids under chronic DSS conditions (Fig. 3.2B, D). This finding was of special interest to us because it suggested a dependency of XBP1 on two factors: first, the duration and intensity of DSS stimulation, or colitis, and second, the presence/absence of *Ormdl3* in the intestinal epithelium.

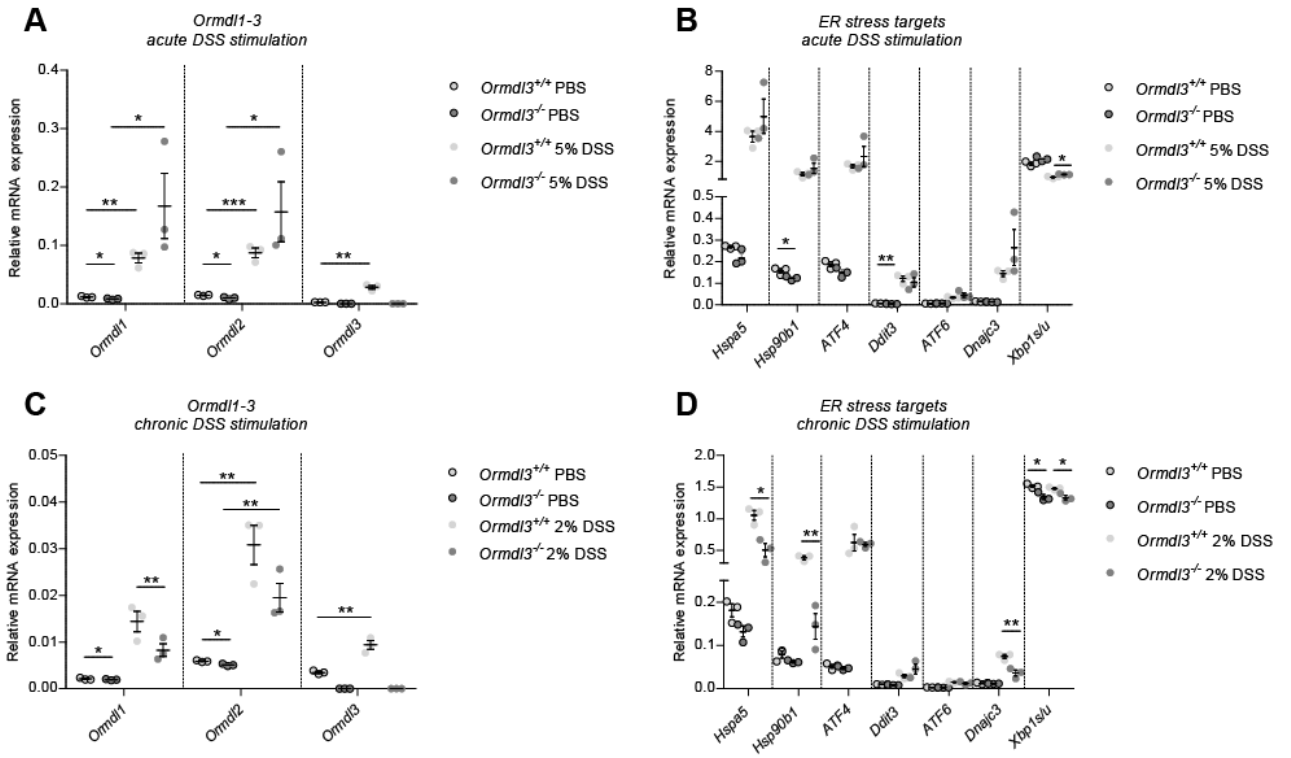

Figure 3.2: DSS stimulation of small intestinal organoids deficient for *Ormdl3* results in activation of the UPR.
(A) Small intestinal organoids from *Ormdl3*$^{+/+}$ and *Ormdl3*$^{-/-}$ mice (n = 3 technical replicates per group) were analyzed for mRNA expression of *Ormdl1*, *Ormdl2* and *Ormdl3* both under homeostasis (PBS) or under acute ER stress conditions (DSS). Organoids were treated with 5 % DSS for 3 h, respectively. Data are normalized to *β-actin*, mean ± s.e.m. **(B)** Small intestinal organoids from *Ormdl3*$^{+/+}$ and *Ormdl3*$^{-/-}$ mice (n = 3 technical replicates per group) were analyzed for mRNA expression of the ER stress markers Heat Shock Protein Family A Member 5 (*Hspa5*), Heat shock protein 90 kDa beta member 1 (*Hsp90b1*), Activating Transcription Factor 4 (*ATF4*), DNA Damage Inducible Transcript 3 (*Ddit3*), Activating Transcription Factor 6 (*ATF6*), Heat Shock Protein Family (Hsp40) Member C3 (*Dnajc3*) and X box-binding protein 1 (*Xbp1*) under homeostasis (PBS) or under acute ER stress conditions (DSS). Organoids were treated with 5 % DSS for 3 h, respectively. Data are normalized to *β-actin*, mean ± s.e.m. **(C)** Small intestinal organoids from *Ormdl3*$^{+/+}$ and *Ormdl3*$^{-/-}$ mice (n = 3 technical replicates per group) were analyzed for mRNA expression of *Ormdl1*, *Ormdl2* and *Ormdl3* both under homeostasis (PBS) or under chronic ER stress conditions (DSS). Organoids were treated with 2 % DSS for 24 h, respectively. Data are normalized to *β-actin*, mean ± s.e.m. **(D)** Small intestinal organoids from *Ormdl3*$^{+/+}$ and *Ormdl3*$^{-/-}$ mice (n = 3 technical replicates per group) were analyzed for mRNA expression of the ER stress markers *Hspa5*, *Hsp90b1*, *ATF4*, *Ddit3*, *ATF6*, *Dnajc3* and *Xbp1* under homeostasis (PBS) or under chronic ER stress conditions (DSS). Organoids were treated with 2 % DSS for 24 h, respectively. Data are normalized to *β-actin*, mean ± s.e.m. Statistical analysis: Two-tailed Students *t* test with * $p < 0.05$, ** $p < 0.01$, *** $p < 0.001$. Xbp1s/u = Xbp1 spliced/unspliced.

3.3 ORMDL3 inhibits the IRE1 pathway of the UPR in murine IECs *in vitro.*

It is common knowledge that ORMDL3 can modify the UPR [130, 138]. Of interest, most studies on this subject provide a link between ORMDL3 and either the PERK or the ATF6 pathway of the UPR. Previous studies from our group, however, suggest that ORMDL3 not only interacts with the two pathways mentioned but can also inhibit the IRE/Xbp1 pathway of the UPR [153]. The possible link between ORMDL3 and XBP1 is of special interest for IBD research since not only ORMDL3 but also XBP1 is a known risk gene for human IBD. Furthermore, deficiency for *Xbp1* specifically in intestinal epithelial cells of mice was shown to induce spontaneous enteritis *in vivo*, suggesting an important role for XBP1 also in murine intestinal inflammation [46].

Previous experiments performed in human HEK-293 cells could show that overexpression of either ORMDL1 or ORMDL3 results in reduced *XBP1* splicing and reduced promoter activity of UPRE, a downstream target of *Xbp1*, while knockdown of ORMDL123 leads to an increase in both *XBP1* splicing and UPRE promoter activity upon ER stress induction [153]. In these experiments, ER stress was induced by stimulation of cells with either tunicamycin or thapsigargin. While tunicamycin inhibits N-glycosylation of proteins, thapsigargin inhibits SERCA. Since these first experiments were performed in HEK-293 cells, and cells were transfected with siRNA directed against all three ORMDL homologues, we decided to confirm these results in murine IECs and with siRNA directed specifically against ORMDL3. Thus, we set out to investigate the siRNA-mediated knockdown of ORMDL3 in the murine IEC line ModeK.

Indeed, we could show that also in IECs siRNA-mediated knockdown of ORMDL3 in ModeK iCtrl cells induces UPRE promoter activity both under control and ER stress conditions (Fig. 3.3B). Since we had already detected a downregulation of *Xbp1* mRNA in *Ormdl3* deficient organoids (see Fig. 3.1B, D for comparison) we were wondering about the gene expression of *Ormdl3* in *Xbp1* deficiency. Of interest, we could see a reduced mRNA expression of *Ormdl3* in both *Xbp1* deficient ModeK cells and small intestinal organoids under control and ER stress conditions (see Fig. 3.3A, C). ModeK iXbp1 cells also exhibited reduced mRNA levels of the other two ORMDL homologues, *Ormdl1* and *Ormdl2*, respectively.

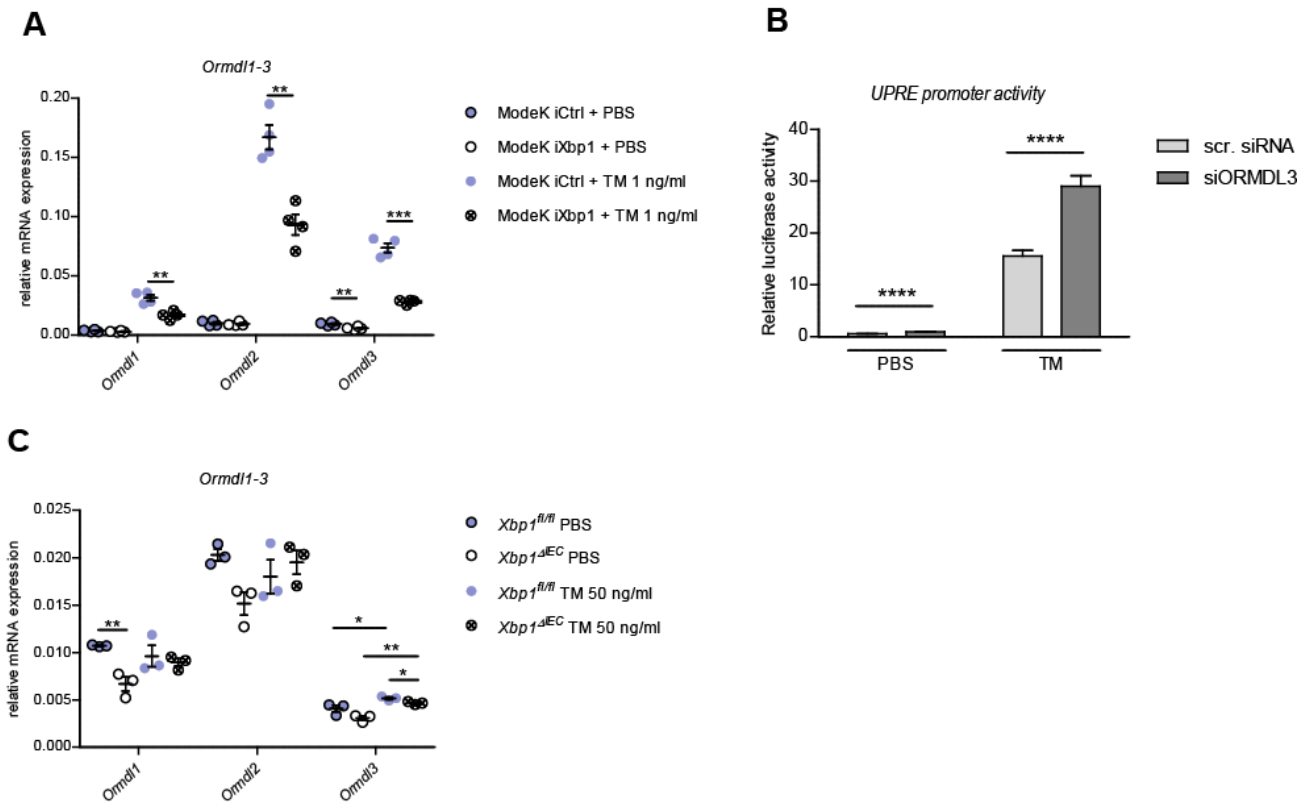

Figure 3.3: ORMDL proteins, and especially ORMDL3, inhibit IRE1 signaling.
(A) mRNA expression of *Ormdl1-3* in ModeK iCtrl and ModeK iXbp1 cells was assessed under homeostasis (untreated) and ER stress conditions (TM 1 ng/ml). Cells were treated with tunicamycin for 24 h prior to experiment. **(B)** UPRE promoter-mediated luciferase assay of murine ModeK iCtrl cells. Cells were transfected with negative control siRNA (scr. siRNA) or ORMDL3-specific siRNA (siORMDL3). After 24 hours, cells were stimulated with tunicamycin (1 μg/ml) or PBS as control for another 24 h (n = 3 independent experiments). Error bars represent mean ± SEM. **(C)** mRNA expression of *Ormdl1-3* in *Xbp1*$^{fl/fl}$ and *Xbp1*$^{\Delta IEC}$ small intestinal organoids was assessed under homeostasis (untreated) and ER stress conditions (TM 50 ng/ml). Cells were treated with tunicamycin for 24 h prior to experiment. Error bars represent mean ± s.e.m. Statistical analysis: Two-tailed Students *t* test with * $p < 0.05$, ** $p < 0.01$, *** $p < 0.001$, **** $p < 0.0001$.

3.4 *Ormdl3/Xbp1* double deficient ModeK cells are less susceptible to ER stress induction than ModeK cells deficient only for *Xbp1*.

After having established a reliable, reproducible *in vitro* model to study *Ormdl3/Xbp1* deficiency, we next aimed at characterizing the extent of ER stress in these IECs. Consequently, we transfected the murine ModeK iXbp1 cell line with siRNA directed specifically against ORMDL3 to create a double deficient cell line. We then compared these cells to ModeK iXbp1 cells transfected only with scrambled siRNA, which represent the *Xbp1* deficient genotype. When investigating the mRNA expression of *Ormdl1-3* and the ER stress related genes *Hspa5*, *ATF4*, *Ddit3*, *ATF6* and *Xbp1u/s* in cells of both genotypes, we could confirm genotype on gene expression level (Fig. 3.4A) but found no other significant differences under homeostatic conditions (Fig. 3.4A, B). Interestingly, mRNA expression levels of the same target genes changed under ER stress conditions when cells were stimulated with tunicamycin (Fig. 3.4C, D). We again could proof the efficiency of siRNA-mediated ORMDL3 knockdown on mRNA expression level. Additionally, we found a significant decrease in *Hspa5* gene expression, an ER chaperone, which is released from the three ER stress sensors (IRE1, ATF6 and PERK) upon accumulation of unfolded or misfolded proteins in the ER, in *Ormdl3/Xbp1* double deficient cells compared to *Xbp1* single deficient control cells (Fig. 3.4D). This finding is of special interest because it suggests that *Ormdl3/Xbp1* double deficient cells exhibit less ER stress on a transcriptional level. To also gain an insight into the translational level we next performed Western blotting of ModeK iXbp1 cells treated either with scrambled siRNA as a control (*Xbp1* single deficiency) or siRNA directed against ORMDL3 (*Ormdl3/Xbp1* double deficiency). To confirm the genotypes, we first detected ORMDL123 protein levels, which we found to be downregulated in ORMDL3 siRNA treated ModeK cells in comparison to control cells (Fig. 3.4E). Furthermore, we studied HSPA5 and HSP90B1 protein levels in cells treated with siRNA under homeostatic (PBS) and ER stress (TM) conditions (Fig. 3.4F). Similar to gene expression, we again found no difference between double (siORM3) and single deficient (scr.) cells under homeostatic conditions. However, we again observed a decrease in HSPA5 and HSP90B1 protein levels upon ER stress induction, suggesting less ER stress in *Ormdl3/Xbp1* double deficiency both on the transcriptional and translational level.

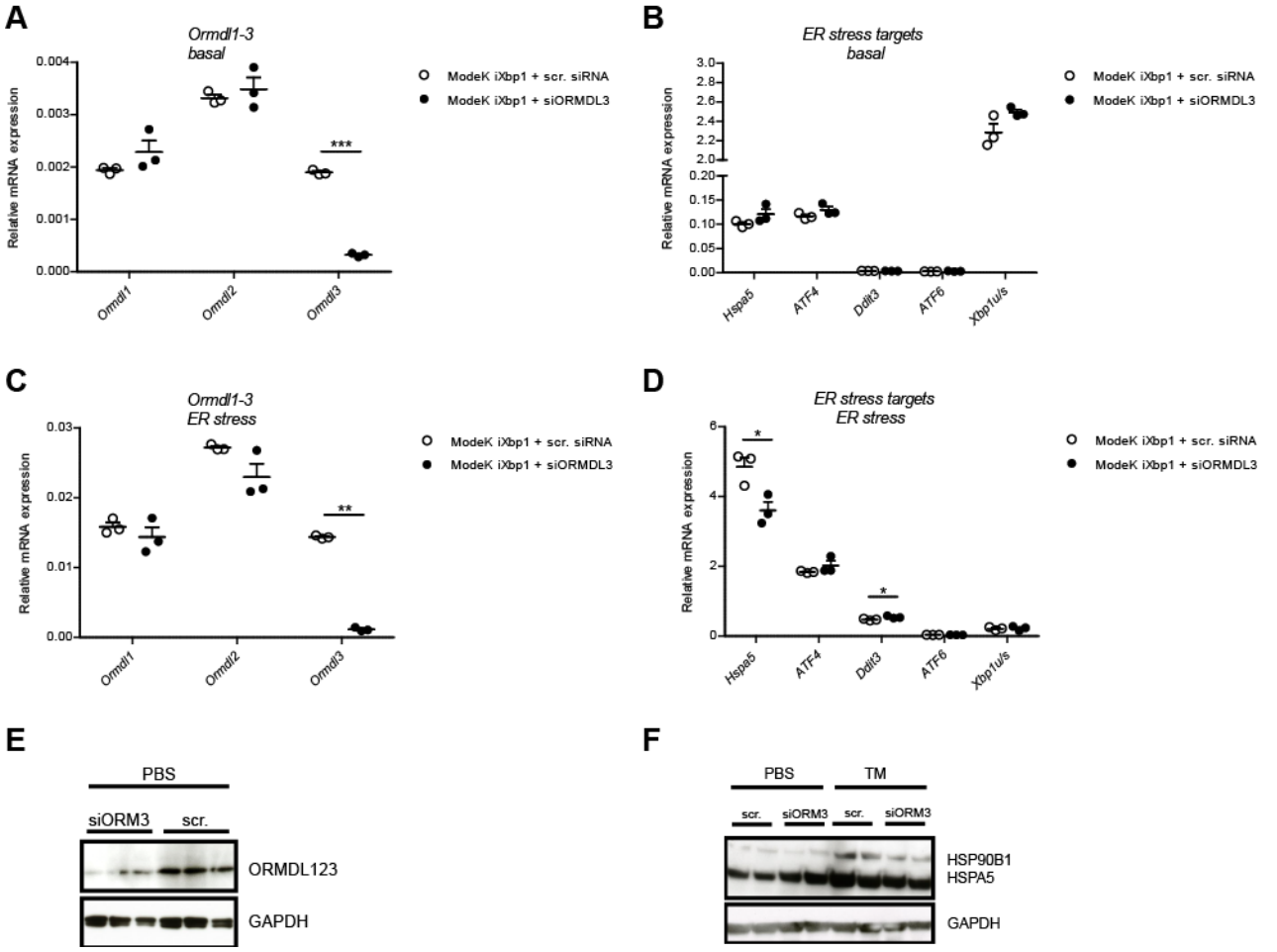

Figure 3.4: *Ormdl3/Xbp1* double deficient ModeK cells are less susceptible to ER stress induction.
(A-D) mRNA expression in murine ModeK iXbp1 cells was assessed under homeostasis (**A+B**) and ER stress conditions (**C+D**). **(A)** RT-PCR for mRNA expression of *Ormdl1-3* in murine ModeK iXbp1 cells. Cells were transfected with negative control siRNA (scr. siRNA) or ORMDL3-specific siRNA (siORMDL3). After 24 hours, cells were stimulated with PBS as control for another 24h (n = 3 technical replicates). **(B)** RT-PCR for mRNA expression of ER stress targets in murine ModeK iXbp1 cells. Cells were transfected with negative control siRNA (scr. siRNA) or ORMDL3-specific siRNA (siORMDL3). After 24 hours, cells were stimulated with PBS as control for another 24h (n = 3 technical replicates). **(C)** *Ormdl1-3* mRNA expression in murine ModeK iXbp1 cells was assessed under ER stress conditions (TM). Cells were transfected with negative control siRNA (scr. siRNA) or ORMDL3-specific siRNA (siORMDL3). After 24 hours, cells were treated with tunicamycin (2 μg/ml) to induce ER stress prior to experiment (n = 3 technical replicates). **(D)** mRNA expression of ER stress targets in murine ModeK iXbp1 cells was assessed under ER stress conditions (TM). Cells were transfected with negative control siRNA (scr. siRNA) or ORMDL3-specific siRNA (siORMDL3). After 24 hours, cells were treated with tunicamycin (2 μg/ml) to induce ER stress prior to experiment (n = 3 technical replicates). Error bars represent mean ± s.e.m. Statistical analysis: Two-tailed Students *t* test with * $p < 0.05$, ** $p < 0.01$, *** $p < 0.001$. **(E)** Immunoblot from ModeK iXbp1 cells transfected with negative control siRNA (scr.) or ORMDL3-specific siRNA (siORM3) 24 h prior to experiment. **(F)** Immunoblot from ModeK cells iXbp1 transfected with negative control siRNA (scr.) or ORMDL3-specific siRNA (siORM3). Cells were treated with PBS as control or tunicamycin (2 μg/ml) to induce ER stress 24 h prior to experiment.

3.5 Characterization of *Ormdl3KO Xbp1VilCre* mice

The *in vitro* studies shown above demonstrate a crosstalk between ORMDL3 and XBP1, which does not only occur in the murine intestinal epithelium but also in human kidney cells. However, the validity of these *in vitro* results is limited due to their simplification of immortalized cell lines in an artificial environment. Therefore, we were especially interested in the crosstalk between ORMDL3 and XBP1 in a mouse model. Since ORMDL3 is associated with a variety of diseases including IBD, we were interested in the effect of its whole-body deletion on the intestinal epithelium. The *Xbp1* deficient ($Xbp1^{-\Delta IEC}$) mouse is a well-established model to study intestinal inflammation *in vivo*. Consequently, we generated *Ormdl3*/*Xbp1* double deficient ($Ormdl3^{-/-}/Xbp1^{-\Delta IEC}$) mice. These mice are characterized by a whole-body knockout of *Ormdl3* and an IEC-specific deletion of *Xbp1*.

Subsequently, mice were characterized under homeostasis as well as under challenging conditions as provided by DSS-induced colitis.

3.5.1 $Ormdl3^{-/-}/Xbp1^{\Delta IEC}$ mice show the expected genetic distribution and follow Mendel's laws.

Ormdl3 and *Xbp1* deficiency was identified by genotyping (see Material and Methods, chapter 2.4.7). Furthermore, the correct genotype of all samples used for subsequent analysis (e.g. isolated IECs or crypts) was again validated by mRNA expression analysis. In the investigated tissues of $Ormdl3^{-/-}/Xbp1^{-\Delta IEC}$ mice no *Ormdl3* transcripts were observed, thus confirming the deletion of *Ormdl3* in the whole organism. To exclude any genetic abnormalities that might have an effect on further experiments, we examined the genetic distribution of offspring. Since breeding was set up between *Ormdl3* heterozygous males and females ($Ormdl3^{+/-}/Xbp1^{-\Delta IEC}$ x $Ormdl3^{+/-}/Xbp1^{-\Delta IEC}$), we expected 50 % of the litter to be heterozygous for *Ormdl3*, and 25 % of the litter to show homozygosity for either the *Ormdl3* wild type or knockout allele, respectively. Indeed, the 116 $Ormdl3KO/Xbp1^{-\Delta IEC}$ mice counted were born in the expected ratios, suggesting that reproduction in this mouse strain follows Mendel's laws (Table 13).

Table 13: Mendelian distribution of *Ormdl3KO Xbp1VilCre* mice.

$Ormdl3^{+/+}/Xbp1^{-\Delta IEC}$	$Ormdl3^{+/-}/Xbp1^{-\Delta IEC}$	$Ormdl3^{-/-}/Xbp1^{-\Delta IEC}$	
32	52	32	observed animal numbers
27	46	27	observed percentage [%]
25	50	25	expected percentage [%]

Genotypes within breeding pairs: $Ormdl3^{+/-}/Xbp1^{\Delta IEC}$ x $Ormdl3^{+/-}/Xbp1^{\Delta IEC}$
$\chi^2 = 0.3896$, p-value = .823015, significance level: $p < 0.05$

3.5.2 Basal phenotype of *Ormdl3*$^{-/-}$*/Xbp1*$^{\Delta IEC}$ mice

Basal phenotyping of mice included assessment of the small intestinal and colonic length, the overall body weight as well as organ weights of spleen, kidney, liver and caecum.

3.5.2.1 The basal phenotype of *Ormdl3*$^{-/-}$*/Xbp1*$^{\Delta IEC}$ mice is not sex-dependent.

It is common sense that some mouse models show sex-dependent phenotypes causing either amelioration or deterioration of the phenotype [184-186]. To exclude any sex-dependent outcome on further experiments we performed basal phenotyping of both 12- to 20-week-old female and male *Ormdl3*$^{-/-}$*/Xbp1*$^{-\Delta IEC}$ mice (Fig. 3.5). Phenotyping included assessment of the parameters body weight, weight of liver, kidney, spleen and caecum. Furthermore, the small intestinal and colonic length were measured. For *Ormdl3*$^{-/-}$ mice sex-dependent IGF1 (insulin growth factor 1) serum levels have been reported, which correlate with a decrease in body size [153]. Neither male nor female *Ormdl3*$^{-/-}$*/Xbp1*$^{-\Delta IEC}$ mice showed a difference in body weight (Fig. 3.5A) or in body size (data not shown). In addition, all organ weights and the colonic length did not significantly differ between the two genotypes in male and female animals (Fig. 3.5B, C). However, both genders showed a genotype-dependent decrease of small intestinal length upon *Ormdl3*/*Xbp1* double deficiency (Fig. 3.5C).

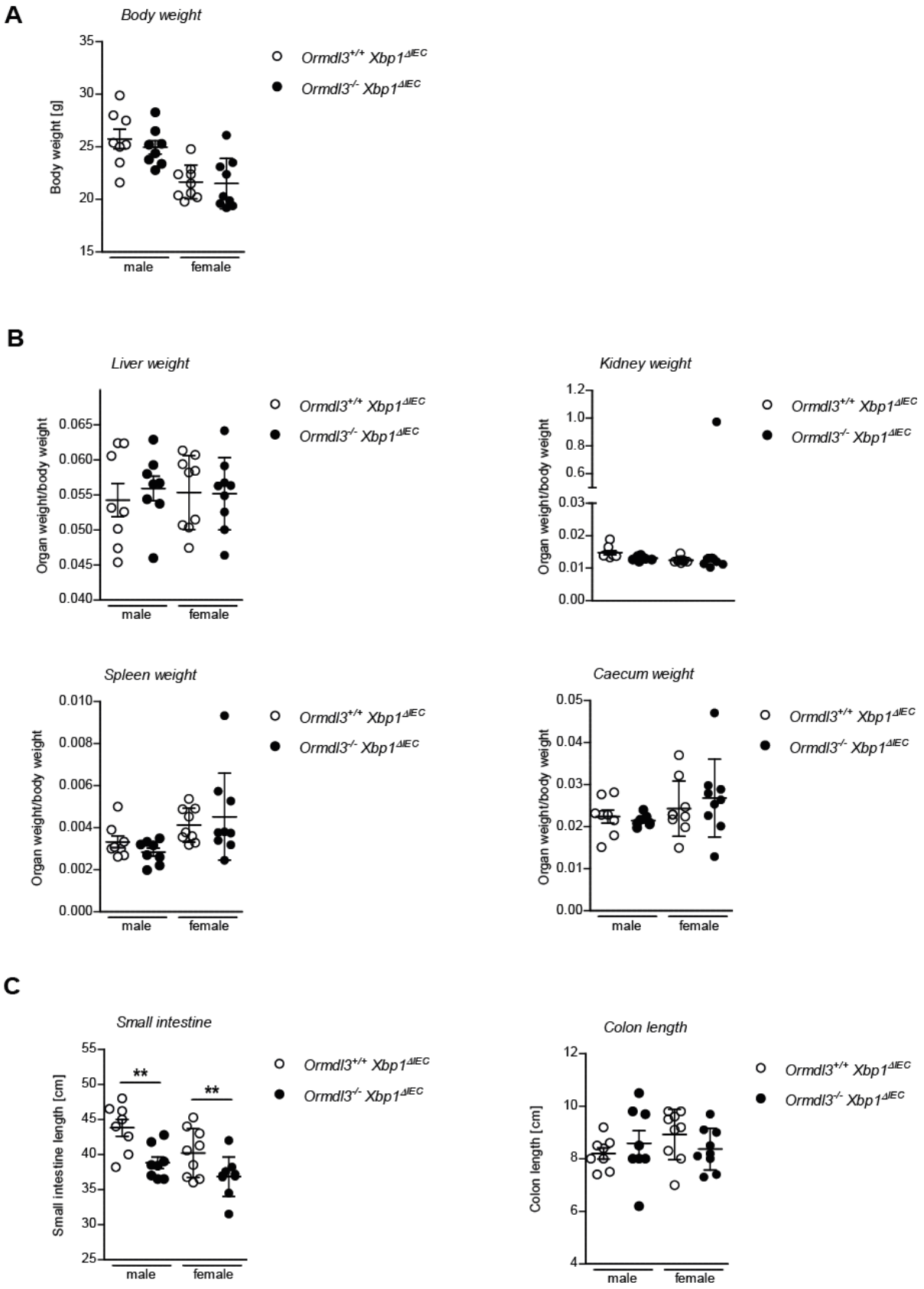

Figure 3.5: Male and female *Ormdl3*$^{-/-}$*/Xbp1*$^{\Delta IEC}$ mice exhibit shortening of small intestine under homeostasis. Female (n = 11 per genotype) and male (n = 9 per genotype) litter pairs were sacrificed between 12-20 weeks of age. **(A)** Body weight in gram. **(B)** Liver, kidney, spleen and caecum weight are displayed as organ weight/total body weight [g/g]. **(C)** Small intestinal and colonic length in cm. Statistical analysis: Two-tailed Students *t* test with ** $p < 0.01$.

3.5.2.2 *Ormdl3*$^{-/-}$*/Xbp1*$^{\Delta IEC}$ mice display significantly more goblet cells in the SI.

After having assessed body and organ weights as well as the intestinal length, we next aimed at characterizing IEC populations. While ISCs and Paneth cells constitute the stem cell niche at the crypt bottom of small intestinal crypts, goblet cells located in the villi secrete high-molecular-weight glycoproteins termed mucins, which represent the main structural component of the mucus layer. For quantification of IEC populations we focussed on the small intestine of *Ormdl3*$^{-/-}$*/Xbp1*$^{\Delta IEC}$ animals due to both its decrease in length and its overall significance for the murine *Xbp1*$^{-\Delta IEC}$ phenotype as described in [46]. Furthermore, unpublished data from our group shows that *Ormdl3* deficiency causes a decrease in Paneth cells in the small intestine. Additionally, Kaser and colleagues [46] showed that IEC-specific deletion of *Xbp1* results in both complete absence of Paneth cells and a reduction in goblet cell numbers and size within the small intestinal epithelium. Consequently, we hypothesized that in case of a double deficiency Paneth cell numbers would be reduced and *lysozyme* expression would be altered.

Of note, mRNA expression levels of all IEC population markers in isolated IECs showed no significant difference between the two genotypes, thus suggesting a role for *Ormdl3* deficiency on translational rather than transcriptional level (Fig. 3.6A). In line with this finding, we observed unchanged cell numbers of the two IEC populations located in small intestinal crypts, Paneth cells and ISCs (Fig. 3.6B-G). Interestingly, goblet cell numbers in small intestinal villi significantly increased upon *Ormdl3/Xbp1* double deficiency (Fig. 3.6H, I) suggesting increased defense against intestinal pathogens. However, this change in goblet cell numbers was, as mentioned above, not reflected by increased mRNA expression of *Muc2*, a marker gene of this specific cell type (Fig. 3.6A).

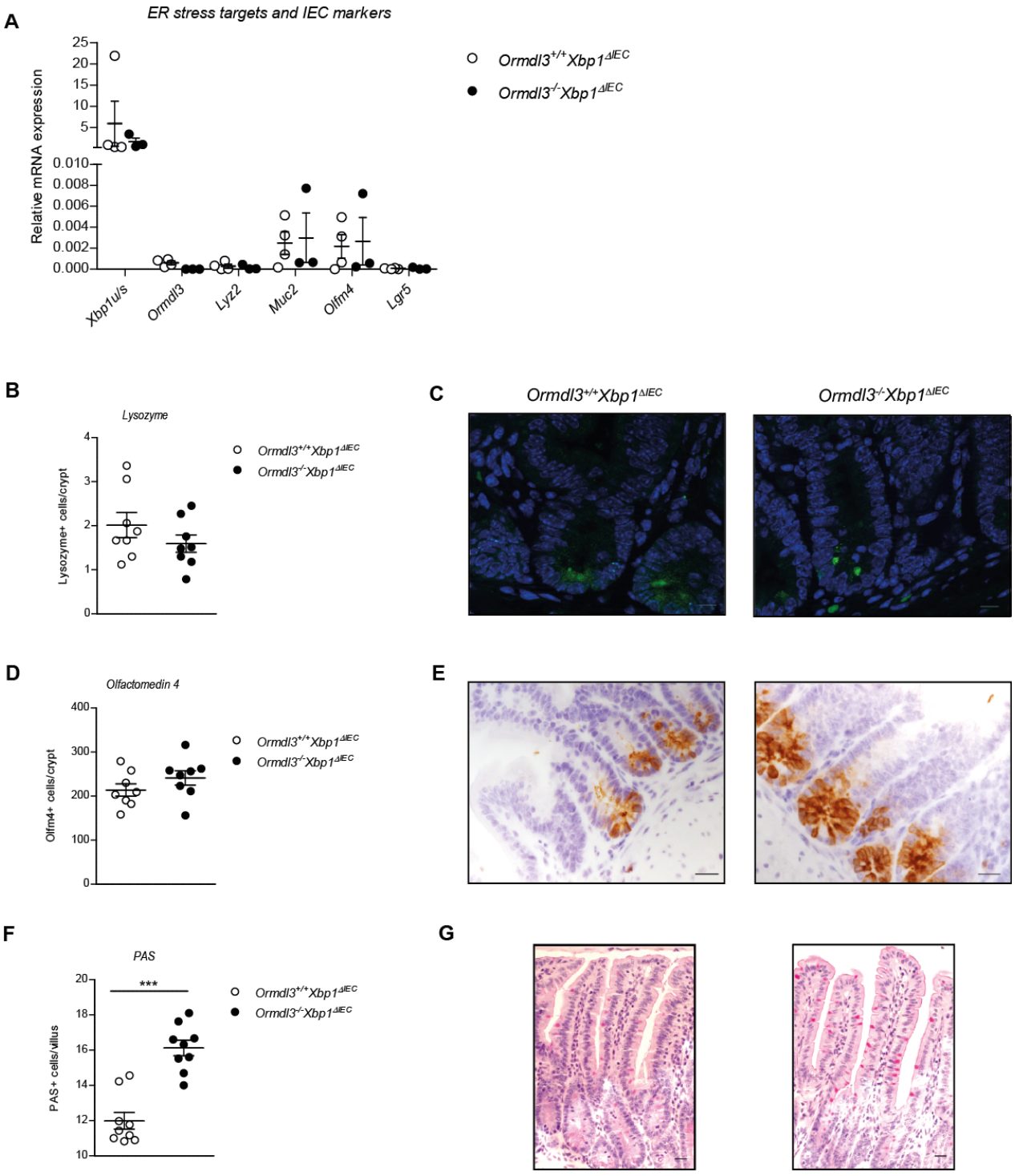

Figure 3.6: *Ormdl3*$^{-/-}$*/Xbp1*$^{\Delta IEC}$ mice exhibit increased goblet cell numbers, while Paneth cell and intestinal stem cell numbers remain unchanged.
(A) Male litter pairs (n = 3 per genotype) were sacrificed between 12-20 weeks of age. Ileum of untreated mice was collected, and intestinal epithelial cells were isolated. The graph shows mRNA expression levels of the target genes X-box protein 1 (*Xbp1*) and Orosomucoid-like 3 (*Ormdl3*) as well as the IEC population marker genes Lysozyme (*Lyz2*), Mucin 2 (*Muc2*), Olfactomedin 4 (*Olfm4*) and Leucin-rich repeat-containing G-protein coupled receptor 5 (*Lgr5*). **(B)** Quantification of lysozyme positive cells per crypt. For quantification, at least 30 crypts per animal were counted. **(C)** Representative images of murine ileal sections (n = 8 per genotype) stained for lysozyme. Scale bar = 20 µm. **(D)** Quantification of Olfactomedin 4 positive cells per crypt. For quantification, at least 30 crypts per animal were counted. **(E)** Representative images of murine ileal sections (n = 8 per genotype) stained for the intestinal stem cell marker Olfactomedin 4. Scale bar = 20 µm. **(F)** Quantification of Mucin 2 positive cells per crypt. For quantification, at least 30 villi per animal were counted. **(G)** Representative images of murine ileal sections (n = 9 per genotype) stained for the intestinal goblet cell marker Mucin 2. Scale bar = 20 µm. Statistical analysis: Two-tailed Students *t* test with *** $p < 0.001$.

3.5.2.3 The *Ormdl3*$^{-/-}$*/Xbp1*$^{\Delta IEC}$ SI shows increased apoptosis.

To further characterize the *Ormdl3*$^{-/-}$*/Xbp1*$^{\Delta IEC}$ mouse model, we tested for phenotypes described for the *Xbp1* deficient mouse such as increased Paneth cell apoptosis [46]. We therefore performed propidium iodide (PI) staining of small intestinal organoids. PI is a membrane interpermeate dye that intercalates exclusively into the double-stranded DNA of dead, apoptotic cells. We found that depending on the organoids used, the genotypic effect may be either stronger or weaker (Fig. 3.7A, B). However, when pooling organoids from two different litter pairs, we observed a trend towards more apoptosis in *Ormdl3*$^{-/-}$*/Xbp1*$^{\Delta IEC}$ mice (Fig. 3.7C). This finding was supported by immunofluorescent staining for caspase 3 of ModeK iXbp1 cells transfected either with scrambled, non-targeted siRNA or siRNA against ORMDL3 (Fig. 3.7D). Caspase 3 (CASP3) is a member of the caspase protein family and is used as a marker for cell apoptosis. Furthermore, TUNEL staining of murine ileal histological sections revealed more apoptotic cells in *Ormdl3*$^{-/-}$*/Xbp1*$^{\Delta IEC}$ mice (Fig. 3.7E, F).

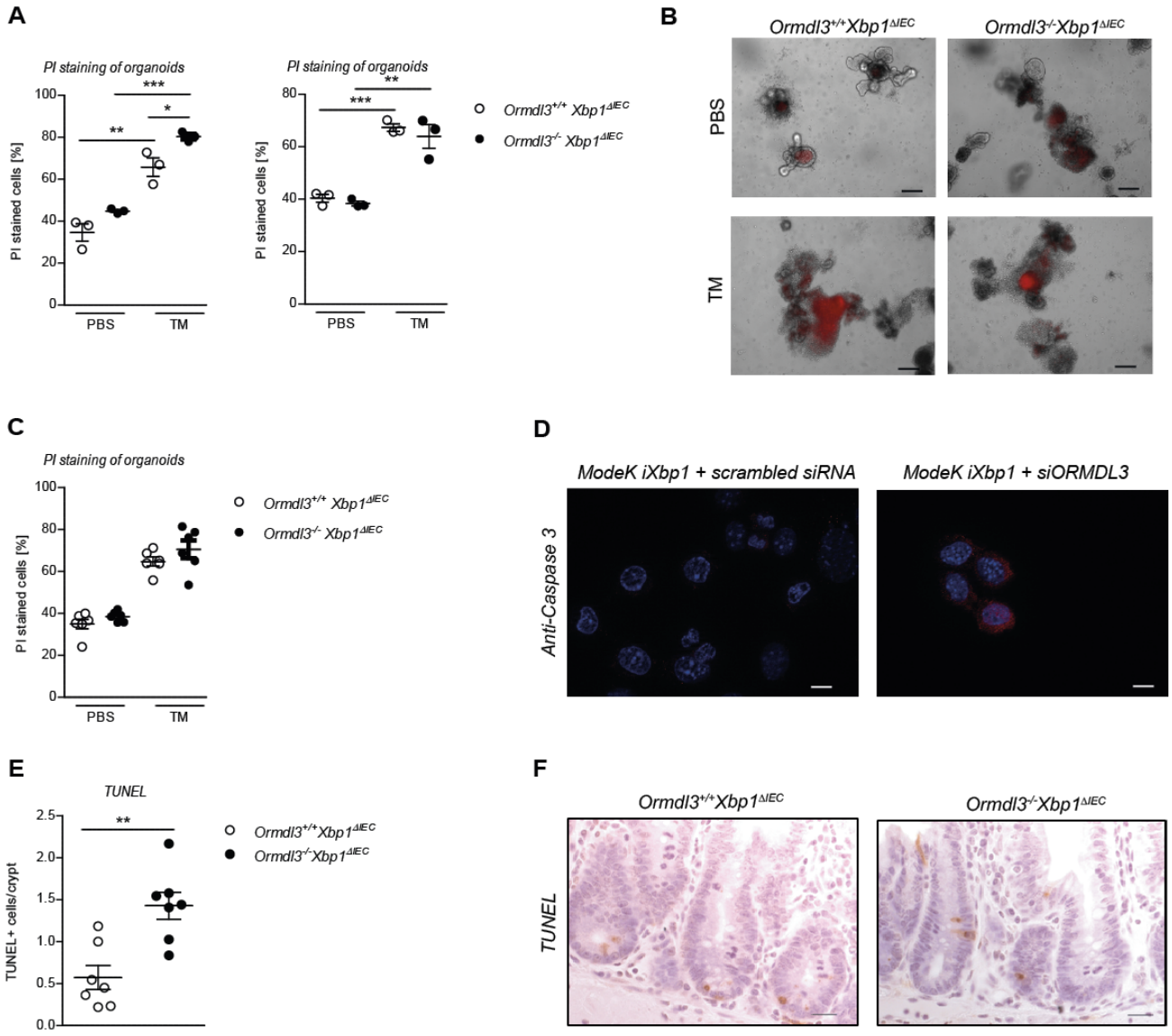

Figure 3.7: *Ormdl3*$^{-/-}$*/Xbp1*$^{\Delta IEC}$ small intestine exhibits elevated levels of cell death.
(A) Male litter pairs (n = 2 per genotype) were sacrificed between 12-20 weeks of age. Ileum of untreated mice was collected, and intestinal epithelial crypts were isolated for generation of small intestinal organoids. Organoids were either treated for 24 hours with PBS as control or tunicamycin (1 µg/ml TM) to induce ER stress. Organoids were dissociated into single cells and subjected to propidium iodide (PI) staining to detect dead cells (n = 3 technical replicates). **(B)** Representative images of SI organoids. Scale bar = 20 µm. **(C)** Quantification of PI positive cells. **(D)** Anti-Caspase 3 immunofluorescence staining of ModeK iXbp1 cells transfected with scrambled, non-targeted siRNA (scrambled siRNA) or siRNA against ORMDL3 (siORMDL3). Blue = DAPI, red = Caspase 3. Scale bar: 10 µm. **(E)** Quantification of terminal deoxynucleotidyl transferase (TUNEL) positive cells per crypts. For quantification, at least 30 crypts per mouse were counted. (n = 7 for *Ormdl3*$^{+/+}$*/Xbp1*$^{\Delta IEC}$ and *Ormdl3*$^{-/-}$*/Xbp1*$^{\Delta IEC}$) **(F)** Representative images of murine ileal sections (n = 7 per genotype) stained for the apoptosis marker TUNEL. Scale bar = 20 µm. Statistical analysis: Two-tailed Students *t* test with * $p < 0.05$, ** $p < 0.01$, *** $p < 0.001$.

3.5.2.4 The *Ormdl3*$^{-/-}$*/Xbp1*$^{\Delta IEC}$ SI shows increased cell proliferation.

Consequently, we next aimed at investigating proliferation within the small intestinal epithelium. Therefore, we cultured single IECs gained from SI organoids for a colony formation assay. This *in vitro* cell survival assay is used to determine a single cell's ability to proliferate into a colony [175]. We counted the number of colonies per well on day 5 and day 10 post-culture and found an increase in *Ormdl3/Xbp1* double deficient colonies on both days (Fig. 3.8A). Additionally, we measured the size of organoid colonies and observed a significant increase in colony size (Fig. 3.8B, C). In line with these findings, we stained the murine SI epithelium for Ki67, a marker for proliferation. When assessing the amount of Ki67^{+} cells, we again found higher numbers of proliferating cells in the *Ormdl3/Xbp1* double deficient epithelium (Fig. 3.8D, E).

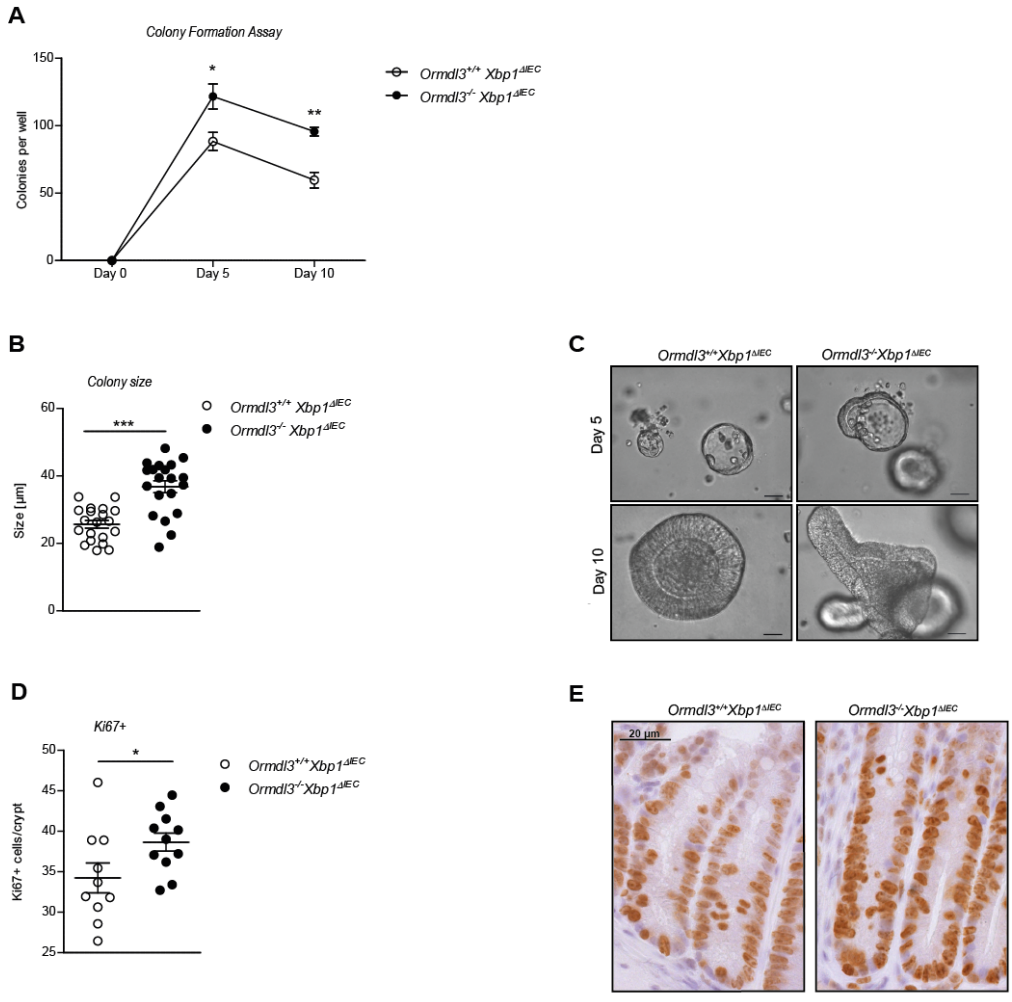

Figure 3.8: *Ormdl3*$^{-/-}$*/Xbp1*$^{\Delta IEC}$ small intestine shows increased cell proliferation.
(A) Male mice (n = 1 per genotype) were sacrificed between 12-20 weeks of age. Ileum of untreated mice was collected, and intestinal epithelial crypts were isolated for generation of small intestinal organoids. Organoids were dissociated into single cells. 5.000 cells/well in 5 wells were cultured with Intesticult in a 96 well-plate for 10 days. Colonies were counted on day 5 and day 10 after seeding. **(B)** Quantification of colony size (n = 20 per genotype). **(C)** Representative images of SI organoids. Scale bar = 20 µm. **(D)** Quantification of Ki67 positive cells per crypt. For quantification, at least 30 crypts per mouse were counted. **(E)** Representative images of murine ileal sections (n = 7 per genotype) stained for the proliferation marker Ki67 (n = 9 for *Ormdl3*$^{+/+}$*/Xbp1*$^{\Delta IEC}$ and *Ormdl3*$^{-/-}$*/Xbp1*$^{\Delta IEC}$). Scale bar = 20 µm. Error bars represent mean ± SEM. Statistical analysis: Two-tailed Students *t* test with * $p < 0.05$, ** $p < 0.01$, *** $p < 0.001$.

3.5.2.5 *Ormdl3*$^{-/-}$*/Xbp1*$^{\Delta IEC}$ mice show signs of spontaneous intestinal inflammation in the SI, but not colon.

We next aimed at investigating the degree of intestinal inflammation on small intestinal and colonic tissue under basal conditions. Therefore, we performed histological scoring of ileal and colonic tissue as described in chapter 2.4.9.4. When investigating the small intestine, we observed higher overall arbitrary units, indicating higher levels of spontaneous inflammation in the *Ormdl3*$^{-/-}$*/Xbp1*$^{-\Delta IEC}$ genotype. This difference, however, was not significant in any of the five categories investigated (Fig. 3.9A, B). In the colon we found overall low arbitrary units, indicating no spontaneous inflammation in either of the two genotypes (Fig. 3.9C, D). When investigating the five distinct categories, we found only low arbitrary units in comparison to the SI and no significant difference for any of the categories (Fig. 3.9D).

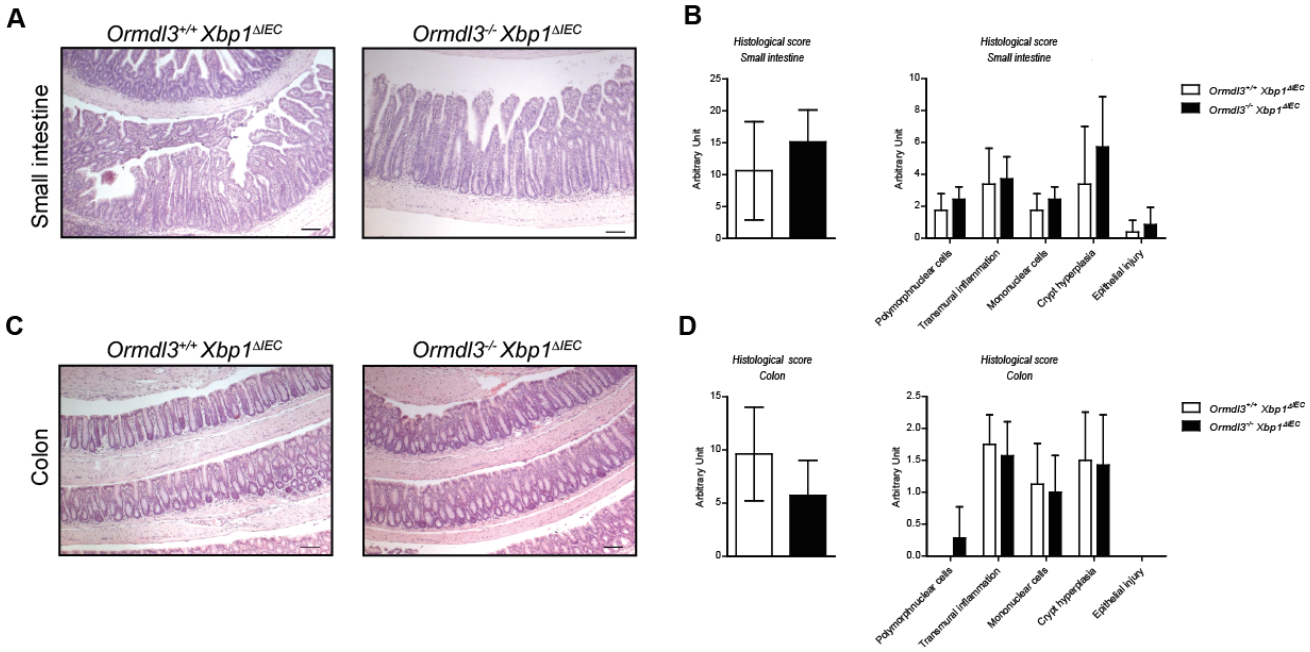

Figure 3.9: *Ormdl3*$^{-/-}$*/Xbp1*$^{\Delta IEC}$ mice develop spontaneous small intestinal inflammation.
Histological scoring of *Ormdl3*$^{+/+}$*/Xbp1*$^{-\Delta IEC}$ (n = 8) and *Ormdl3*$^{-/-}$*/Xbp1*$^{-\Delta IEC}$ (n = 7) small intestine and colon (littermates, male and female mice, age 12-20 weeks). **(A)** Typical small intestinal histology under homeostasis. Scale bars represent 200 µm. **(B)** Inflammation of small intestinal tissue was scored blindly as described in Methods. Data presents mean ± s.d. Mann-Whitney test was performed and showed no significance for any of the categories tested. **(C)** Typical basal colonic histology. Scale bars represent 200 µm. **(D)** Inflammation of colonic tissue was scored blindly as described in Methods. Data presents mean ± s.d. Mann-Whitney test was performed and showed no significance for any of the categories tested.

3.5.2.6 Presence/Absence of *Ormdl3* influences MHCII expression on IECs.

When studying isolated IECs and cells of the LP fraction of the small intestine of both *Ormdl3*$^{+/+}$*/Xbp1*$^{-\Delta IEC}$ and *Ormdl3*$^{-/-}$*/Xbp1*$^{-\Delta IEC}$ mice we frequently observed lower surface expression levels of MHCII proteins on cells of the double deficient small intestine (data not shown). Of note, this decrease in MHCII proteins could not be linked to any antigen-presenting cell (APC) population, e.g. macrophages or dendritic cells. In accordance with studies from various groups, we therefore concluded that the events we detected might arise from MHCII positive IECs, which have been described to

function as non-professional APCs [76]. This effect of MHCII presentation on IECs is of special interest because it has previously been linked to human IBD [77, 187-190].

To characterize a possible interplay between *Ormdl3* sufficient and deficient IECs and MHCII further, we first investigated gene expression of MHCII-related genes in SI organoids (Fig. 3.10A-D). We chose H2-Ab1 (H-2 class II histocompatibility antigen, A beta chain), a gene involved in the production of the beta chain of the MHCII molecule, as a first target. Interestingly, we found significantly lower gene expression of *H2-Ab1* in *Ormdl3* deficient organoids both under basal and ER stress (as represented by TM treatment) or inflammatory (DSS) conditions (Fig. 3.10A-C). We then assessed mRNA expression of CIITA (Class II major histocompatibility complex transactivator), which acts as a positive regulator of MHCII gene transcription. Therefore, we stimulated SI organoids from *Ormdl3* sufficient ($Ormdl3^{+/+}$), *Ormdl3* deficient ($Ormdl3^{-/-}$), $Ormdl3^{+/+}/Xbp1^{\Delta IEC}$ and $Ormdl3^{-/-}/Xbp1^{\Delta IEC}$ mice either with PBS or TM. Fig. 3.10D displays the result of qPCR analysis. Of interest, *CIITA* mRNA expression levels of double deficient organoids resemble those of *Ormdl3* single deficient rather than $Ormdl3^{+/+}$ $Xbp^{\Delta IEC}$ control organoids. While *Ormdl3* single deficient organoids show no significant differences in *CIITA* gene expression compared to WT organoids both under homeostatic (PBS) and ER stress (TM) conditions, the gene expression of $Ormdl3^{-/-}/Xbp1^{\Delta IEC}$ organoids is significantly reduced compared to $Ormdl3^{+/+}/Xbp^{\Delta IEC}$ organoids. To further visualize our findings, we performed immunofluorescence staining for MHCII on $Ormdl3^{+/+}/Xbp^{\Delta IEC}$ and $Ormdl3^{-/-}/Xbp1^{\Delta IEC}$ SI organoids where again *Ormdl3*/*Xbp1* double deficient organoids exhibit a higher amount of stained, and thus MHCII positive, cells (data not shown). To confirm our finding that double deficiency causes a decrease in both MHCII-related gene expression and MHCII protein levels in comparison to $Ormdl3^{+/+}/Xbp^{\Delta IEC}$, we performed flow cytometric analysis of murine ModeK cells. We transfected ModeK iXbp1 cells either with scrambled RNA to mimic the $Ormdl3^{+/+}/Xbp^{\Delta IEC}$ genotype or siRNA directed against ORMDL3 to mimic $Ormdl3^{-/-}/Xbp1^{\Delta IEC}$ (Fig. 3.10E). Furthermore, we included non-transfected ModeK iCtrl cells as a wild type control. Strinkingly, we found significantly elevated MHCII protein levels in both *Xbp1* deficient genotypes (ModeK iXbp1) compared to control cells (ModeK iCtrl), pointing towards *Xbp1* deficiency as the main driver of this upregulation (Fig. 3.10E). Moreover, we show that double deficient ModeK cells, like organoids, exhibit a decrease in MHCII protein levels compared to *Xbp1* single deficient cells (Fig. 3.10E). These results correspond to findings described for $Ormdl3^{-/-}$ mice, which not only exhibited less MHCII positive cells in the colon but also showed decreased IFNγ serum levels compared to $Ormdl3^{+/+}$ mice [153]. IFNγ is necessary for maintenance of the homeostasis of intestinal epithelium [191] and induces MHCII expression [192]. Notably, mRNA expression analysis of IECs of young and old $Ormdl3^{-/-}/Xbp1^{\Delta IEC}$ mice show lower *IFNγ* levels, accompanied with significantly decreased *Cxcl10* levels, with the latter being a target of IFNγ (data not shown).

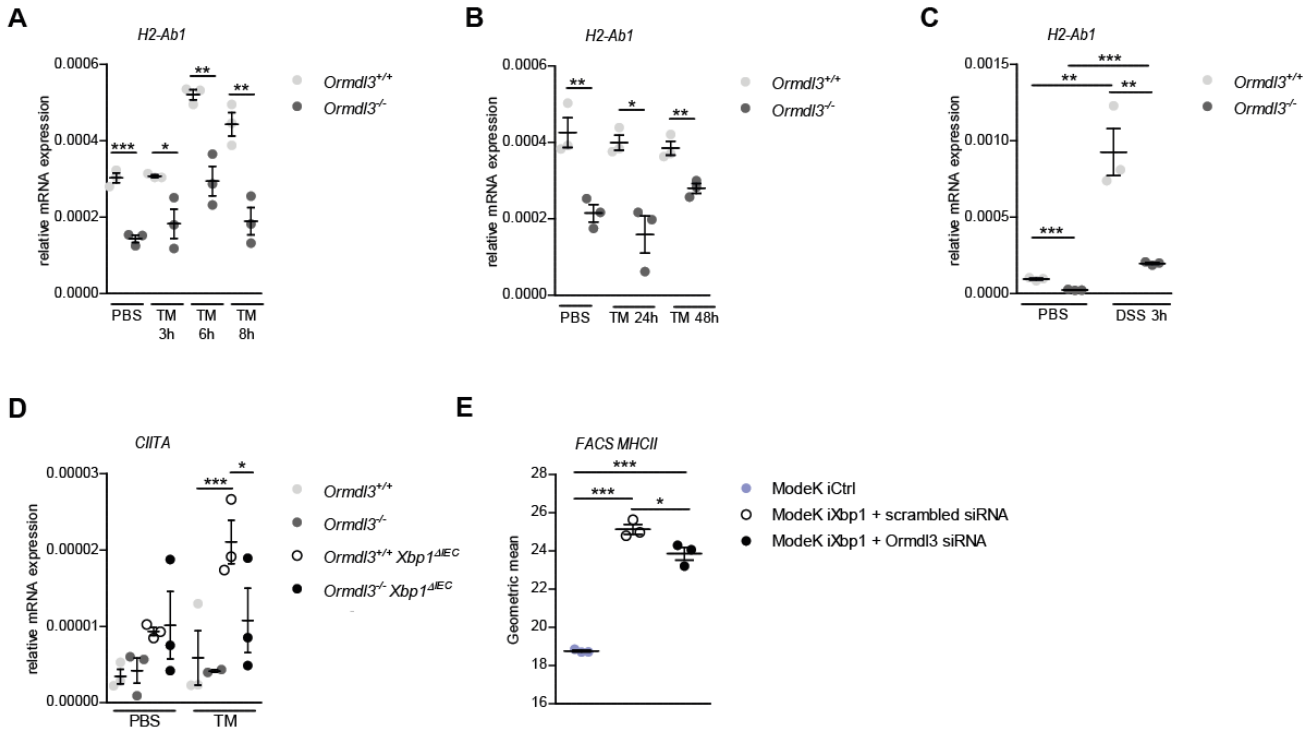

Figure 3.10: *Ormdl3* deficiency causes significant downregulation of MHCII-related genes and decreased surface expression of MHCII in intestinal epithelial cells.
(A) *Ormdl3*$^{+/+}$ and *Ormdl3*$^{-/-}$ SI organoids (n = 3 technical replicates) were either treated with PBS as control or with tunicamycin (1 µg/ml TM) for 3, 6 or 8 hours. Next, RNA was isolated and RT-PCR analysis of *H2-Ab1* (H-2 class II histocompatibility antigen, A beta chain) was performed. **(B)** *Ormdl3*$^{+/+}$ and *Ormdl3*$^{-/-}$ SI organoids (n = 3 technical replicates) were either treated with PBS as control or with tunicamycin (1 µg/ml TM) for 24 or 48 hours. Next, RNA was isolated and RT-PCR analysis of *H2-Ab1* (H-2 class II histocompatibility antigen, A beta chain) was performed. **(C)** *Ormdl3*$^{+/+}$ and *Ormdl3*$^{-/-}$ SI organoids (n = 3 technical replicates) were either treated with PBS as control or with 5 % DSS for 3 hours prior to harvesting of organoids. Next, RNA was isolated and RT-PCR analysis of *H2-Ab1* (H-2 class II histocompatibility antigen, A beta chain) was performed. **(D)** *Ormdl3*$^{+/+}$, *Ormdl3*$^{-/-}$, *Ormdl3*$^{+/+}$/*Xbp1*$^{\Delta IEC}$ and *Ormdl3*$^{-/-}$/*Xbp1*$^{\Delta IEC}$ SI organoids (n = 3 technical replicates) were either treated with PBS as control or with tunicamycin (1 µg/ml TM) for 24 hours. Next, RNA was isolated and RT-PCR analysis of *CIITA* (MHC class II transactivator) was performed. Statistical analysis: 2way ANOVA with *p < 0.05 and **p < 0.01. **(E)** Flow cytometric analysis of MHCII protein levels on ModeK iCtrl, ModeK iXbp1 transfected with scrambled siRNA (= *Ormdl3*$^{+/+}$/*Xbp1*$^{\Delta IEC}$) or siRNA against ORMDL3 (= *Ormdl3*$^{-/-}$/*Xbp1*$^{\Delta IEC}$) 24 hours prior to experiment. Statistical analysis unless otherwise indicated: Student's *t* test (unpaired) with *p < 0.05, **p < 0.01.

3.5.2.7 RNA sequencing of small intestinal organoids reveals strong effect of XBP1 on the *Ormdl3/Xbp1* double deficient genotype

To further characterize any basal transcriptional differences between the *Ormdl3*$^{+/+}$/*Xbp1*$^{-\Delta IEC}$ and *Ormdl3*$^{-/-}$/*Xbp1*$^{-\Delta IEC}$ genotypes, we performed RNA sequencing of small intestinal organoids. As control, we included *Ormdl3*$^{+/+}$ wild type organoids. We were very surprised to find that, while *Ormdl3*$^{+/+}$ and *Ormdl3*$^{+/+}$/*Xbp1*$^{-\Delta IEC}$ shared 2940 differentially expressed genes (DEG) and *Ormdl3*$^{+/+}$ and *Ormdl3*$^{-/-}$/*Xbp1*$^{-\Delta IEC}$ even 4382, *Ormdl3*$^{+/+}$/*Xbp1*$^{-\Delta IEC}$ and *Ormdl3*$^{-/-}$/*Xbp1*$^{-\Delta IEC}$ organoids shared only 14 DEGs, with one of them being *Ormdl3* itself (Fig. 3.11A). These findings suggest a strong effect of the *Xbp1* deficient phenotype in the double deficient organoids (Fig. 3.11B). Interestingly, despite the low number of DEGs between *Ormdl3*$^{+/+}$/*Xbp1*$^{-\Delta IEC}$ and *Ormdl3*$^{-/-}$/*Xbp1*$^{-\Delta IEC}$, we found a majority of them to be associated with Paneth cells (data not shown). However, we could not replicate our findings *in vitro* (data not shown) and thus did not follow up on these results.

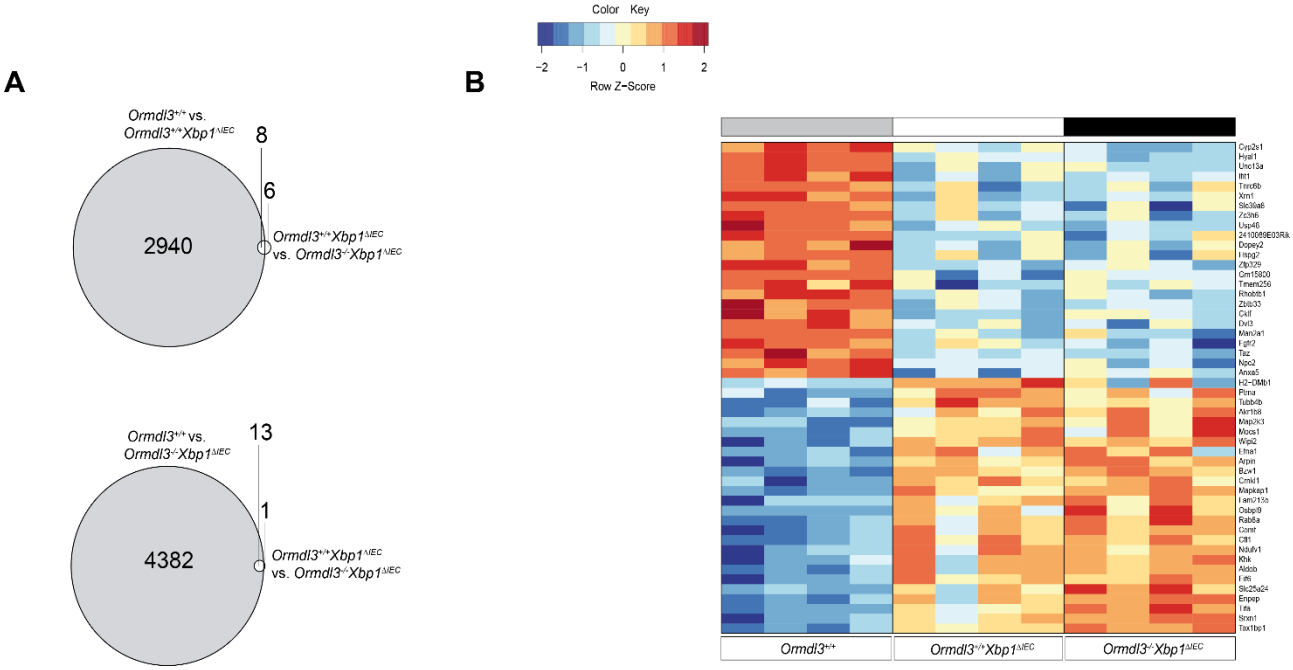

Figure 3.11: RNA sequencing of murine *Ormdl3*$^{+/+}$, *Ormdl3*$^{+/+}$/*Xbp1*$^{\Delta IEC}$ and *Ormdl3*$^{-/-}$/*Xbp1*$^{\Delta IEC}$ small intestinal organoids reveals strong effect of Xbp1 on the transcriptional level.
Bioinformatic analysis performed by Dr. Joana Pimenta Bernardes. **(A+B)** Small intestinal organoids of *Ormdl3*$^{+/+}$ (n = 3), *Ormdl3*$^{+/+}$/*Xbp1*$^{-\Delta IEC}$ (n = 3) and *Ormdl3*$^{+/+}$/*Xbp1*$^{-\Delta IEC}$ (n = 3) mice were used for RNA sequencing. Organoids were grown in Intesticult medium prior to experiment and harvested on day 4 after last passaging. **(A)** Venn diagram of differentially expressed genes shared between *Ormdl3*$^{+/+}$ and *Ormdl3*$^{+/+}$/*Xbp1*$^{-\Delta IEC}$ (2940) or *Ormdl3*$^{+/+}$/*Xbp1*$^{-\Delta IEC}$ and *Ormdl3*$^{-/-}$/*Xbp1*$^{-\Delta IEC}$ (8+6), respectively (upper circle) or *Ormdl3*$^{+/+}$ and *Ormdl3*$^{-/-}$/*Xbp1*$^{-\Delta IEC}$ (4382) or *Ormdl3*$^{+/+}$/*Xbp1*$^{-\Delta IEC}$ and *Ormdl3*$^{-/-}$/*Xbp1*$^{-\Delta IEC}$ (13+1), respectively (lower circle). **(B)** Top 50 differentially expressed genes between *Ormdl3*$^{+/+}$(grey panel) and *Ormdl3*$^{+/+}$/*Xbp1*$^{-\Delta IEC}$ (white panel) compared to *Ormdl3*$^{-/-}$/*Xbp1*$^{-\Delta IEC}$ (black panel).

3.5.2.8 Aging of *Ormdl3*$^{-/-}$*/Xbp1*$^{\Delta IEC}$ mice does not have an impact on the intestinal phenotype.

Due to the fact that human IBDs exhibit a specific age of onset, we hypothesized that this might also hold true for an inflammatory intestinal phenotype in mice. Having characterized young mice up to 20 weeks of age, we consequently now aimed at investigating the intestinal phenotype in aged, 1-year-old mice. When assessing body weight as well as organ weights (data of the latter not shown) and SI and colon length, we found no significant differences between old *Ormdl3*$^{+/+}$*/Xbp1*$^{-\Delta IEC}$ and *Ormdl3*$^{-/-}$*/Xbp1*$^{-\Delta IEC}$ mice (Fig. 3.12A+B). However, since we included only n = 5 and n = 4 animals, respectively, it is possible that the groups were simply too small to detect any phenotypic differences. This might especially hold true for the SI length (Fig. 3.12B), which shows a strong trend towards shortening of the *Ormdl3*$^{-/-}$*/Xbp1*$^{-\Delta IEC}$ small intestine, as it was also observed in younger mice. We further performed mRNA expression analysis of ER stress target genes and the three *Ormdl* genes in isolated IECs of aged mice (Fig. 3.12C+D). Notably, only *Ormdl3* was differentially expressed between the two genotypes (Fig. 3.12D). To conclude the phenotyping of aged mice, we assessed possible spontaneous inflammation in the small intestine and colon using histological scoring (Fig. 3.12E-H; see chapter 2.4.9.4). The results for SI and colon both indicate slightly more signs of inflammation in *Ormdl3*$^{-/-}$*/Xbp1*$^{-\Delta IEC}$ mice, even though the overall arbitrary units are distinctly low (Fig. 3.12F+H). Consequently, we also only observed low numbers throughout the five categories (Fig. 3.12F+H), suggesting that neither the *Ormdl3*$^{+/+}$*/Xbp1*$^{-\Delta IEC}$ nor the *Ormdl3*$^{-/-}$*/Xbp1*$^{-\Delta IEC}$ genotype results in spontaneous intestinal inflammation upon aging of the animals.

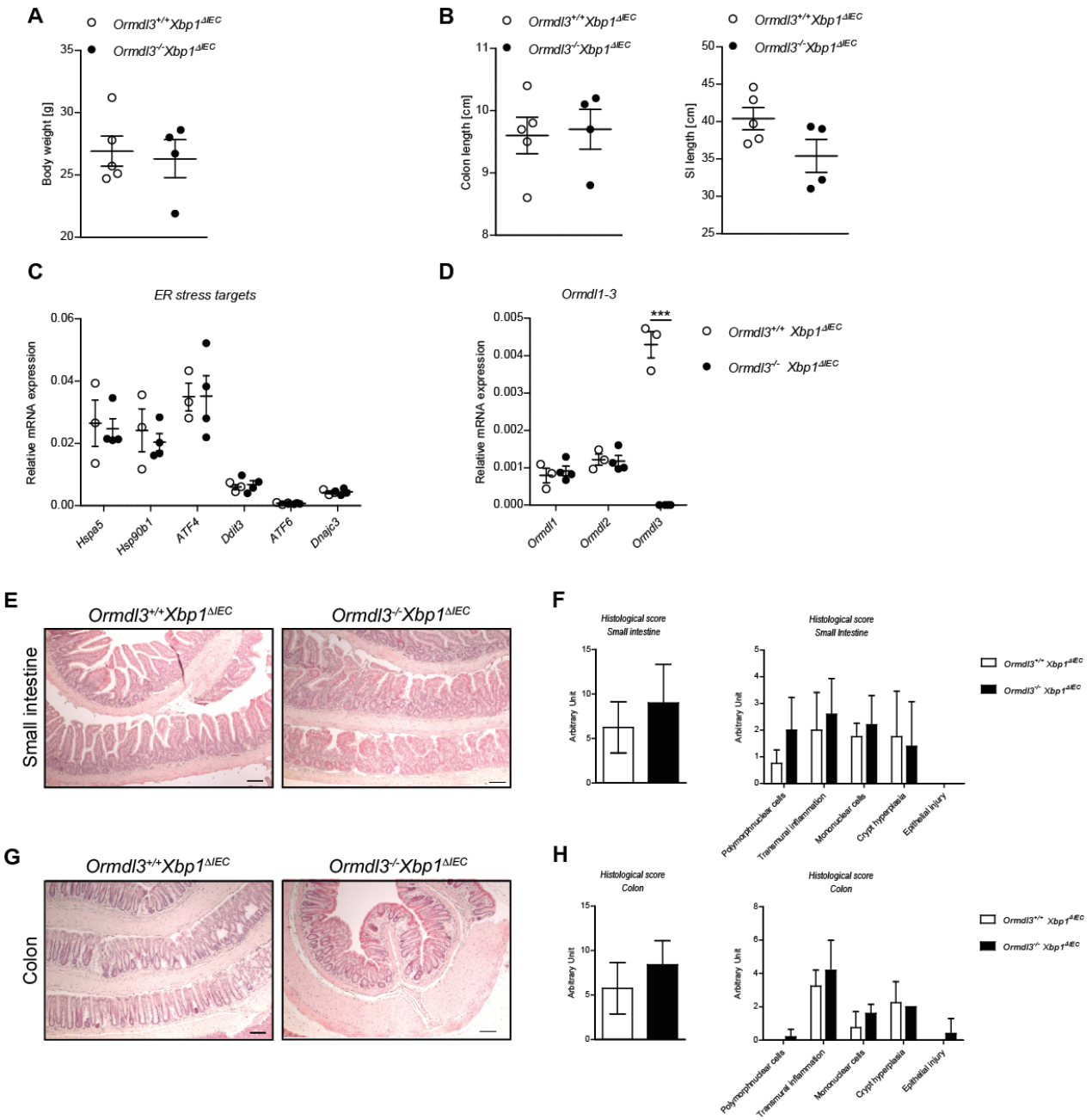

Figure 3.12: Basal phenotyping of aged *Ormdl3*$^{-/-}$*/Xbp1*$^{\Delta IEC}$ mice neither shows differences in their intestinal phenotype nor in gene expression of ER stress target genes and *Ormdl* genes.
Ormdl3$^{+/+}$*/Xbp1*$^{-\Delta IEC}$ (n = 5) and *Ormdl3*$^{-/-}$*/Xbp1*$^{-\Delta IEC}$ (n = 4) male and female mice were sacrificed at 1 year of age. **(A)** Body weight as measured on day of sacrifice. Data presents mean ± s.e.m. **(B)** Length of small intestine and colon as measured on day of sacrifice. Data presents mean ± s.e.m. **(C)** Isolated IECs of *Ormdl3*$^{+/+}$*/Xbp1*$^{-\Delta IEC}$ and *Ormdl3*$^{-/-}$*/Xbp1*$^{-\Delta IEC}$ small intestines (n = 3 per genotype) were assessed by qPCR for gene expression of the ER stress targets Heat Shock Protein Family A Member 5 (*Hspa5*), Heat Shock Protein 90 Beta Family Member 1 (*Hsp90b1*), Activating Transcription Factor 4 (*ATF4*), DNA Damage Inducible Transcript 3 (*Ddit3*), Activating Transcription Factor 6 (*ATF6*) and DnaJ Heat Shock Protein Family Member C3 (*Dnajc3*). Data are normalized to *β-actin*, mean ± s.e.m. **(D)** Isolated IECs of *Ormdl3*$^{+/+}$*/Xbp1*$^{-\Delta IEC}$ and *Ormdl3*$^{-/-}$*/Xbp1*$^{-\Delta IEC}$ small intestines (n = 3 per genotype) were assessed by qPCR for gene expression of Orosomucoid-like 1-3 (*Ormdl1-3*). Data are normalized to *β-actin*, mean ± s.e.m. **(E-H)** Histological scoring of *Ormdl3*$^{+/+}$*/Xbp1*$^{-\Delta IEC}$ (n = 4) and *Ormdl3*$^{-/-}$*/Xbp1*$^{-\Delta IEC}$ (n = 5) small intestine and colon (littermates, male and female mice, age 1 year). **(E)** Typical small intestinal histology under homeostasis. Scale bars represent 200 µm. **(F)** Inflammation of small intestinal tissue was scored blindly as described in Methods. Left: Overall histological score. Right: Scoring of the five parameters polymorph nuclear cell infiltrates, transmural inflammation, mononuclear cell infiltrates, crypt hyperplasia and epithelial injury. Data presents mean ± s.d. Mann-Whitney test was performed and showed no significance for any of the categories tested. **(G)** Typical basal colonic histology. Scale bars represent 200 µm. **(H)** Inflammation of colonic tissue was scored blindly as described in Methods. Left: Overall histological score. Right: Scoring of the five parameters polymorph nuclear cell infiltrates, transmural inflammation, mononuclear cell infiltrates, crypt hyperplasia and epithelial injury. Data presents mean ± s.d. Mann-Whitney test was performed and showed no significance for any of the categories tested.

3.5.3 Phenotype of *Ormdl3*$^{-/-}$*/Xbp1*$^{\Delta IEC}$ mice upon induced DSS colitis

While ORMDL3 has been identified as a susceptibility locus for both subsets of IBD, CD and UC, in humans [47, 48], *Ormdl3*$^{-/-}$*/Xbp1*$^{\Delta IEC}$ mice show rather distinct signs of inflammation under basal conditions (see Fig. 3.9 for comparison). To investigate the role of *Ormdl3/Xbp1* double deficiency both during acute and chronic intestinal inflammation, *Ormdl3*$^{+/+}$*/Xbp1*$^{\Delta IEC}$ control mice and *Ormdl3*$^{-/-}$*/Xbp1*$^{\Delta IEC}$ mice were challenged with 2 % DSS in their drinking water either for 5 consecutive days (acute DSS colitis) or for 3 cycles of 5 consecutive days (chronic DSS colitis). During DSS colitis, the body weight of all animals was assessed daily and monitored closely. Animals that had lost more than 20 % of their original body weight were excluded from the experiment and sacrificed immediately. Mice were sacrificed and their organs harvested on day 10 (acute DSS colitis) or day 30 (chronic DSS colitis), respectively.

3.5.3.1 *Ormdl3 Xbp1* double deficiency does not induce higher susceptibility to intestinal inflammation in an acute DSS colitis model.

During acute colitis, mice of both genotypes exhibited a sudden weight loss after day 5 of DSS treatment but recovered until day 9 of colitis. Even though *Ormdl3*$^{-/-}$*/Xbp1*$^{\Delta IEC}$ mice seem to have lost less weight in comparison to *Ormdl3*$^{+/+}$*/Xbp1*$^{\Delta IEC}$ mice, this finding is not significant (Fig. 3.13A). This observation is supported by the results of histological scoring of SI and colon tissue, which also showed no significant differences between the two genotypes. Of interest, the overall arbitrary units indicate that the SI was more affected by DSS treatment than the colon (3.13C-F), even though the DSS colitis model itself has been described to primarily affect colonic IECs.

We next characterized Paneth cells, the cell type to be described as most affected by *Xbp1* deficiency [46]. Compared to basal conditions, we found no difference in *Lyz*+ cell numbers between *Ormdl3*$^{+/+}$*/Xbp1*$^{\Delta IEC}$ control mice and their *Ormdl3*$^{-/-}$*/Xbp1*$^{\Delta IEC}$ littermates (Fig. 3.13G+H). Moreover, we observed no difference in proliferating IECs, as indicated by Ki67 staining (Fig. 3.13I+J). Notably and in accordance with baseline conditions, *Ormdl3*$^{-/-}$*/Xbp1*$^{\Delta IEC}$ mice exhibited higher numbers of TUNEL+ cells, which are indicative of increased apoptosis (Fig. 3.13K+L).

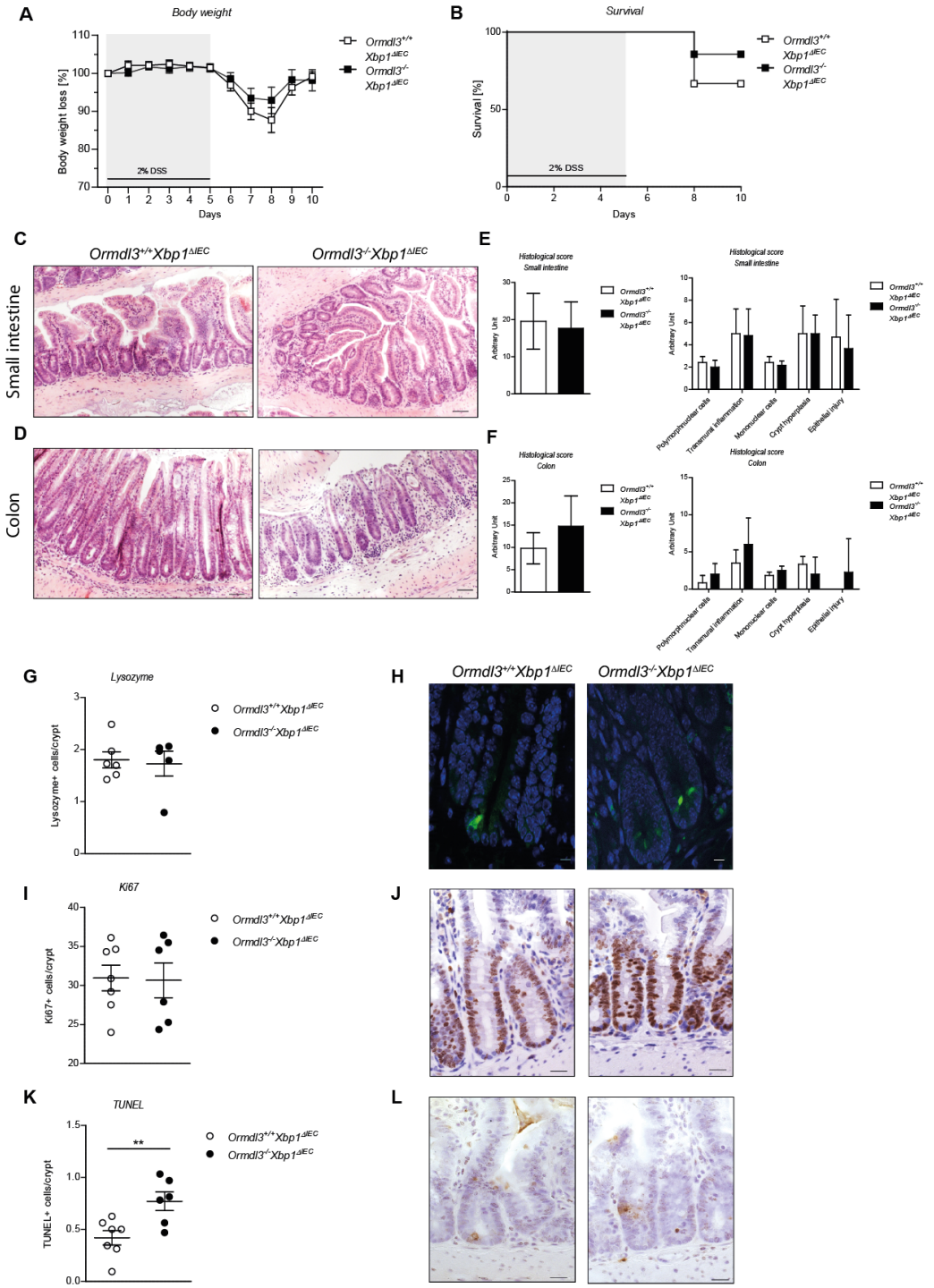

Figure 3.13: *Ormdl3/Xbp1* double deficiency does not cause higher susceptibility but induces cell death in an acute DSS colitis.

(A) 2 % dextran sodium sulfate (DSS) was administered for 5 days and then replaced by regular drinking water in *Ormdl3*$^{+/+}$/*Xbp1*$^{\Delta IEC}$ (n = 7) and *Ormdl3*$^{-/-}$/*Xbp1*$^{\Delta IEC}$ (n = 6) littermates (mice of both genders, age 8-15 weeks). Wasting is presented as percentage (%) of initial body weight. Data presents mean ± s.e.m. Two-tailed Student's *t* test was performed. **(B)** Survival of animals during DSS colitis was assessed daily. Data presents mean ± s.e.m. **(C)** Typical small intestinal histology on day 7 of DSS colitis. Scale bars represent 200 µm. **(D)** Typical colonic histology on day 7 of DSS colitis. Scale bars represent 200 µm. **(E)** Inflammation of small intestinal tissue harvested on day 7 of DSS colitis was scored blindly as described in Methods. Data presents mean ± s.d. Mann-Whitney test was performed and showed no significance for any of the categories tested. **(F)** Inflammation of colonic tissue harvested on day 7 of DSS colitis was scored blindly as described in Methods. Data presents mean ± s.d. Mann-Whitney test was performed and showed no significance for any of the categories tested. **(G-L)** Histological evaluation of small intestinal sections with quantification and representative images for the Paneth cell marker lysozyme **(G+H)**, proliferation marker Ki67 **(I+J)** and cell death marker TUNEL **(K+L)**. s.e.m. = standard error of the mean, s.d. = standard deviation, Ki67 = Kiel67, TUNEL = Terminal deoxynucleotidyl transferase dUTP nick end labelling. Statistical analysis: Two-tailed Students *t* test with ** $p < 0.01$.

3.5.3.2 *Ormdl3/Xbp1* double deficiency does not induce higher susceptibility to intestinal inflammation in a chronic DSS colitis model.

After having found that acute DSS colitis leads to increased apoptosis, as also observed under basal conditions, *Ormdl3*$^{-/-}$/*Xbp1*$^{\Delta IEC}$ mice were further subjected to chronic DSS colitis. This model was used to assess the effect of *Ormdl3/Xbp1* double deficiency in IECs under long-term ER stress conditions. During the first and second DSS cycle of colitis, *Ormdl3*$^{-/-}$/*Xbp1*$^{\Delta IEC}$ mice lost and gained weight on the same level as *Ormdl3*$^{+/+}$/*Xbp1*$^{\Delta IEC}$ control animals (Fig. 3.14A). While the body weight curve of control animals reached a plateau during cycle three, the body weight of *Ormdl3*$^{-/-}$/*Xbp1*$^{\Delta IEC}$ mice dropped again slightly, though not to a significant extent. At the end of the experiment, mice of both strains had gained back their previously lost weight to about 100 % of the original body weight (Fig. 3.14A). Not surprisingly, histological scoring of both SI and colon tissue harvested on day 30 of the experiment revealed overall low levels of intestinal inflammation (Fig. 3.14C-F). When investigating overall survival of the animals, we found that 2 animals from each strain had to be excluded from the experiment during the second cycle (Fig. 3.14B). A characterization of Paneth cells again revealed equal numbers of *Lyz*+ cells in both genotypes (Fig. 3.14G+H). Even though the differences were not significant, the *Ormdl3*$^{-/-}$/*Xbp1*$^{\Delta IEC}$ epithelium displayed slightly higher levels of proliferation (Fig. 3.14I+J) and apoptosis (Fig. 3.14K+L).

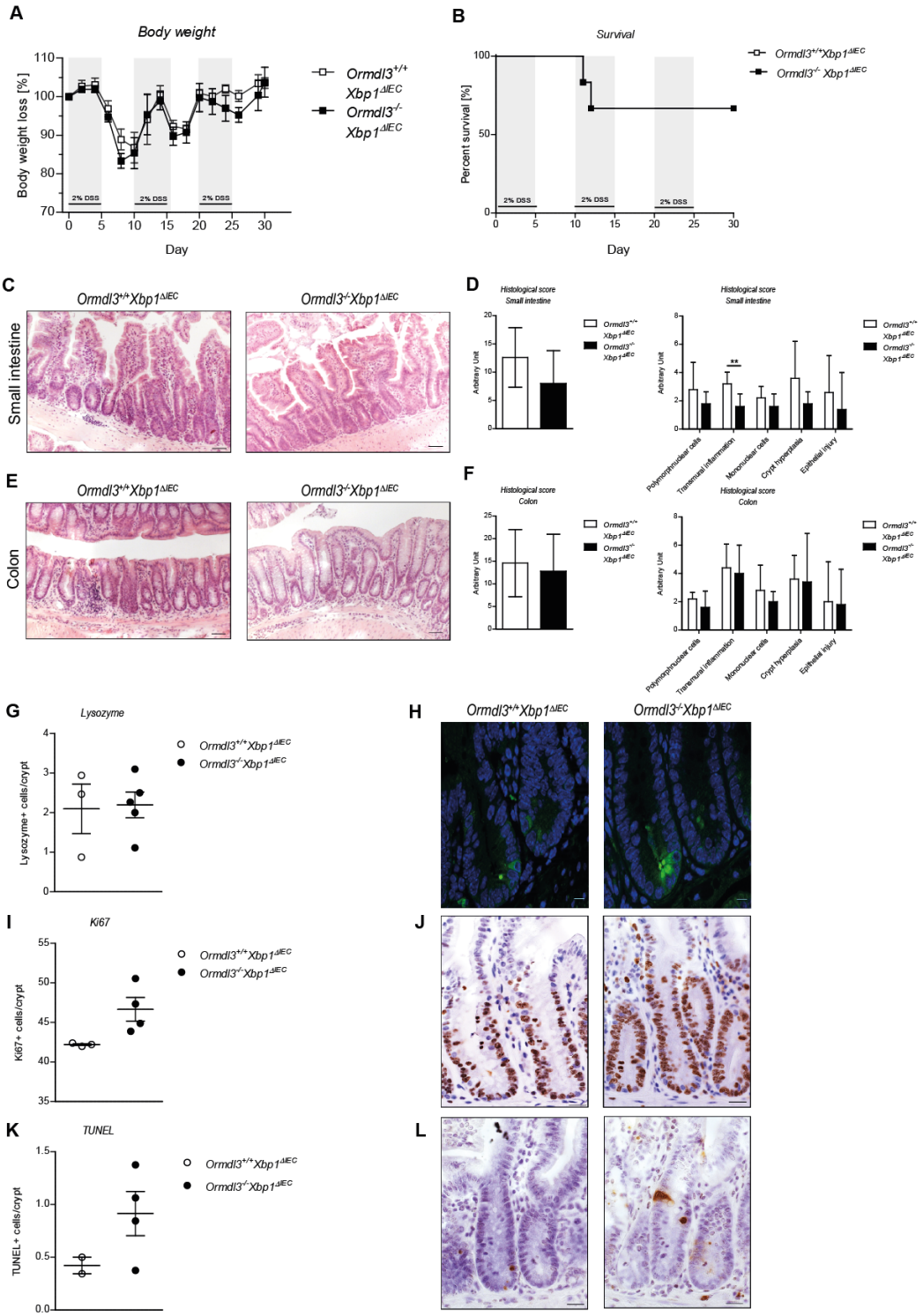

Figure 3.14: *Ormdl3/Xbp1* double deficiency does not cause higher susceptibility to chronic DSS colitis but seems to affect intestinal epithelial cell proliferation and cell death.
(A) 2 % dextran sodium sulfate (DSS) was administered in three cycles of 5 days, each followed by 5 days with regular drinking water in *Ormdl3*$^{+/+}$/*Xbp1*$^{\Delta IEC}$ (n = 4) and *Ormdl3*$^{-/-}$/*Xbp1*$^{\Delta IEC}$ (n = 4) littermates (mice of both genders, age 8-15 weeks). Wasting is presented as percent (%) of initial body weight. Data presents mean ± s.e.m. Two-tailed Student's *t* test was performed. **(B)** Survival of animals during DSS colitis was assessed daily. Data presents mean ± s.e.m. **(C)** Typical small intestinal histology on day 30 of DSS colitis. Scale bars represent 200 µm. **(D)** Inflammation of small intestinal tissue harvested on day 30 of DSS colitis was scored blindly as described in Methods. Data presents mean ± s.d. Mann-Whitney test was performed with ** $p < 0.01$. **(E)** Typical colonic histology on day 30 of DSS colitis. Scale bars represent 200 µm. **(F)** Inflammation of colonic tissue harvested on day 30 of DSS colitis was scored blindly as described in Methods. Data presents mean ± s.d. Mann-Whitney test was performed and showed no significance for any of the categories tested. **(G-L)** Histological evaluation of small intestinal sections with quantification and representative images for the Paneth cell marker lysozyme (**G**+**H**), proliferation marker Ki67 (**I**+**J**) and cell death marker TUNEL (**K**+**L**). s.e.m. = standard error of the mean, s.d. = standard deviation, Ki67 = Kiel67, TUNEL = Terminal deoxynucleotidyl transferase dUTP nick end labeling

3.6 The *Ormdl2* deficient mouse model under inflammatory conditions

3.6.1 *Ormdl2KO* mice show the expected genetic distribution and follow Mendel's laws.

ORMDL3 has been described to function as a risk gene for human IBD. However, only little is known about the inflammatory potential of its two homologues, ORMDL1 and ORMDL2. Thus, our group investigated gene expression of all three ORMDL homologues in whole colon biopsies from IBD patients in comparison to healthy patients. Surprisingly, mRNA expression of *ORMDL1* and *ORMDL2* was upregulated in both CD and UC, while *ORMDL3* expression was downregulated in IBD patients (Fig. 3.15).

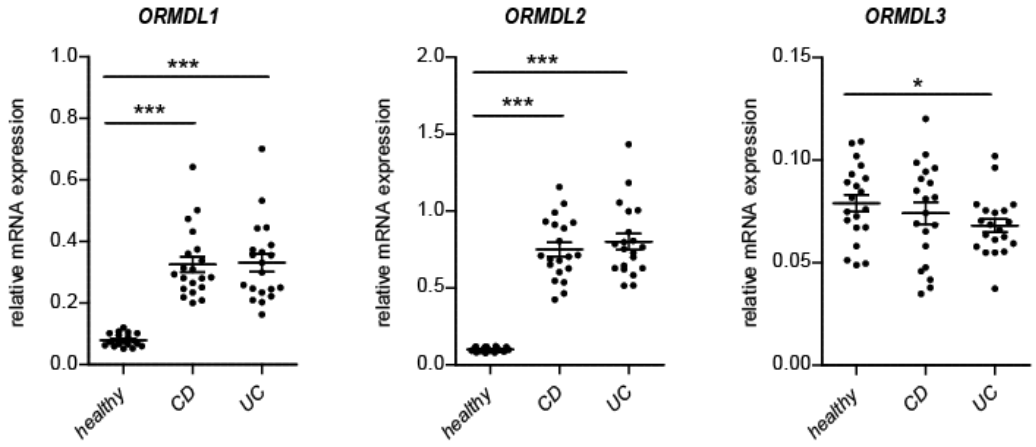

Figure 3.15: *ORMDL1* and *ORMDL2* but not *ORMDL3* mRNA expression are significantly elevated in whole biopsies from IBD patients.
Whole biopsies of colonic tissue of healthy subjects, Crohn's disease (CD) and Ulcerative colitis (UC) patients (n = 20 per group) were used for RNA isolation and cDNA synthesis. The graph shows mRNA expression levels of the target genes Orosomucoid-like 1-3 (*ORMDL1-3*). Statistical analysis: 1-way ANOVA with * $p < 0.05$, *** $p < 0.001$.

This finding made us wonder if the heterogenous nature of the biopsies (including IECs and lamina propria) caused this phenomenon. Consequently, we investigated mRNA expression of *Ormdl1-3* in isolated IECs and the lamina propria of C57BL6/J WT mice both under homeostatic and inflammatory conditions. Notably, *Ormdl2* mRNA expression was significantly upregulated in IECs while *Ormdl3* showed the strongest upregulation in the LP fraction under basal and inflammatory conditions (Fig. 3.16A+B). These results made us question the importance especially of ORMDL2 during intestinal inflammation.

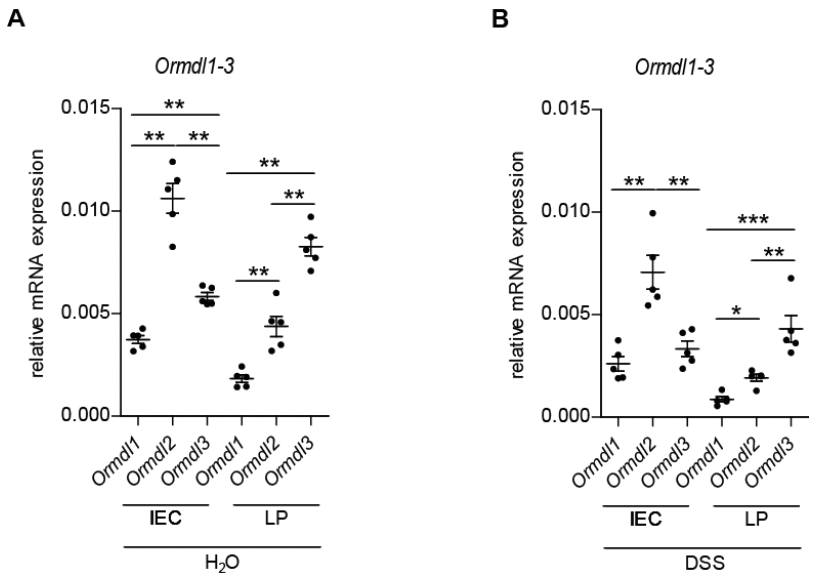

Figure 3.16: mRNA expression levels of *Ormdl2* are significantly elevated in intestinal epithelial cells, whereas *Ormdl3* mRNA expression is significantly increased in the lamina propria of C57BL6/J mice.
Samples were kindly provided by Dr. Maren Falk-Paulsen. C57BL6/J mice (n = 5 per group) were either subjected to chronic DSS-induced colitis or normal drinking water as control. Colitis was induced by two cycles of 2.5 % dextran sodium sulfate administration via drinking water for 5 days, each followed by another 5 days with normal drinking water. Mice were sacrificed on day 20. Colonic IECs and LP were used for RNA isolation and cDNA synthesis. **(A)** qPCR analysis of *Ormdl1-3* within the IEC and LP fraction of the control group, which only received normal drinking water. **(B)** qPCR analysis of *Ormdl1-3* within the IEC and LP fraction of the DSS group. Data are normalized to *β-actin*, mean ± s.e.m. Statistical analysis: Two-tailed Students *t* test with * $p < 0.05$, ** $p < 0.01$, *** $p < 0.001$. IEC = intestinal epithelial cell, LP = lamina propria, H_2O = water, DSS = dextran sodium sulfate

Previous studies from our group aimed at examining the role of *Ormdl1* and *Ormdl3* deficiency in intestinal inflammation in mice (unpublished data). The results suggest a compensatory effect of the respective remaining two ORMDL homologues in case of a single gene deficiency *in vivo*. Of interest, while ORMDL1 was shown to affect all three UPR pathways *in vitro*, no significant differences between *Ormdl1*$^{+/+}$ and *Ormdl1*$^{-/-}$ mice could be observed both under basal conditions and in a DSS colitis. The IBD risk gene ORMDL3, however, not only modulated the UPR pathways *in vitro* but was also shown to play an important role in maintaining intestinal homeostasis under inflammatory conditions. Both *Ormdl3*$^{-/-}$ and *Ormdl3*$^{\Delta IEC}$ mice showed increased susceptibility or longer recovery time upon acute DSS colitis, respectively [153]. However, the homologue of *Ormdl1* and *Ormdl3*, *Ormdl2*, has not been studied in the context of intestinal inflammation yet. To provide a possible missing link for the *in vivo* phenotypes observed in *Ormdl3* deficient animals, we aimed at characterizing the impact of *Ormdl2* deficiency in intestinal inflammation.

To exclude any genetic abnormalities that might have an outcome on further experiments we examined the genetic distribution of *Ormdl2KO* offspring. Since breeding was set up between heterozygous males and females, we expected 50 % of litter to be heterozygous for *Ormdl2* and 25 % of litter to show homozygosity for either the *Ormdl2* wild type or knockout allele, respectively. Indeed, the 72 *Ormdl2KO* mice counted were born in the expected ratios, suggesting that this mouse strain follows Mendel's laws (Table 14).

Table 14: Mendelian distribution of *Ormdl2KO* mice.

Ormdl2$^{+/+}$	*Ormdl2*$^{+/-}$	*Ormdl2*$^{-/-}$	
24	31	17	observed animal numbers
33	43	24	observed percentage [%]
25	50	25	expected percentage [%]

Genotypes within breeding pairs: *Ormdl2*$^{+/-}$ x *Ormdl2*$^{+/-}$
$\chi^2 = 1.6507$, p-value = .438073, significance level: $p < 0.05$

3.6.2 *Ormdl2* deficiency does not induce higher susceptibility to intestinal inflammation in an acute DSS colitis model.

To examine the role of *Ormdl2* deficiency in intestinal inflammation *in vivo*, *Ormdl2KO* mice were subjected to an acute DSS colitis (Fig. 3.17). Mice were challenged with 2 % DSS in their drinking water for 6 consecutive days to induce colitis followed by four days of normal drinking water to mediate recovery. The severity of intestinal inflammation was monitored daily by assessment of body weight. Mice with more than 20 % weight loss as compared to their initial body weight were excluded from the experiment. Interestingly, both *Ormdl2*$^{+/+}$ and *Ormdl2*$^{-/-}$ mice show a similar course of body weight loss with only little (*Ormdl2*$^{-/-}$) to no weight loss (*Ormdl2*$^{+/+}$) until day 3 of the colitis. Starting from day 4, however, mice of both genotypes show a strong reduction in weight indicative for the success of DSS treatment and no visible recovery phase until the end of colitis on day 10 (Fig. 3.17A). Because of the high weight loss, which was accompanied by similarly increasing disease activity as assessed by scoring of stool consistency, blood in the stool and body weight loss, two mice of both genotypes had to be excluded from the experiment (Fig. 3.17B, C). Another important marker for the severity of intestinal inflammation in a DSS colitis is the shortening in colon length [174]. Not surprisingly, the colon length was not altered in *Ormdl2*$^{-/-}$ mice in comparison to their WT littermates. Further measurements of the small intestinal length as well as caecum, spleen, liver and kidney weights also showed no significant differences between the two genotypes (Fig. 3.17E). To assess clinical parameters of inflammation, a histological scoring of both small intestinal and colonic tissue was performed. This histological score combines parameters like mononuclear and polymorph nuclear cell infiltrates in the epithelium, transmural inflammation, crypt hyperplasia and epithelial injury. While the overall score indicates presence of intestinal inflammation in both genotypes thus indicating the successful induction of colitis, the results are not significantly different between the two groups (Fig. 3.17F-I). QPCR analysis of the pro-inflammatory cytokines *Tnfa* and *Cxcl1* in small intestinal crypts also showed no significant differences between the genotypes (Fig. 3.17D).

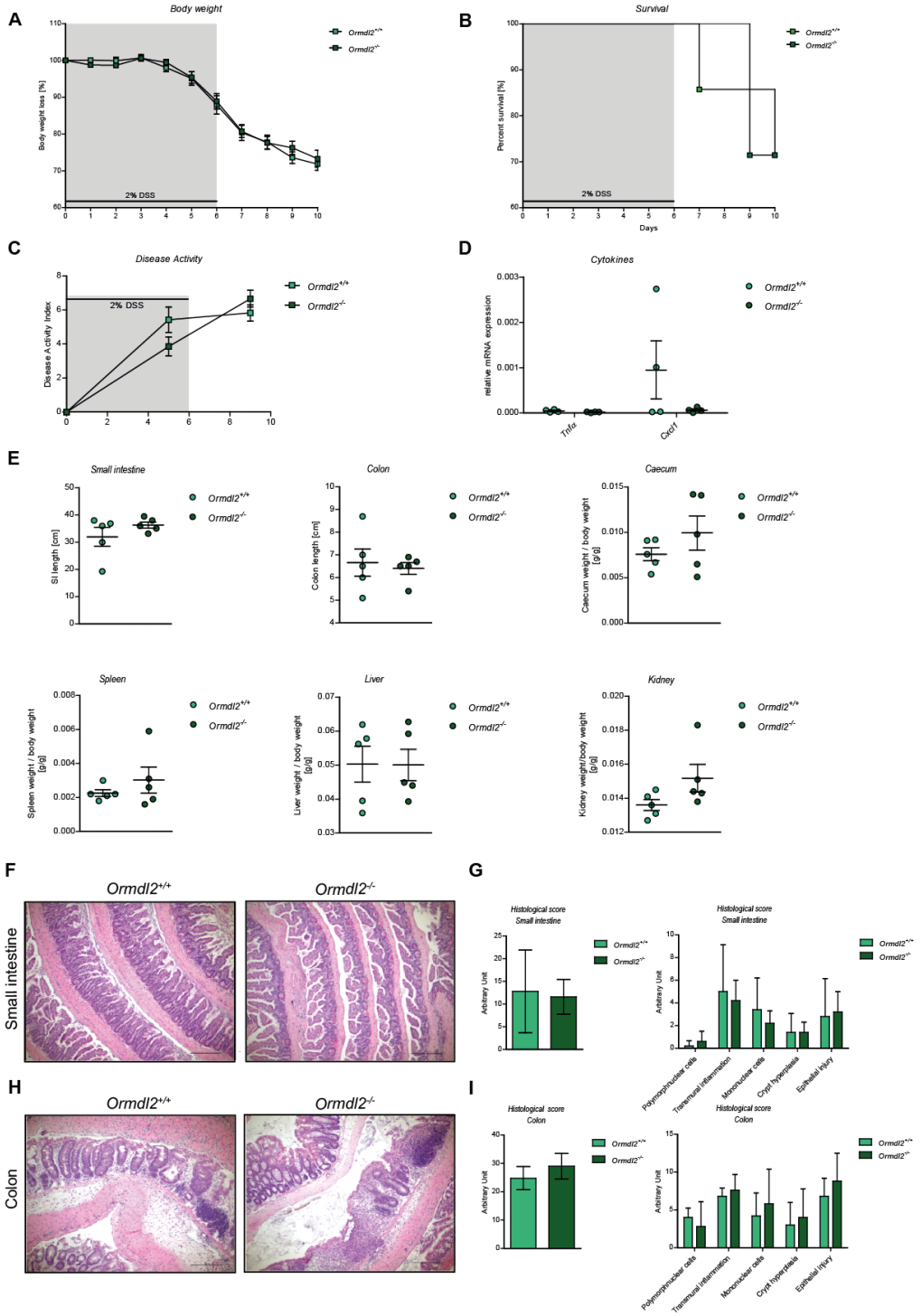

Figure 3.17: *Ormdl2* deficiency does not cause higher susceptibility to dextran sodium sulfate (DSS)-induced colitis. **(A)** 2 % DSS was administered for 6 days and then replaced by regular drinking water in *Ormdl2*$^{+/+}$ (n = 5) and *Ormdl2*$^{-/-}$ (n = 5) littermates (male mice, age 9-11 weeks). Wasting is presented as % of initial body weight. Data presents mean ± s.e.m. **(B)** Survival curve according to Kaplan-Meier estimate. **(C)** Disease activity index (DAI) comprised of body weight loss, stool consistency and blood in the stool was assessed daily and scored as described in Methods. Data presents mean ± s.e.m. **(D)** Small intestinal crypts of *Ormdl2*$^{+/+}$ and *Ormdl2*$^{-/-}$ littermates (n = 4 per genotype) were assessed by qPCR for the two cytokines Tumor necrosis factor alpha (*Tnfa*) and C-X-C motif ligand 1 (*Cxcl1*). Data presents mean ± s.e.m. **(E)** Length of small intestine and colon, weight of caecum, spleen, liver and kidney as measured on day of sacrifice. Data presents mean ± s.e.m. **(F)** Typical small intestinal histology on day 7 of DSS colitis. Scale bars represent 200 µm. **(G)** Inflammation of small intestinal tissue harvested on day 7 of DSS colitis was scored blindly as described in methods. Left: Overall histological score. Right: Scoring of the five parameters polymorph nuclear cell infiltrates, transmural inflammation, mononuclear cell infiltrates, crypt hyperplasia and epithelial injury. Data presents mean ± s.d. **(H)** Typical colonic histology on day 7 of DSS colitis. Scale bars represent 200 µm. **(I)** Inflammation of colonic tissue harvested on day 7 of DSS colitis was scored blindly as described in methods. Left: Overall histological score. Right: Scoring of the five parameters polymorph nuclear cell infiltrates, transmural inflammation, mononuclear cell infiltrates, crypt hyperplasia and epithelial injury. Data presents mean ± s.d.

3.6.3 *Ormdl2* deficiency does not result in significant compensatory upregulation of the other two ORMDL homologues or alteration of ER stress target gene expression upon intestinal inflammation.

To test our initial hypothesis of a compensatory effect of ORMDL proteins upon deletion of *Ormdl2* we performed qPCR to measure mRNA expression of *Ormdl1*, *Ormdl2* and *Ormdl3* in small intestinal crypts, which were isolated on day 10 of the acute DSS colitis. To assess the role of ORMDL2 in regulation of the UPR, we additionally investigated several ER stress target genes by qPCR. These results suggest that *Ormdl2* deficiency does not cause a significant upregulation of either *Ormdl1* or *Ormdl3* mRNA in comparison with *Ormdl2*$^{+/+}$ (Fig. 3.18A). However, since the results indicate a trend towards higher mRNA expression of *Ormdl3* in *Ormdl2*$^{-/-}$ we hypothesized that via *Ormdl3* mRNA upregulation *Ormdl2* deficient crypts might exhibit more ER stress. Of note, *Ormdl2* deficiency does not result in upregulation of the ER stress related genes *Hspa5*, *ATF4*, *Ddit3*, *ATF6* and *Xbp1* (Fig. 3.18B).

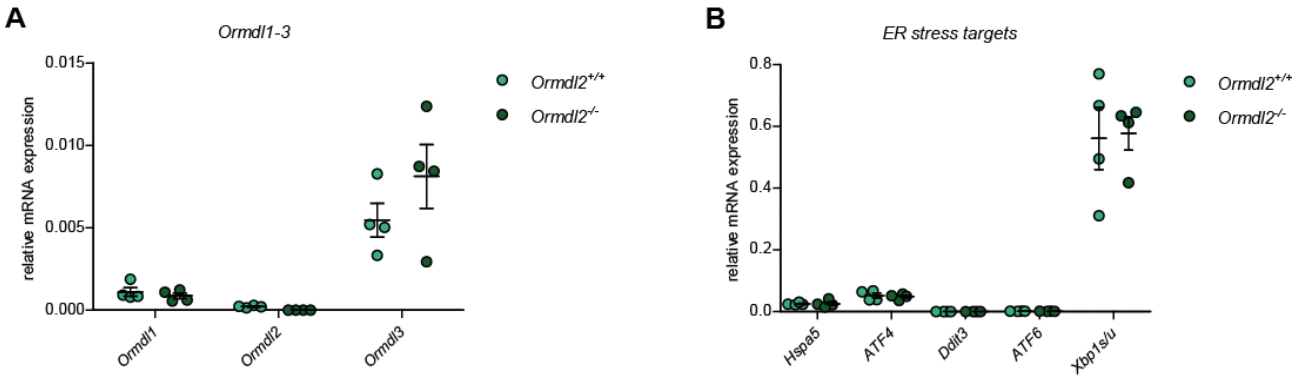

Figure 3.18: *Ormdl2* deficiency does not cause significant differences of *Ormdl1/3* and ER stress target gene mRNA expression upon intestinal inflammation.
2 % DSS was administered for 6 days and then replaced by regular drinking water in *Ormdl2*$^{+/+}$ and *Ormdl2*$^{-/-}$ littermates (male mice, age 9-11 weeks). **(A)** Isolated crypts from *Ormdl2*$^{+/+}$ (n = 4) and *Ormdl2*$^{-/-}$ (n = 4) mice were analyzed for mRNA expression of *Ormdl1-3*. **(B)** Isolated crypts from *Ormdl2*$^{+/+}$ (n = 4) and *Ormdl2*$^{-/-}$ (n = 4) mice were analyzed for mRNA expression of the ER stress markers Heat Shock Protein Family A (Hsp70) Member 5 (*Hspa5*), Activating Transcription Factor 4 (*ATF4*), DNA Damage Inducible Transcript 3 (*Ddit3*), Activating Transcription Factor 6 (*ATF6*) and X-box binding protein 1 (*Xbp1*). Data are normalized to *β-actin*, mean ± s.e.m.

4 Discussion

IBD, with its two subtypes Crohn's disease and ulcerative colitis, is characterized by chronic relapsing-remitting inflammatory episodes of the gastrointestinal tract. Today, it is common knowledge that the four pillars genetics, epigenetics, environmental factors, and the microbiome influence the development of IBD. Although recent studies addressed and continuously increased the knowledge on genetic background and the etiology of IBD, the exact mechanisms of action of most genetic risk loci remain largely unknown. One of the risk loci identified for IBD, and more specifically CD [48], development is the ER stress- and UPR-associated ORMDL3 [46, 193]. Since genetic variants in the gene encoding for the UPR factor XBP1 have been identified as an IBD risk factor, too, previous studies from our group aimed at characterizing the impact of ORMDL proteins, and especially ORMDL3, on ER stress- and UPR-associated intestinal inflammation [153, 162]. While first *in vitro* studies could already show an impact of ORMDL3 on the IRE1/XBP1 pathway of the UPR, only little is known about the influence of ORMDL3 on the same pathway of the UPR in intestinal inflammation.

This study for the first time investigates the impact of ORMDL3 on *Xbp1* deficiency-derived intestinal inflammation *in vivo*. Furthermore, we characterized the role of the homologue of ORMDL3, ORMDL2, in intestinal inflammation.

4.1 ORMDL3 functions as a regulator of the UPR in the murine epithelium.

Usually, ER stress in cells causes upregulation of UPR-related genes. Studies in mouse models with genetic deletion of ER stress related genes have shown that deficiency of these genes can result in enhanced ER stress. A study by Kaser *et al.* in *Xbp1* deficient mice has revealed significantly increased levels of *Hspa5* and *CHOP* in the murine epithelium [46]. Moreover, the authors showed that biopsies of CD and UC patients exhibited both increased *XBP1* splicing, indicative of enhanced IRE1 pathway activity, and increased *HSPA5* mRNA expression, indicative of enhanced ER stress. Since ORMDL3 has also previously been described to be associated with ER stress [130, 149, 153, 194], we investigated the impact of ER stress on the intestinal homeostasis especially in mouse intestinal epithelial cells. We here show that ER stress induction under *Ormdl3* deficient conditions leads to significant upregulation of several ER stress target genes (Fig. 3.1 and Fig. 3.2). This finding demonstrates not only that ORMDL3 is associated with ER stress and the UPR in murine IECs but also shows that *Ormdl3* deficiency directly results in ER stress and induction of all three UPR pathways in these cells. Interestingly, this observation contrasts previous findings from our group, which described an inhibitory effect of ORMDL proteins on the IRE1/XBP1 pathway on the one hand and an activating effect on the PERK/ATF4 and the ATF6 pathway of the UPR on the other hand [153]. However, this previous study was performed in the human kidney cell line HEK-293, suggesting a species-, tissue- and cell-type specific effect of ORMDL proteins, and specifically ORMDL3. It may be speculated that this effect arises due to the cells' exposure and

susceptibility to external stressors. The highly secretory IECs are constantly challenged by microbial and food antigens, while immune cells such as macrophages or monocytes usually are recruited to sites of immunological challenges and undergo significant transcriptional changes upon activation. This effect may be responsible for the contrasting results regarding the cell's response to ER stress induction. Noteworthy, a study of Khongwichit *et al.* supports the hypothesis that UPR responses strongly depend on the investigated cell type [195]. In their study, the authors found that infection of the human Hela and HepG2 cell lines with chikungunya virus led to different UPR responses in the two cell lines. Virus infection of Hela cells caused activation of the PERK/eIF2α UPR pathway, whereas virus infection of HepG2 cells led to activation of the IRE1/XBP1 UPR pathway. Khongwichit *et al.* thus concluded that the cell type represents a key factor in the host cell's response to infection. It may well be assumed that ER stress conditions in different mouse cell populations lead to different UPR responses and importantly, to differential expression of the ORMDL proteins. Furthermore, it can be speculated that changes in ORMDL expression have an impact on tissue function and disease severity during pathophysiological conditions. Of note, even though ORMDL3 expression has been described to be altered in IBD [25, 47, 196], ileal and colonic biopsies of both CD and UC patients showed no significant difference in mRNA expression compared to healthy controls (Fig. 3.15). This finding underscores the importance of further studies regarding ORMDL proteins and their cell-type specific function in IBD.

As mentioned beforehand, a previous study from our group has already demonstrated a repressive effect of ORMDL proteins on the IRE1/XBP1 pathway of the UPR in human intestinal cell lines *in vitro* [153]. This finding was supported by Mc Govern *et al.*, who used HEK-293 cells transfected with siRNA directed against ORMDL3 to show elevated UPRE promoter activity [47]. Surprisingly, a study by Miller *et al.*, which was conducted in the lung epithelial cell line A549 transfected with ORMDL3 could not confirm any changes in *XBP1* splicing levels [147]. Another study by Löser *et al.* [197] conducted in *Ormdl3*$^{+/+}$ and *Ormdl3*$^{-/-}$ mouse lung cells *ex vivo* also showed no difference neither in *Xbp1* mRNA expression nor *Xbp1* splicing under homeostatic conditions. Furthermore, data from Dang *et al.* suggests that altered ORMDL3 expression also in the human Raji B cell line neither alters *XBP1* mRNA expression nor *XBP1* splicing [160].

Results obtained in murine IECs during this study supported the findings from Jentzsch [153] and Mc Govern and colleagues [47]: Deficiency for *Ormdl3* in mouse IECs caused higher UPRE promoter activity both under homeostatic and ER stress conditions and increased *Xbp1* mRNA expression (Fig. 3.3). Besides, we here show that ER stress induction in *Xbp1* deficiency leads to a decrease in *Ormdl3* mRNA expression (Fig. 3.3). Of note, while *Ormdl3*/*Xbp1* double deficient cells showed no alterations in mRNA expression of ER stress related target genes under homeostatic conditions, induction of ER stress via tunicamycin led to decreased levels of *Hspa5* both on mRNA and protein level (Fig. 3.4). These results are of special interest because they suggest a destructive role for ORMDL3 in IECs upon ER stress

conditions. Together, these results underscore the mutual relation between ORMDL3 and XBP1 in murine cells. Also, these contrasting results underscore the importance of distinct cell-type specific differences of endogenous ORMDL protein function also in mice.

4.2 Genetic deletion of either of the *Ormdl* genes only partially results in compensatory upregulation of the remaining *Ormdl* genes.

ORMDL proteins are characterized by their high sequence identity and ubiquitous expression patterns in human adult and fetal tissues [129]. Of note, ORMDL1 and ORMDL2 expression have been described to vary between human and mouse tissues, with the latter being particularly abundant in the murine liver and kidney [198]. In this study we detected only partial compensatory upregulation of *Ormdl1*, *Ormdl2*, or *Ormdl3* – especially in the case of single deficiency for either *Ormdl2* or *Ormdl3*. These results are supported by Clarke *et al.* who found a partial compensatory effect of the individual ORMDLs in the control of sphingolipid levels and the prevention of expression of severe phenotypes in *Ormdl3* and *Ormdl1/3* deficient mice [156, 197]. Consequently, Clarke *et al.* speculate that redundancy of ORMDL proteins may serve as both organismal and evolutionary advantage in the control of the sphingolipid pathway. The existence of several ORMDL genes may point towards different functions for each of the three proteins in a tissue-specific manner. This hypothesis is supported by data in *Ormdl1/3* deficient brains, which exhibited low levels of dihydroceramides with very long chain fatty acids, whereas *Ormdl1/3* deficient sciatic nerve exhibited high levels of these dihydroceramides [156]. Moreover, data obtained in Hela cells transfected with siRNA directed against each of the three single ORMDLs showed that all three ORMDL homologues had to be knocked down to ensure complete loss of SPT regulation [199]. There results demonstrate that, at least in sphingolipid synthesis, the three ORMDL proteins exert compensatory functions. However, because of the high sequence identity of the three genes, the investigation of ORMDL protein levels is technically very challenging. To this day, only antibodies directed against all three ORMDL proteins exist, which means that a characterization of single homologues on protein level is not possible (yet). Thus, there remains the possibility that even though some studies show uniform mRNA expression of the ORMDLs, the protein levels may still be differentially regulated in a tissue- or cellular compartment-specific manner.

4.3 Deletion of *Ormdl3* in a model of *Xbp1* deficiency alters intestinal homeostasis.

Xbp1 deficient mice develop spontaneous intestinal inflammation with histopathological features like those observed in human IBD, and especially CD [46]. *Ormdl3* deficient mice, however, have not yet been described to display a spontaneous inflammatory phenotype in the intestine [153, 162]. We here show that *Ormdl3/Xbp1* double deficiency causes a significant shortening of the small intestine. Generally, intestinal length is considered to be dependent on smooth muscle function. Since the histological scoring

of both small intestinal and colon tissue showed no differences between the two genotypes, it may be assumed that the SI shortening in *Ormdl3*$^{-/-}$/*Xbp1*$^{-\Delta IEC}$ animals arises from altered function of the underlying muscularis propria [200]. Of interest, human IBD as a transmural disease is characterized by thickening of the bowel wall with involvement of the muscularis propria, among others. Moreover, the IBD risk gene *ORMDL3* has previously been associated with the contractility of airway smooth muscle [201]. This may point towards a role of ORMDL3 to maintain muscle function not only in asthma but also in IBD.

Along with the shortening of the small intestine, *Ormdl3*/*Xbp1* double deficiency further caused development of spontaneous small intestinal inflammation under homeostatic conditions. As mentioned above, *Ormdl3* deficient mice in our group do not exhibit any signs of spontaneous intestinal inflammation and are thus in sharp contrast to the *Ormdl3*$^{-/-}$/*Xbp1*$^{-\Delta IEC}$ phenotype. One possible explanation for this discrepancy may be the different animal facilities that these strains were kept in. While *Ormdl3*$^{-/-}$/*Xbp1*$^{-\Delta IEC}$ mice and their *Ormdl3*$^{+/+}$/*Xbp1*$^{-\Delta IEC}$ littermates were kept in the Victor Hensen Animal Facility of Kiel University, *Ormdl3*$^{+/+}$ and *Ormdl3*$^{-/-}$ mice were housed in the Zentrale Tierhaltung of the University Medical Center Kiel. The phenomenon of animal facility-specific phenotypes has already been described in literature. Today, it is common sense that the hygiene status of the respective animal facility strongly impacts on disease development [202, 203]. A study by Yang *et al.* has shown that both the intestinal microbiota composition and the severity of *Helicobacter hepaticus*-induced colitis in *IL-10* deficient mice varies not only between two different SPF facilities but also inside a single facility [204]. Taken together, it can be assumed that the development of spontaneous intestinal inflammation may be dependent on the housing conditions of the animals.

Knockdown of *Ormdl3* has already been linked to apoptosis of B cells in mouse spleen as characterized, among others, by increased activation of caspase-3 [160]. The study by Dang and colleagues described a role for ORMDL3 in mediating B cell survival by induction of autophagy via a ATF6-Beclin1 pathway, which suppresses apoptosis in these cells, thus linking ORMDL3, autophagy and apoptosis. This data is supported by a previous study from our group, which could successfully show that *Ormdl3* deficiency impairs autophagy in murine IECs [162], thus underscoring the importance of ORMDL3 in regulation of the intestinal homeostasis. Furthermore, it has been described that *Xbp1* deficient mice show elevated levels of Paneth cell apoptosis due to failure to cope with ER stress [46]. Also, *Xbp1* deficient mice were described to exhibit IRE1α-dependent expansion of proliferating ISCs along the crypt-villus axis [126]. Strikingly, *Ormdl3*/*Xbp1* double deficiency also causes both increased apoptosis and cell proliferation within the small intestinal epithelium. This finding is especially interesting because increased epithelial apoptosis has been described as a feature of human IBD, which is also thought to contribute to leakage of the epithelial barrier [205]. However, since epithelial barrier permeability of the *Ormdl3*$^{-/-}$/*Xbp1*$^{-\Delta IEC}$

epithelium was not assessed within this study, it can only be speculated that the epithelial barrier function is impaired upon double deficiency.

4.3.1 *Ormdl3/Xbp1* double deficiency specifically influences Goblet cells.

The gastrointestinal mucosa is continuously exposed to food antigens and bacterial antigens. Therefore, the intestinal epithelium is protected from the resident microbiota by a physical barrier: the mucous layer. Mucous, which is composed of an inner, sterile layer and an outer, commensal bacteria containing layer, is secreted by goblet cells. Mucous has been described to be important for prevention of bacterial invasion into the underlying epithelium. Interestingly, studies in *Muc2* deficient mice have shown that these mice not only develop colitis and exhibit increased risk for colorectal cancer but also reveal disrupted intestinal barrier function [206-208]. This histopathological phenotype is described to arise from the presence of bacteria in direct contact with the intestinal epithelium. Of interest, no mutation in the human *MUC2* gene has been associated with disrupted intestinal barrier function [209]. However, inflamed ileum of CD patients has shown to exhibit reduced *MUC1* mRNA expression, while non-inflamed ileal tissue exhibited reduced *MUC3*, *4* and *5B* mRNA expression [210]. Paneth cells in the small intestine are needed for secretion of antimicrobial peptides like lysozyme to fight against invasion of pathogenic bacteria. ISCs are multipotent adult stem cells, which continuously self-renew by division and differentiation into the specialized IEC populations.

An earlier characterization of IEC populations in *Ormdl3*$^{-/-}$ mice has shown that the single deficient epithelium exhibits a significant decrease in Paneth cell numbers, along with altered bacterial killing capacity [162]. An investigation of goblet cells, another highly secretory cell type within the crypt compartment, furthermore unraveled decreased numbers of PAS positive goblet cells in colonic sections of *Ormdl3*$^{-/-}$ mice along with decreased *Muc2* expression both in ileal and colonic tissue of *E.coli* LF82 infected animals [162]. A study by Kaser *et al.* conducted in *Xbp1* deficient mice described a complete absence of Paneth cells in the small intestine, which was accompanied by substantially reduced mRNA expression of Paneth cell markers such as cryptdins and lysozyme [46]. Furthermore, the authors described a reduction of number and size of goblet cells in the small intestine in comparison to *Xbp1*$^{+/+}$ control mice [46]. Also, the group found reduced secretory granules and a decrease in *Muc2* mRNA expression in the SI, pointing towards a minor defect in goblet cells.

Based on these results we hypothesized that *Ormdl3*$^{-/-}$/*Xbp1*$^{\Delta IEC}$ mice would exhibit both alterations of Paneth cell and goblet cell function. To our surprise, we found an increase in PAS positive goblet cells, but no alteration of Paneth cell or ISC numbers or gene expression of their corresponding marker genes in the SI epithelium of *Ormdl3*$^{-/-}$/*Xbp1*$^{\Delta IEC}$ mice, respectively. In airway cells, an increase in goblet cell numbers has been described to emerge from chronic airway insult and to result in an increase in mucus production and output [211]. Consequently, it can be hypothesized that the spontaneous intestinal

inflammation in the SI of *Ormdl3*$^{-/-}$/*Xbp1*$^{\Delta IEC}$ mice caused the elevated goblet cell numbers in response to mild, but chronic inflammation under homeostasis.

4.3.2 ORMDL3 influences the immune system.

ORMDL3 is a risk gene for human autoimmune diseases like asthma and IBD, thus underscoring the importance of ORMDL3 in the regulation of the immune system. Of interest, WT mice show elevated levels of *Ormdl3* in cells from the lamina propria, a thin layer underneath the epithelium that contains a variety of immune cells, thus suggesting that also in the mouse model ORMDL3 is needed for the regulation of immune responses (Fig. 3.15). These observations are further supported by data suggesting a role for ORMDL3 in B cell development and function in mice [160]. We found that *Ormdl3*$^{-/-}$/*Xbp1*$^{\Delta IEC}$ mice exhibited significantly low levels of MHCII on IECs of the small intestine. Interestingly, IECs express MHCI and MHCII similarly to professional APCs. The antigen presentation by IECs thereby depends on inflammatory stimuli: Under homeostatic conditions, IECs mediate induction of CD4+ T cells with a regulatory phenotype while inflammatory stimuli cause IECs to activate CD4+ T cells with the capacity to secrete proinflammatory cytokines [75, 76]. Noteworthy, knockdown of *ORMDL3* in T cells has been described to cause changes in cytokine production e.g. of IFNγ, which is a proinflammatory cytokine secreted by the Th1 subset of T cells [212]. The latter is of special interest because IFNγ is necessary for maintenance of the homeostasis of intestinal epithelium [191]. Furthermore, IFNγ is known to induce MHCII expression [192]. Of note, mRNA expression analysis of IECs of young and old *Ormdl3*$^{-/-}$/*Xbp1*$^{\Delta IEC}$ mice show lower *IFNγ* levels, accompanied with significantly decreased *Cxcl10* levels with the latter being a target of IFNγ (data not shown). These results correspond to findings described for *Ormdl3*$^{-/-}$ mice, which not only exhibited less MHCII positive cells in the colon but also showed decreased IFNγ serum levels compared to *Ormdl3*$^{+/+}$ mice [153]. Taken together, it can be proposed that future research should explore the impact of ER stress associated IBD risk genes on MHCII expression on intestinal epithelial cells in the context of human IBD. This is especially important because elevated levels of MHCII, as seen in *Xbp1* single deficiency in mice, have frequently been observed in the context of mucosal inflammation as occurring in human CD [77]. However, the question remains to be answered if the impact of *Ormdl3* knockout on MHCII expression is a direct or indirect effect that may be mediated by the proinflammatory cytokine IFNγ.

4.3.3 Aging only has mild effects on the intestinal homeostasis.

Inflammatory bowel disease in humans is a complex chronic disease affecting both young and old individuals. Notably, CD has two incidence peaks with the first in the group of 20- to 30-year-old young adults and the second in the group of 60- to 70-year-old elderly. About 8-20 % of IBD patients are assumed to be older than 60 years [213, 214]. Moreover, the aging process itself is characterized by a

chronic, low-grad inflammation termed inflammaging [215]. Because of the age distribution in human IBD and the naturally occurring inflammaging process, we hypothesized that aging in mice may lead to the same spontaneous intestinal phenotype as observed in younger mice. To characterize the impact of aging specifically on the SI homeostasis, we characterized 1-year-old *Ormdl3*$^{+/+}$/*Xbp1*$^{\Delta IEC}$ and *Ormdl3*$^{-/-}$/*Xbp1*$^{\Delta IEC}$ animals (Fig. 3.12). While overall body weight and colon length of the aged animals seemed inconspicuous, the SI length in *Ormdl3*$^{-/-}$/*Xbp1*$^{\Delta IEC}$ mice showed a clear, however not significant, trend towards SI shortening similar to the observation in young mice. Since the histological score shows no significant differences between the genotypes it may well be assumed that the difference in SI length is caused by an alteration in muscularis propria function. However, since a more thorough characterization of the SI, involving e.g. assessing of IEC proliferation, apoptosis or IEC population numbers, is lacking in aged mice, further studies are needed to assess the impact of *Ormdl3*/*Xbp1* double deficiency on the aged mucosa.

4.4 The role of *Ormdl3*/*Xbp1* double deficiency in DSS-induced intestinal inflammation

A properly functioning UPR is indispensable for the maintenance of intestinal homeostasis and particularly under demanding conditions [119]. The chemical DSS is commonly used to induce colitis in mice and has been described to cause an inflammatory condition, which resembles human IBD. Even though the exact mechanism by which DSS induces colitis is unknown, studies point towards a disruption of intestinal barrier function by destruction of IECs within the basal crypt and disturbance of the microbiome [216]. Furthermore, DSS causes ER stress in IECs [119], making it a suitable tool to study specifically the function of ER stress related genes such as ORMDL3 in IECs. A previous study from our group investigated the role of ORMDL3 during intestinal inflammation in both *Ormdl3*$^{-/-}$ and *Ormdl3*$^{\Delta IEC}$ mice [153]. Of note, both *Ormdl3* deficient strains showed higher susceptibility and slower recovery to acute DSS treatment than their control littermates. Because of the association of ORMDL proteins with ER stress and the UPR, we investigated the role of *Ormdl3*/*Xbp1* double deficiency during intestinal inflammation, induced by treatment with DSS.

4.4.1 *Ormdl3*/*Xbp1* double deficiency induces apoptosis in acute inflammatory conditions.

Contrasting the results from *Ormdl3* deficient mice, which have been shown to be more susceptible than their wild type littermates, *Ormdl3*$^{-/-}$/*Xbp1*$^{\Delta IEC}$ mice showed a similar course of disease as their *Ormdl3*$^{+/+}$/*Xbp1*$^{\Delta IEC}$ littermates during acute DSS colitis, as visualized by comparable body weight loss and survival of the two genotypes (Fig. 3.13). In line with this finding, histological scoring of ileal and colonic tissue indicated equally strong levels of intestinal inflammation in mice of both genotypes and Paneth cell numbers remained unaltered by *Ormdl3*/*Xbp1* double deficiency also during intestinal

inflammation.

Noteworthy, during recovery, meaning the time span following DSS treatment in which the animals only received normal drinking water, *Ormdl3/Xbp1* double deficient animals exhibited less weight loss than their littermates. This observation suggests that *Ormdl3/Xbp1* double deficiency may be beneficial for recovery following acute inflammation. A similar effect has been found for *CHOP* deficient mice. CHOP is activated by ER stress and promotes apoptosis [217, 218]. Namba *et al.* describe *CHOP*-null mice to be resistant to development of colitis upon DSS treatment [122]. Since some mouse models with genetic deletion of other members of the ER stress response have shown contrasting phenotypes upon DSS treatment, the authors suggest that some members of the UPR are positively correlated with the development of experimental colitis while others show a negative correlation. Examples for positively correlated members are e.g. the *Xbp1* deficient mouse model or the *IRE1β* deficient mouse model, which both show increased susceptibility to DSS-induced colitis [46, 125].

Xbp1$^{-\Delta IEC}$ mice not only develop spontaneous enteritis under homeostatic conditions but are also more susceptible to DSS-induced colitis than their wild type littermates [46]. DSS-treated *Xbp1*$^{-\Delta IEC}$ colonic tissues were found to show increased levels of the pro-inflammatory cytokine tumor necrose facto alpha (TNFα). DSS-treated *Ormdl3*$^{-/-}$ mice also exhibited elevated serum levels of TNFα [153]. In human IBD, this cytokine has been described to facilitate transmural inflammation, a hallmark of CD [219]. Of note, TNFα is known to function as a potent inducer of apoptosis [220]. Therapies that target the inflammatory cytokine TNF have been found to inhibit IEC apoptosis in patients with IBD, although the exact mechanism of IEC apoptosis remains unclear [221]. Surprisingly, while IEC proliferation was unaltered, IEC apoptosis of *Ormdl3/Xbp1* double deficient animals was elevated not only under basal but also under inflammatory conditions. Preliminary results of *TNFa* mRNA expression analysis in SI crypts showed a trend towards higher *TNFa* levels in DSS-treated *Ormdl3/Xbp1* double deficient mice (data not shown). Thus, it may be speculated that the clear increase in apoptotic IECs could be a direct consequence of elevated TNFα levels within the intestinal epithelium and especially the small intestinal epithelium.

4.4.2 *Ormdl3/Xbp1* double deficiency results in increased proliferation and apoptosis under chronic inflammatory conditions.

During chronic DSS colitis, *Ormdl3*$^{-/-}$/*Xbp1*$^{-\Delta IEC}$ mice showed a similar course of disease as their *Ormdl3*$^{+/+}$/*Xbp1*$^{-\Delta IEC}$ littermates, as visualized by comparable body weight loss and survival of the two genotypes (Fig. 3.16). During chronic inflammatory conditions both IEC proliferation and IEC apoptosis were slightly, though not significantly elevated in *Ormdl3*$^{-/-}$/*Xbp1*$^{-\Delta IEC}$ mice. This finding may indicate that the intestinal barrier function in the double deficient epithelium is restored over time, thus rendering the animals more protected to prolonged ER stress by chronic exposure to DSS. The overall relatively low

units in the histological score of both SI and colon tissue as well as the body weight curve underscore this hypothesis. Thus, the outcome of this experiment proposes that *Ormdl3*$^{-/-}$/*Xbp1*$^{-\Delta IEC}$ mice are more protected under chronic inflammatory conditions than under acute inflammatory conditions. Further supported is this hypothesis by the described protective effect of *Ormdl3* deletion upon chronic DSS colitis in *Ormdl3*$^{-\Delta IEC}$ mice [153]. In summary, results of both DSS colitis experiments suggest that both ORMDL3 and XBP1 are indispensable for a proper fine-tuning of the ER stress response in inflammatory conditions.

4.5 The role of *Ormdl2* deficiency in DSS-induced intestinal inflammation

A properly functioning UPR is indispensable for the maintenance of intestinal homeostasis and particularly under demanding conditions [119]. Because of the association of ORMDL proteins with ER stress and the UPR, we investigated the role of *Ormdl2* deficiency during DSS-induced acute intestinal inflammation.

4.5.1 *Ormdl2* deficiency does not cause higher susceptibility to colitis.

QPCR data of biopsies from IBD patients show a significant upregulation of *Ormdl2* as well as *Ormdl1* in both UC and CD patients in comparison to the healthy control group. This data led us to believe that not only ORMDL3 but also ORMDL2 might be important for disease development. Thus, during this work, *Ormdl2* deficient mice were subjected to an acute DSS colitis. Since both *Ormdl1* and *Ormdl3* deficient mice have been the subject of previous studies, we herewith provide a novel insight into the pathophysiology of the *Ormdl2* deficient mouse strain. Also, the DSS-induced colitis experiment was performed based on the hypothesis that ORMDL proteins might compensate for the respective loss of one of the other two ORMDL proteins. We therefore aimed at investigating the role of *Ormdl1* and *Ormdl3*, respectively, in *Ormdl2* deficiency specifically under inflammatory conditions.

When subjecting *Ormdl2* deficient mice to acute DSS colitis, these animals showed a similar course of disease as their wild type littermates as indicated by equal levels of body weight loss and disease activity, and similar histological scores for both small intestine and colon. The outcome of the DSS treatment of *Ormdl2*$^{-/-}$ animals thus indicates that ORMDL2 does not distinctly influence the intestinal homeostasis during acute intestinal inflammatory conditions. These findings are supplemented by data from Clarke *et al.* who performed a study in *Ormdl2KO* mouse brains [156]. The authors found that the brain of *Ormdl2KO* mice contained sphingolipid levels similar to those in wild type mice, whereas *Ormdl3KO* mice showed significant phenotypical differences to their wild type littermates. These data underscore the hypothesis that among the ORMDL proteins ORMDL2 might be the most dispensable for pathological abnormalities in mice.

Of note, while Clarke *et al.* describe a partial compensatory upregulation of the three ORMDL proteins important for the control of sphingolipid levels and prevention of pathological phenotypes [156], we

found only a slight upregulation of *Ormdl3* in *Ormdl2* deficient IECs, which, however, did not result in increased ER stress. Thus, we propose that compensatory upregulation of the other two ORMDLs is dispensable in the *Ormdl2* deficient mouse model.

4.6 Conclusion and Outlook

This study´s aim was to characterize the complex function of ORMDL proteins both in the UPR and in intestinal homeostasis during basal and inflammatory conditions.

Consequently, the impact of *Ormdl3*/*Xbp1* double deficiency specifically on the murine small intestinal epithelium was investigated. Of interest, I detected elevated levels of proliferation and apoptosis, along with an increase in goblet cell numbers in the double deficient epithelium in comparison to $Ormdl3^{+/+}/Xbp1^{\Delta IEC}$. The biological origin of these phenotypes is still missing and needs further investigation. Nonetheless, it may be speculated that an increase in goblet cell numbers may lead to elevated levels of mucin production and bacterial clearance. Since *Muc2* mRNA expression was not altered, it can be assumed that *Ormdl3 Xbp1* double deficiency either affects other mucins or it alters MUC2 on a translational rather than on a transcriptional level. Possible experiments to study a goblet cell phenotype could involve the cultivation of $Ormdl3^{-/-}/Xbp1^{\Delta IEC}$ and $Ormdl3^{+/+}/Xbp1^{\Delta IEC}$ small intestinal organoids with specific medium to enrich for goblet cells [222]. Also, a repetition of RNA sequencing using goblet cell-enriched organoids would be an asset because it can be assumed that this organoid phenotype reflects the *in vivo* $Ormdl3^{-/-}/Xbp1^{\Delta IEC}$ phenotype more closely.

Additionally, a closer characterization of the post-transcriptional function of the other two UPR pathways, the ATF6 and the PERK/ATF4 pathway in $Ormdl3^{-/-}/Xbp1^{\Delta IEC}$ mice, would be of significance. The results of this investigation might be of special relevance because knockdown of ATF6 has been shown to decrease apoptosis [223]. Thus, an association of *Ormdl3*/*Xbp1* deficiency with elevated ATF6 levels may provide an explanation for the increase in apoptosis.

One major limitation of the animal model used in this study is the problem of comparing the contrasting finding to "normal" wild type controls. Particularly in the comparison of the transcriptomal patterns of $Ormdl3^{+/+}/Xbp1^{\Delta IEC}$ and $Ormdl3^{-/-}/Xbp1^{\Delta IEC}$ mice, the strong effect of the *Xbp1* deficiency may have overruled possible fragile effects of the *Ormdl3* presence or absence. Thus, further investigation of this mouse strain should involve a wild type control to enable a differentiation between $Xbp1^{fl/fl}$, $Ormdl3^{+/+}/Xbp1^{\Delta IEC}$ and $Ormdl3^{-/-}/Xbp1^{\Delta IEC}$ phenotypes.

Besides, I here show that *Ormdl2*, the homologue of the IBD risk gene *Ormdl3* does not influence the susceptibility to DSS-induced colitis in mice. However, since only a small number of mice ($Ormdl2^{+/+}$ with n = 4, $Ormdl2^{-/-}$ with n = 5) survived until the last day of acute DSS colitis, it may be reasonable to replicate these findings with more animals.

Moreover, I investigated a possible compensatory upregulation of the ORMDL homologues in case of single deficiencies. Since partial functional compensation could be observed under ER stress conditions in *Ormdl3* deficiency but not *Ormdl2* deficiency, the characterization of *Ormdl1/2/3*$^{\Delta IEC}$ mice in comparison to single deficient mice might be reasonable to elucidate possible overlapping functions of the three ORMDLs specifically in the IECs more closely.

All in all, I here further characterize the role of ORMDL3 and its homologue ORMDL2 during intestinal inflammation. This thesis thereby provides an insight into the proper interaction of ORMDL3 with the IRE1/XBP1 signaling pathway of the UPR. Thus, this study may serve as a starting point to learn more about ORMDL proteins and their role in UPR-mediated intestinal inflammation.

5 Summary

The endoplasmic reticulum (ER) in eukaryotic cells is needed for both the translation as well as the proper folding of proteins. Furthermore, the ER functions as quality control unit and is thus indispensable in the maintenance of intestinal homeostasis. Improper protein folding and accumulation of misfolded proteins in the ER cause a condition termed ER stress, which initiates the unfolded protein response (UPR) to ensure restoration of the cell's homeostasis e.g. by increased synthesis of chaperones that ensure proper protein folding. Activation of the UPR usually leads to initiation of three different signaling pathways, namely the IRE1α/XBP1, PERK/ATF4 and the ATF6 pathway.

Both ER stress and the UPR are important cellular mechanisms that occur in the intestinal epithelium of patients suffering from Inflammatory Bowel Disease (IBD). While there have been numerous studies on the UPR, only little is known about the role of the transmembrane protein ORMDL3 in IBD pathogenesis. Notably, ORMDL3 has been associated with both IBD development and the UPR and thus represents an interesting target for investigation of the UPR in IBD. To date, ORMDL3's two homologues ORMDL1 and ORMDL2 have rarely been investigated in the context of disease development, which is especially interesting because the three ORMDL proteins exhibit a high sequence identity.

Chapter 3 of this thesis demonstrates the results obtained in the present study. We show that ORMDL3 is linked to ER stress development and the activation of UPR also in murine cells. Besides, we demonstrate on gene expression level that deletion of one of the three ORMDLs in intestinal epithelial cells (IECs) can cause compensatory upregulation of the other two genes depending on the cell type investigated and the extent of cellular stress. We also show that in murine IEC lines ORMDL3 inhibits the IRE1α/XBP1 signaling pathway of the UPR.

To study the function of ORMDL3 in a specific UPR signaling pathway, we generated and characterized *Ormdl3*$^{-/-}$/*Xbp1*$^{-\Delta IEC}$ mice with a whole-body deletion of *Ormdl3* and an IEC-specific deletion of *Xbp1*. We were especially interested in characterizing the interplay between ORMDL3 and the IRE1α/XBP1 signaling pathway because XBP1 has also been characterized as IBD risk gene. Of interest, IEC-specific deletion of *Xbp1* in mice was shown to cause spontaneous intestinal inflammation in the SI epithelium, which resembles that of human IBD [46].

When comparing *Ormdl3*$^{-/-}$/*Xbp1*$^{-\Delta IEC}$ mice with *Ormdl3*$^{+/+}$/*Xbp1*$^{-\Delta IEC}$ control animals, we found the SI of the double deficient animals to be significantly shortened. Moreover, the SI displayed signs of spontaneous intestinal inflammation as well as increased levels of apoptosis and proliferation in the epithelium. We further noted lower levels of MHCII on IECs of *Ormdl3*$^{-/-}$/*Xbp1*$^{-\Delta IEC}$ mice. Interestingly, the basal SI phenotype described above, is not reflected in elevated mRNA expression levels of IEC marker genes or histological scores when compared to *Ormdl3*$^{+/+}$/*Xbp1*$^{-\Delta IEC}$ controls. We describe that

aging of *Ormdl3*$^{-/-}$/*Xbp1*$^{-\Delta IEC}$ mice causes a SI phenotype similar to that observed in young animals. This phenomenon has also been observed in human IBD, where mostly two incidence peaks exist: one being at about 20-30 of age in young people and the other being at about 60-70 years of age, respectively.

Additional to the results of basal phenotyping, we also show the outcome of both an acute and a chronic DSS-induced colitis. While chronic DSS colitis seemed to have an overall mild effect on cellular processes like apoptosis or proliferation in the *Ormdl3*$^{-/-}$/*Xbp1*$^{-\Delta IEC}$ mouse model, acute DSS colitis significantly induced apoptosis. This observation led us to believe that the *Ormdl3*$^{-/-}$/*Xbp1*$^{-\Delta IEC}$ mouse is generally more susceptible to acute ER stress conditions, e.g. caused by DSS treatment or spontaneous basal inflammatory responses, than to chronic ER stress.

Due to the high amino acid homology of the three ORMDL proteins and because of a lack of data on the topic, we further investigated *Ormdl2* deficiency in an acute DSS colitis. The data obtained from this experiment suggest that ORMDL2 seems to be dispensable for maintaining intestinal homeostasis in murine IECs since both *Ormdl2*$^{-/-}$ mice and control animals show equal levels of susceptibility to colitis.

Taken together, ORMDL proteins and especially ORMDL3 play a major role in maintaining intestinal homeostasis both under basal and inflammatory conditions. Moreover, the interaction between ORMDL3 and XBP1 is a key component in regulation of homeostasis, which is also underscored by the characterization of both genes as IBD risk genes.

6 Zusammenfassung

Das Endoplasmatische Retikulum (ER) in eukaryotischen Zellen dient der Translation von Proteinen sowie der Proteinfaltung. Da dem ER außerdem die Aufgabe der Qualitätskontrolle zukommt, ist dieses Organell ein entscheidender Faktor in der Aufrechterhaltung der Zellfunktion. Bei fehlerhafter Faltung von Proteinen sowie deren Anhäufung im ER wird eine Stressantwort ausgelöst (genannt ER-Stress), welche die sogenannte *Unfolded Protein Response* (UPR) aktiviert. Letztere dient der Wiederherstellung der zellulären Homöostase, z.B. durch den Abbau fehlerhaft gefalteter Proteine und der Synthese von solchen Chaperonen, die für eine einwandfreie Proteinfaltung benötigt werden. Die Aktivierung der UPR erfolgt mittels der zwei Kinasen IRE1α und PERK sowie dem Transmembran-Transkriptionsfaktor ATF6α, welche jeweils unterschiedliche UPR-Signalwege auslösen.

Interessanterweise spielen sowohl ER-Stress als auch die *UPR* im intestinalen Epithel von Patienten mit chronisch-entzündlichen Darmerkrankungen (CED) eine entscheidende Rolle. Während die UPR an sich bereits Gegenstand vieler Studien war, ist über die Rolle des Transmembranproteins ORMDL3, das als CED-Risikogen identifiziert wurde und mit der UPR assoziiert ist, in der CED-Krankheitsentstehung bislang wenig bekannt. Auch die zwei homologen Gene von *ORMDL3*, *ORMDL1* und *ORMDL2* wurden im Zusammenhang mit CED bisher nur selten untersucht.

In Kapitel 3 dieser Arbeit werden die Ergebnisse dieser Studie dargestellt und erläutert. Wir zeigen, dass ORMDL3 auch in murinen Zellen mit der Entstehung von ER-Stress und der Aktivierung der *UPR* assoziiert ist. Auf Genexpressions-Level kann die Deletion eines ORMDL-Homologs in intestinalen Epithelzellen (*intestinal epithelial cells, IECs*) zu einer Funktionsübernahme durch die anderen beiden Gene führen, wie es durch die hohe Sequenz-Identität zu vermuten wäre. Diese Funktionsübernahme ist dabei abhängig vom untersuchten Zelltypen sowie der Art und Dauer des zellulären Stresses. Außerdem zeigen wir, dass ORMDL3 in der murinen Zelllinie ModeK den IRE1/XBP1-Signalweg der *UPR* inhibiert.

Um die Funktion von ORMDL3 vor dem Hintergrund eines einzelnen UPR-Signalweges studieren zu können, wurden *Ormdl3*$^{-/-}$/*Xbp1*$^{\perp IEC}$-Mäuse generiert, welche eine Deletion von *Ormdl3* im gesamten Organismus sowie eine *IEC*-spezifische Deletion von *Xbp1* aufweisen. Der IRE1/Xbp1-Signalweg der UPR war deshalb von besonderem Interesse, weil XBP1 ebenfalls als CED-Risikogen beschrieben wurde und in einem Mausmodell eine spontane intestinale Entzündung zeigte, die derjenigen der menschlichen CED sehr ähnelt [46]. Diese Studie zeigt auf, dass die *Ormdl3*$^{-/-}$/*Xbp1*$^{\perp IEC}$-Maus im Vergleich zu *Ormdl3*$^{+/+}$/*Xbp1*$^{\perp IEC}$-Kontrolltieren einen verkürzten Dünndarm mit erhöhter Apoptose und Proliferation aufweist, der zudem eine spontane Entzündung unter basalen Bedingungen entwickelt. Außerdem weist die *Ormdl3*$^{-/-}$/*Xbp1*$^{\perp IEC}$-Maus geringere MHCII-Level auf *IECs* auf als die *Ormdl3*$^{+/+}$/*Xbp1*$^{\perp IEC}$-Kontrolltiere. Interessanterweise bezieht sich der beschriebene basale Phänotyp nur auf den Dünndarm der Tiere und spiegelt sich nicht in einer erhöhten Genexpression von IEC-

Markergenen oder einem histologischen Score im Vergleich zu *Ormdl3*$^{+/+}$/*Xbp1*$^{-\Delta IEC}$-Kontrolltieren wider. Die zusätzliche Untersuchung des Phänotyps während des Alterungsprozesses der *Ormdl3*$^{-/-}$/*Xbp1*$^{-\Delta IEC}$-Maus präsentiert einen ähnlichen Phänotypen wie denjenigen in jüngeren Tieren. Dieses Phänomen spiegelt somit die menschlichen CED wider, in denen hauptsächlich junge (20-30 Jahre) und alte Personen (60-70 Jahre) diagnostiziert werden.

Zusätzlich zu der basalen Phänotypisierung zeigen wir außerdem die Ergebnisse einer akuten sowie einer chronischen DSS-Kolitis. Während die chronische Kolitis nur einen geringen Einfluss auf zelluläre Prozesse wie Apoptose und Proliferation in der *Ormdl3*$^{-/-}$/*Xbp1*$^{-\Delta IEC}$-Maus zu haben scheint, induziert die akute Kolitis erhöhte Apoptose. In Anbetracht dieser Ergebnisse vermuten wir, dass die *Ormdl3*$^{-/-}$ *Xbp1*$^{-\Delta IEC}$-Maus generell suszeptibler für akuten ER-Stress, ausgelöst durch DSS-Behandlung oder spontane basale Entzündungsreaktionen, als für chronischen ER-Stress ist.

Aufgrund der bereits erwähnten hohen Sequenz-Identität der drei ORMDL-Homologe sowie der bislang noch fehlenden Ergebnisse, wurde zudem eine *Ormdl2*-Defizienz in einer akuten DSS-Kolitis untersucht. Die in diesem Versuch gewonnenen Ergebnisse zeigen, dass ORMDL2 in der intestinalen Homöostase von murinen IECs keine entscheidende Funktion inne zu haben scheint, da dieses Mausmodell ähnliche Suszeptibilität zeigt wie die Kontrolltiere.

Zusammenfassend lässt sich festhalten, dass ORMDL-Proteine, und insbesondere ORMDL3, eine entscheidende Rolle in der Aufrechterhaltung der intestinalen Homöostase unter basalen und entzündlichen Bedingungen spielen. Zudem scheint der Interaktion von ORMDL3 und XBP1 eine besondere Rolle zuzukommen, was durch die Charakterisierung beider Gene als CED-Risikogene unterstrichen wird.

7 References

1. Ventham, N.T., et al., *Beyond gene discovery in inflammatory bowel disease: the emerging role of epigenetics.* Gastroenterology, 2013. **145**(2): p. 293-308.
2. Aden, K., et al., *Classic IL-6R signalling is dispensable for intestinal epithelial proliferation and repair.* Oncogenesis, 2016. **5**(11): p. e270.
3. Zheng, J.J., et al., *Crohn's disease in mainland China: a systematic analysis of 50 years of research.* Chin J Dig Dis, 2005. **6**(4): p. 175-81.
4. Ng, S.C., et al., *Worldwide incidence and prevalence of inflammatory bowel disease in the 21st century: a systematic review of population-based studies.* Lancet, 2018. **390**(10114): p. 2769-2778.
5. Molodecky, N.A., et al., *Increasing incidence and prevalence of the inflammatory bowel diseases with time, based on systematic review.* Gastroenterology, 2012. **142**(1): p. 46-54.e42; quiz e30.
6. El-Matary, W., S.P. Moroz, and C.N. Bernstein, *Inflammatory bowel disease in children of Manitoba: 30 years' experience of a tertiary center.* J Pediatr Gastroenterol Nutr, 2014. **59**(6): p. 763-6.
7. Benchimol, E.I., et al., *Inflammatory bowel disease in immigrants to Canada and their children: a population-based cohort study.* Am J Gastroenterol, 2015. **110**(4): p. 553-63.
8. Benchimol, E.I., et al., *Epidemiology of pediatric inflammatory bowel disease: a systematic review of international trends.* Inflamm Bowel Dis, 2011. **17**(1): p. 423-39.
9. Ponder, A. and M.D. Long, *A clinical review of recent findings in the epidemiology of inflammatory bowel disease.* Clin Epidemiol, 2013. **5**: p. 237-47.
10. Parente, J.M., et al., *Inflammatory bowel disease in an underdeveloped region of Northeastern Brazil.* World J Gastroenterol, 2015. **21**(4): p. 1197-206.
11. Bernstein, C.N. and F. Shanahan, *Disorders of a modern lifestyle: reconciling the epidemiology of inflammatory bowel diseases.* Gut, 2008. **57**(9): p. 1185-91.
12. Shanahan, F. and C.N. Bernstein, *The evolving epidemiology of inflammatory bowel disease.* Curr Opin Gastroenterol, 2009. **25**(4): p. 301-5.
13. Li, X., et al., *Risk of inflammatory bowel disease in first- and second-generation immigrants in Sweden: a nationwide follow-up study.* Inflamm Bowel Dis, 2011. **17**(8): p. 1784-91.
14. Luther, J., et al., *Association between Helicobacter pylori infection and inflammatory bowel disease: a meta-analysis and systematic review of the literature.* Inflamm Bowel Dis, 2010. **16**(6): p. 1077-84.
15. Calkins, B.M., *A meta-analysis of the role of smoking in inflammatory bowel disease.* Dig Dis Sci, 1989. **34**(12): p. 1841-54.
16. Bernstein, C.N., et al., *The epidemiology of inflammatory bowel disease in Canada: a population-based study.* Am J Gastroenterol, 2006. **101**(7): p. 1559-68.
17. Ouyang, Q., et al., *The emergence of inflammatory bowel disease in the Asian Pacific region.* Curr Opin

Gastroenterol, 2005. **21**(4): p. 408-13.

18. Loftus, E.V., Jr., *Clinical epidemiology of inflammatory bowel disease: Incidence, prevalence, and environmental influences.* Gastroenterology, 2004. **126**(6): p. 1504-17.
19. Sakamoto, N., et al., *Dietary risk factors for inflammatory bowel disease: a multicenter case-control study in Japan.* Inflamm Bowel Dis, 2005. **11**(2): p. 154-63.
20. Amre, D.K., et al., *Imbalances in dietary consumption of fatty acids, vegetables, and fruits are associated with risk for Crohn's disease in children.* Am J Gastroenterol, 2007. **102**(9): p. 2016-25.
21. Reif, S., et al., *Pre-illness dietary factors in inflammatory bowel disease.* Gut, 1997. **40**(6): p. 754-60.
22. Halfvarson, J., et al., *Environmental factors in inflammatory bowel disease: a co-twin control study of a Swedish-Danish twin population.* Inflamm Bowel Dis, 2006. **12**(10): p. 925-33.
23. Baron, S., et al., *Environmental risk factors in paediatric inflammatory bowel diseases: a population based case control study.* Gut, 2005. **54**(3): p. 357-63.
24. Plat, J. and R.P. Mensink, *Food components and immune function.* Curr Opin Lipidol, 2005. **16**(1): p. 31-37.
25. Jostins, L., et al., *Host-microbe interactions have shaped the genetic architecture of inflammatory bowel disease.* Nature, 2012. **491**(7422): p. 119-24.
26. Wei, S.C., et al., *SLCO3A1, A novel crohn's disease-associated gene, regulates nf-kappaB activity and associates with intestinal perforation.* PLoS One, 2014. **9**(6): p. e100515.
27. Ozen, S.C., et al., *NOD2/CARD15, NOD1/CARD4, and ICAM-1 gene polymorphisms in Turkish patients with inflammatory bowel disease.* J Gastroenterol, 2006. **41**(4): p. 304-10.
28. Juyal, G., et al., *An investigation of genome-wide studies reported susceptibility loci for ulcerative colitis shows limited replication in north Indians.* PLoS One, 2011. **6**(1): p. e16565.
29. Guo, Q.S., et al., *NOD2 3020insC frameshift mutation is not associated with inflammatory bowel disease in Chinese patients of Han nationality.* World J Gastroenterol, 2004. **10**(7): p. 1069-71.
30. Inoue, N., et al., *Lack of common NOD2 variants in Japanese patients with Crohn's disease.* Gastroenterology, 2002. **123**(1): p. 86-91.
31. Ozaki, K., et al., *Functional SNPs in the lymphotoxin-alpha gene that are associated with susceptibility to myocardial infarction.* Nat Genet, 2002. **32**(4): p. 650-4.
32. Mirkov, M.U., B. Verstockt, and I. Cleynen, *Genetics of inflammatory bowel disease: beyond NOD2.* Lancet Gastroenterol Hepatol, 2017. **2**(3): p. 224-234.
33. Huang, H.L., et al., *Fine-mapping inflammatory bowel disease loci to single-variant resolution.* Nature, 2017. **547**(7662): p. 173-178.
34. Lee, J.C., et al., *Genome-wide association study identifies distinct genetic contributions to prognosis and susceptibility in Crohn's disease.* Nat Genet, 2017. **49**(2): p. 262-268.
35. Hugot, J.P., et al., *Association of NOD2 leucine-rich repeat variants with susceptibility to Crohn's disease.*

Nature, 2001. **411**(6837): p. 599-603.

36. Ogura, Y., et al., *A frameshift mutation in NOD2 associated with susceptibility to Crohn's disease.* Nature, 2001. **411**(6837): p. 603-6.
37. Shaw, M.H., et al., *NOD-like receptors (NLRs): bona fide intracellular microbial sensors.* Curr Opin Immunol, 2008. **20**(4): p. 377-82.
38. Rivas, M.A., et al., *Deep resequencing of GWAS loci identifies independent rare variants associated with inflammatory bowel disease.* Nat Genet, 2011. **43**(11): p. 1066-73.
39. Feerick, C.L. and D.P. McKernan, *Understanding the regulation of pattern recognition receptors in inflammatory diseases - a 'Nod' in the right direction.* Immunology, 2017. **150**(3): p. 237-247.
40. Hugot, J.P., et al., *Prevalence of CARD15/NOD2 mutations in Caucasian healthy people.* Am J Gastroenterol, 2007. **102**(6): p. 1259-67.
41. Hampe, J., et al., *A genome-wide association scan of nonsynonymous SNPs identifies a susceptibility variant for Crohn disease in ATG16L1.* Nat Genet, 2007. **39**(2): p. 207-11.
42. Rioux, J.D., et al., *Genome-wide association study identifies new susceptibility loci for Crohn disease and implicates autophagy in disease pathogenesis.* Nat Genet, 2007. **39**(5): p. 596-604.
43. Wellcome Trust Case Control, C., *Genome-wide association study of 14,000 cases of seven common diseases and 3,000 shared controls.* Nature, 2007. **447**(7145): p. 661-78.
44. Adolph, T.E., et al., *Paneth cells as a site of origin for intestinal inflammation.* Nature, 2013. **503**(7475): p. 272-6.
45. Zheng, W., et al., *Evaluation of AGR2 and AGR3 as candidate genes for inflammatory bowel disease.* Genes Immun, 2006. **7**(1): p. 11-8.
46. Kaser, A., et al., *XBP1 links ER stress to intestinal inflammation and confers genetic risk for human inflammatory bowel disease.* Cell, 2008. **134**(5): p. 743-56.
47. McGovern, D.P., et al., *Genome-wide association identifies multiple ulcerative colitis susceptibility loci.* Nat Genet, 2010. **42**(4): p. 332-7.
48. Barrett, J.C., et al., *Genome-wide association defines more than 30 distinct susceptibility loci for Crohn's disease.* Nat Genet, 2008. **40**(8): p. 955-62.
49. Moffatt, M.F., et al., *Genetic variants regulating ORMDL3 expression contribute to the risk of childhood asthma.* Nature, 2007. **448**(7152): p. 470-3.
50. Duerr, R.H., et al., *A genome-wide association study identifies IL23R as an inflammatory bowel disease gene.* Science, 2006. **314**(5804): p. 1461-3.
51. Sivanesan, D., et al., *IL23R (Interleukin 23 Receptor) Variants Protective against Inflammatory Bowel Diseases (IBD) Display Loss of Function due to Impaired Protein Stability and Intracellular Trafficking.* J Biol Chem, 2016. **291**(16): p. 8673-85.
52. Schreiber, S., et al., *Immunoregulatory role of interleukin 10 in patients with inflammatory bowel disease.*

Gastroenterology, 1995. **108**(5): p. 1434-44.

53. Murata, Y., et al., *The role of proinflammatory and immunoregulatory cytokines in the pathogenesis of ulcerative colitis.* J Gastroenterol, 1995. **30 Suppl 8**: p. 56-60.
54. Tagore, A., et al., *Interleukin-10 (IL-10) genotypes in inflammatory bowel disease.* Tissue Antigens, 1999. **54**(4): p. 386-90.
55. Ahmad, T., S.-E. Marshall, and D. Jewell, *Genetics of inflammatory bowel disease: the role of the HLA complex.* World J Gastroenterol, 2006. **12**(23): p. 3628-3635.
56. Degenhardt, F., et al., *Trans-ethnic analysis of the human leukocyte antigen region for ulcerative colitis reveals shared but also ethnicity-specific disease associations.* Hum Mol Genet, 2021.
57. Spence, J.R., R. Lauf, and N.F. Shroyer, *Vertebrate intestinal endoderm development.* Dev Dyn., 2011. **240**(3): p. 501-520.
58. Sangiorgi, E. and M.R. Capecchi, *Bmi1 is expressed in vivo in intestinal stem cells.* Nat Genet, 2008. **40**(7): p. 915-20.
59. Yan, K.S., et al., *The intestinal stem cell markers Bmi1 and Lgr5 identify two functionally distinct populations.* Proc Natl Acad Sci U S A, 2012. **109**(2): p. 466-71.
60. Powell, A.E., et al., *The pan-ErbB negative regulator Lrig1 is an intestinal stem cell marker that functions as a tumor suppressor.* Cell, 2012. **149**(1): p. 146-58.
61. Wong, V.W., et al., *Lrig1 controls intestinal stem-cell homeostasis by negative regulation of ErbB signalling.* Nat Cell Biol, 2012. **14**(4): p. 401-8.
62. Flier, L.G.v.d. and H. Clevers, *Stem Cells, Self-Renewal, and Differentiation in the Intestinal Epithelium.* Annu Rev Physiol. , 2009. **71**(1): p. 241-260.
63. Breese, E., et al., *Interleukin-2- and interferon-gamma-secreting T cells in normal and diseased human intestinal mucosa.* Immunology, 1993. **78**(1): p. 127-131.
64. Noguchi, M., et al., *Enhanced interferon-gamma production and B7-2 expression in isolated intestinal mononuclear cells from patients with Crohn's disease.* J Gastroenterol, 1995. **30 Suppl 8**: p. 52-5.
65. Camoglio, L., et al., *Altered expression of interferon-gamma and interleukin-4 in inflammatory bowel disease.* Inflamm Bowel Dis, 1998. **4**(4): p. 285-90.
66. Heller, F., et al., *Interleukin-13 is the key effector Th2 cytokine in ulcerative colitis that affects epithelial tight junctions, apoptosis, and cell restitution.* Gastroenterology, 2005. **129**(2): p. 550-64.
67. Fuss, I.J., et al., *Nonclassical CD1d-restricted NK T cells that produce IL-13 characterize an atypical Th2 response in ulcerative colitis.* J Clin Invest, 2004. **113**(10): p. 1490-7.
68. Vainer, B., et al., *Colonic expression and synthesis of interleukin 13 and interleukin 15 in inflammatory bowel disease.* Cytokine, 2000. **12**(10): p. 1531-6.
69. Wilson, M.S., et al., *Colitis and intestinal inflammation in IL10-/- mice results from IL-13Ra2-mediated attenuation of IL-13 activity.* Gastroenterology, 2011. **140**(1): p. 254-64.

70. Rovedatti, L., et al., *Differential regulation of interleukin 17 and interferon gamma production in inflammatory bowel disease.* Gut, 2009. **58**(12): p. 1629-36.
71. Sugihara, T., et al., *The increased mucosal mRNA expressions of complement C3 and interleukin-17 in inflammatory bowel disease.* Clin. Exp. Immunol., 2010. **160**(3): p. 386-393.
72. Morrissey, P.J. and K. Charrier, *Induction of wasting disease in SCID mice by the transfer of normal CD4+/CD45RBhi T cells and the regulation of this autoreactivity by CD4+/CD45RBlo T cells.* Res Immunol, 1994. **145**(5): p. 357-62.
73. Powrie, F., et al., *Inhibition of Th1 responses prevents inflammatory bowel disease in scid mice reconstituted with CD45RBhi CD4+ T cells.* Immunity, 1994. **1**(7): p. 553-62.
74. Cahill, R.J., et al., *Inflammatory bowel disease: an immunity-mediated condition triggered by bacterial infection with Helicobacter hepaticus.* Infect Immun, 1997. **65**(8): p. 3126-31.
75. Hershberg, R.M., et al., *Intestinal epithelial cells use two distinct pathways for HLA class II antigen processing.* J Clin Invest, 1997. **100**(1): p. 204-215.
76. Hershberg, R.M. and L.F. Mayer, *Antigen processing and presentation by intestinal epithelial cells - polarity and complexity.* Immunol Today, 2000. **21**(3): p. 123-8.
77. Bar, F., et al., *Inflammatory bowel diseases influence major histocompatibility complex class I (MHC I) and II compartments in intestinal epithelial cells.* Clin Exp Immunol, 2013. **172**(2): p. 280-9.
78. Bianconi, E., et al., *An estimation of the number of cells in the human body.* Ann. Hum. Biol, 2013. **40**(6): p. 463-471.
79. Sender, R., S. Fuchs, and R. Milo, *Revised Estimates for the Number of Human and Bacteria Cells in the Body.* PLoS Biol, 2016. **14**(8): p. e1002533.
80. Rautava, S. and W.A. Walker, *Commensal bacteria and epithelial cross talk in the developing intestine.* Curr Gastroenterol Rep, 2007. **9**(5): p. 385-92.
81. Gophna, U., et al., *Differences between tissue-associated intestinal microfloras of patients with Crohn's disease and ulcerative colitis.* J. Clin. Microbiol., 2006. **44**(11): p. 4136-4141.
82. Frank, D.N., et al., *Molecular-phylogenetic characterization of microbial community imbalances in human inflammatory bowel diseases.* Proc Natl Acad Sci U S A, 2007. **104**(34): p. 13780-5.
83. Gevers, D., et al., *The treatment-naive microbiome in new-onset Crohn's disease.* Cell Host Microbe, 2014. **15**(3): p. 382-392.
84. Kostic, A.D., R.J. Xavier, and D. Gevers, *The microbiome in inflammatory bowel disease: current status and the future ahead.* Gastroenterology, 2014. **146**(6): p. 1489-99.
85. Faitova, J., et al., *Endoplasmic reticulum stress and apoptosis.* Cell Mol Biol Lett, 2006. **11**(4): p. 488-505.
86. Bertolotti, A., et al., *Dynamic interaction of BiP and ER stress transducers in the unfolded-protein response.* Nat Cell Biol, 2000. **2**(6): p. 326-32.

87. Wu, J., et al., *ATF6alpha optimizes long-term endoplasmic reticulum function to protect cells from chronic stress.* Dev Cell, 2007. **13**(3): p. 351-64.

88. Haze, K., et al., *Mammalian transcription factor ATF6 is synthesized as a transmembrane protein and activated by proteolysis in response to endoplasmic reticulum stress.* Mol Biol Cell, 1999. **10**(11): p. 3787-99.

89. Ron, D. and P. Walter, *Signal integration in the endoplasmic reticulum unfolded protein response.* Nat Rev Mol Cell Biol, 2007. **8**(7): p. 519-29.

90. Yamamoto, K., et al., *Transcriptional induction of mammalian ER quality control proteins is mediated by single or combined action of ATF6alpha and XBP1.* Dev Cell, 2007. **13**(3): p. 365-76.

91. Fu, S., et al., *Aberrant lipid metabolism disrupts calcium homeostasis causing liver endoplasmic reticulum stress in obesity.* Nature, 2011. **473**(7348): p. 528-31.

92. Volmer, R., K. van der Ploeg, and D. Ron, *Membrane lipid saturation activates endoplasmic reticulum unfolded protein response transducers through their transmembrane domains.* Proc Natl Acad Sci U S A, 2013. **110**(12): p. 4628-33.

93. Chan, C.P., et al., *Internal ribosome entry site-mediated translational regulation of ATF4 splice variant in mammalian unfolded protein response.* Biochim Biophys Acta, 2013. **1833**(10): p. 2165-75.

94. Palam, L.R., T.D. Baird, and R.C. Wek, *Phosphorylation of eIF2 facilitates ribosomal bypass of an inhibitory upstream ORF to enhance CHOP translation.* J Biol Chem, 2011. **286**(13): p. 10939-49.

95. Harding, H.P., et al., *Regulated translation initiation controls stress-induced gene expression in mammalian cells.* Mol Cell, 2000. **6**(5): p. 1099-108.

96. Marciniak, S.J., et al., *CHOP induces death by promoting protein synthesis and oxidation in the stressed endoplasmic reticulum.* Genes Dev, 2004. **18**(24): p. 3066-77.

97. Song, B., et al., *Chop deletion reduces oxidative stress, improves beta cell function, and promotes cell survival in multiple mouse models of diabetes.* J Clin Invest, 2008. **118**(10): p. 3378-89.

98. Claudio, N., et al., *Mapping the crossroads of immune activation and cellular stress response pathways.* EMBO J, 2013. **32**(9): p. 1214-24.

99. Ravindran, R., et al., *The amino acid sensor GCN2 controls gut inflammation by inhibiting inflammasome activation.* Nature, 2016. **531**(7595): p. 523-527.

100. Hetz, C. and L.H. Glimcher, *Fine-tuning of the unfolded protein response: Assembling the IRE1alpha interactome.* Mol Cell, 2009. **35**(5): p. 551-61.

101. Hetz, C., et al., *The unfolded protein response: integrating stress signals through the stress sensor IRE1alpha.* Physiol Rev, 2011. **91**(4): p. 1219-43.

102. Chen, Y. and F. Brandizzi, *AtIRE1A/AtIRE1B and AGB1 independently control two essential unfolded protein response pathways in Arabidopsis.* Plant J, 2012. **69**(2): p. 266-77.

103. Nagashima, Y., et al., *Arabidopsis IRE1 catalyses unconventional splicing of bZIP60 mRNA to produce the active transcription factor.* Sci Rep, 2011. **1**: p. 29.

104. Acosta-Alvear, D., et al., *XBP1 controls diverse cell type- and condition-specific transcriptional regulatory networks.* Mol Cell, 2007. **27**(1): p. 53-66.

105. Lee, A.H., N.N. Iwakoshi, and L.H. Glimcher, *XBP-1 regulates a subset of endoplasmic reticulum resident chaperone genes in the unfolded protein response.* Mol Cell Biol, 2003. **23**(21): p. 7448-59.

106. Yamamoto, K., et al., *Human HRD1 promoter carries a functional unfolded protein response element to which XBP1 but not ATF6 directly binds.* J Biochem, 2008. **144**(4): p. 477-86.

107. Yoshida, H., et al., *ATF6 activated by proteolysis binds in the presence of NF-Y (CBF) directly to the cis-acting element responsible for the mammalian unfolded protein response.* Mol Cell Biol, 2000. **20**(18): p. 6755-67.

108. Yoshida, H., et al., *XBP1 mRNA is induced by ATF6 and spliced by IRE1 in response to ER stress to produce a highly active transcription factor.* Cell, 2001. **107**(7): p. 881-91.

109. Yoshida, H., A. Uemura, and K. Mori, *pXBP1(U), a negative regulator of the unfolded protein response activator pXBP1(S), targets ATF6 but not ATF4 in proteasome-mediated degradation.* Cell Struct Funct, 2009. **34**(1): p. 1-10.

110. Ma, Y., et al., *Two distinct stress signaling pathways converge upon the CHOP promoter during the mammalian unfolded protein response.* J Mol Biol, 2002. **318**(5): p. 1351-65.

111. Okada, T., et al., *Distinct roles of activating transcription factor 6 (ATF6) and double-stranded RNA-activated protein kinase-like endoplasmic reticulum kinase (PERK) in transcription during the mammalian unfolded protein response.* Biochem J, 2002. **366**(Pt 2): p. 585-94.

112. Chang, T.-K., et al., *Coordination between Two Branches of the Unfolded Protein Response Determines Apoptotic Cell Fate.* Molecular Cell, 2018. **71**(4): p. 629-636.e5.

113. Selsted, M.E. and A.J. Ouellette, *Mammalian defensins in the antimicrobial immune response.* Nat Immunol, 2005. **6**(6): p. 551-7.

114. Salzman, N.H., et al., *Enteric defensins are essential regulators of intestinal microbial ecology.* Nat Immunol, 2010. **11**(1): p. 76-83.

115. Vaishnava, S., et al., *Paneth cells directly sense gut commensals and maintain homeostasis at the intestinal host-microbial interface.* Proc Natl Acad Sci U S A, 2008. **105**(52): p. 20858-63.

116. Shkoda, A., et al., *Interleukin-10 blocked endoplasmic reticulum stress in intestinal epithelial cells: impact on chronic inflammation.* Gastroenterology, 2007. **132**(1): p. 190-207.

117. Wang, Z., Y. Hao, and A.W. Lowe, *The adenocarcinoma-associated antigen, AGR2, promotes tumor growth, cell migration, and cellular transformation.* Cancer Res, 2008. **68**(2): p. 492-7.

118. Zhao, F., et al., *Disruption of Paneth and goblet cell homeostasis and increased endoplasmic reticulum stress in Agr2-/- mice.* Dev Biol, 2010. **338**(2): p. 270-9.

119. Cao, S.S., et al., *The unfolded protein response and chemical chaperones reduce protein misfolding and colitis in mice.* Gastroenterology, 2013. **144**(5): p. 989-1000 e6.

120. Liu, B., et al., *Essential roles of grp94 in gut homeostasis via chaperoning canonical Wnt pathway.* Proc Natl Acad Sci U S A, 2013. **110**(17): p. 6877-82.

121. Brandl, K., et al., *Enhanced sensitivity to DSS colitis caused by a hypomorphic Mbtps1 mutation disrupting the ATF6-driven unfolded protein response.* Proc Natl Acad Sci U S A, 2009. **106**(9): p. 3300-5.

122. Namba, T., et al., *Positive role of CCAAT/enhancer-binding protein homologous protein, a transcription factor involved in the endoplasmic reticulum stress response in the development of colitis.* Am J Pathol, 2009. **174**(5): p. 1786-98.

123. Reimold, A.M., et al., *An essential role in liver development for transcription factor XBP-1.* Genes Dev, 2000. **14**(2): p. 152-7.

124. Zhang, K., et al., *The unfolded protein response sensor IRE1alpha is required at 2 distinct steps in B cell lymphopoiesis.* J Clin Invest, 2005. **115**(2): p. 268-81.

125. Bertolotti, A., et al., *Increased sensitivity to dextran sodium sulfate colitis in IRE1beta-deficient mice.* J Clin Invest, 2001. **107**(5): p. 585-93.

126. Niederreiter, L., et al., *ER stress transcription factor Xbp1 suppresses intestinal tumorigenesis and directs intestinal stem cells.* J Exp Med, 2013. **210**(10): p. 2041-56.

127. Yu, H., D. Pardoll, and R. Jove, *STATs in cancer inflammation and immunity: a leading role for STAT3.* Nat Rev Cancer, 2009. **9**(11): p. 798-809.

128. Vallabhapurapu, S. and M. Karin, *Regulation and function of NF-kappaB transcription factors in the immune system.* Annu Rev Immunol, 2009. **27**: p. 693-733.

129. Hjelmqvist, L., et al., *ORMDL proteins are a conserved new family of endoplasmic reticulum membrane proteins.* Genome Biol, 2002. **3**(6): p. Research0027.

130. Cantero-Recasens, G., et al., *The asthma-associated ORMDL3 gene product regulates endoplasmic reticulum-mediated calcium signaling and cellular stress.* Hum Mol Genet, 2010. **19**(1): p. 111-21.

131. Hirota, T., et al., *Genetic polymorphism regulating ORM1-like 3 (Saccharomyces cerevisiae) expression is associated with childhood atopic asthma in a Japanese population.* J Allergy Clin Immunol, 2008. **121**(3): p. 769-70.

132. Sleiman, P.M., et al., *ORMDL3 variants associated with asthma susceptibility in North Americans of European ancestry.* J Allergy Clin Immunol, 2008. **122**(6): p. 1225-7.

133. Tavendale, R., et al., *A polymorphism controlling ORMDL3 expression is associated with asthma that is poorly controlled by current medications.* J Allergy Clin Immunol, 2008. **121**(4): p. 860-3.

134. Moffatt, M.F., et al., *A large-scale, consortium-based genomewide association study of asthma.* N Engl J Med, 2010. **363**(13): p. 1211-1221.

135. Fang, Q., et al., *Association of genetic variants in chromosome 17q21 and adult-onset asthma in a Chinese Han population.* BMC Med Genet, 2011. **12**: p. 133.

136. Hoefkens, E., et al., *Genetic association and functional role of Crohn disease risk alleles involved in microbial*

sensing, autophagy, and endoplasmic reticulum (ER) stress. Autophagy, 2013. **9**(12): p. 2046-55.

137. Barrett, J.C., et al., *Genome-wide association defines more than 30 distinct susceptibility loci for Crohn's disease.* Nat Genet, 2008. **40**(8): p. 955-62.

138. Hsu, K.J. and S.E. Turvey, *Functional analysis of the impact of ORMDL3 expression on inflammation and activation of the unfolded protein response in human airway epithelial cells.* Allergy Asthma Clin Immunol, 2013. **9**(1): p. 4.

139. Lees, C.W., et al., *New IBD genetics: common pathways with other diseases.* Gut, 2011. **60**(12): p. 1739-53.

140. Hitomi, Y., et al., *Identification of the functional variant driving ORMDL3 and GSDMB expression in human chromosome 17q12-21 in primary biliary cholangitis.* Sci. Rep., 2017. **7**(1): p. 2904-2904.

141. Qiu, F., et al., *A genome-wide association study identifies six novel risk loci for primary biliary cholangitis.* Nat. Commun., 2017. **8**(1): p. 14828.

142. Kurreeman, F.A., et al., *Use of a multiethnic approach to identify rheumatoid- arthritis-susceptibility loci, 1p36 and 17q12.* Am J Hum Genet, 2012. **90**(3): p. 524-32.

143. Ma, X., et al., *ORMDL3 contributes to the risk of atherosclerosis in Chinese Han population and mediates oxidized low-density lipoprotein-induced autophagy in endothelial cells.* Sci Rep, 2015. **5**: p. 17194.

144. Qiu, R., et al., *Genetic variants on 17q21 are associated with ankylosing spondylitis susceptibility and severity in a Chinese Han population.* Scand J Rheumatol, 2013. **42**(6): p. 469-72.

145. Smith, J.A., et al., *Endoplasmic reticulum stress and the unfolded protein response are linked to synergistic IFN-beta induction via X-box binding protein 1.* Eur J Immunol, 2008. **38**(5): p. 1194-203.

146. DeLay, M.L., et al., *HLA-B27 misfolding and the unfolded protein response augment interleukin-23 production and are associated with Th17 activation in transgenic rats.* Arthritis Rheum, 2009. **60**(9): p. 2633-43.

147. Miller, M., et al., *ORMDL3 transgenic mice have increased airway remodeling and airway responsiveness characteristic of asthma.* J Immunol, 2014. **192**(8): p. 3475-87.

148. Miller, M., et al., *ORMDL3 is an inducible lung epithelial gene regulating metalloproteases, chemokines, OAS, and ATF6.* Proc Natl Acad Sci U S A, 2012. **109**(41): p. 16648-53.

149. Liu, Y.P., et al., *Association of ORMDL3 with rhinovirus-induced endoplasmic reticulum stress and type I Interferon responses in human leucocytes.* Clin. Exp. Allergy, 2017. **47**(3): p. 371-382.

150. Carreras-Sureda, A., et al., *ORMDL3 modulates store-operated calcium entry and lymphocyte activation.* Hum Mol Genet, 2013. **22**(3): p. 519-30.

151. Han, S., et al., *Orm1 and Orm2 are conserved endoplasmic reticulum membrane proteins regulating lipid homeostasis and protein quality control.* Proc. Natl. Acad. Sci. U.S.A., 2010. **107**(13): p. 5851-5856.

152. Tsuru, A., et al., *Novel mechanism of enhancing IRE1a-XBP1 signalling via the PERK-ATF4 pathway.* Scientific Reports, 2016. **6**: p. 24217.

153. Jentzsch, M., *Functional characterization of ORMDL proteins involved in endoplasmic reticulum stress and intestinal inflammation.* Dissertation, 2015.

154. Toncheva, A.A., et al., *Childhood asthma is associated with mutations and gene expression differences of ORMDL genes that can interact.* Allergy, 2015. **70**(10): p. 1288-99.

155. Zhu, W.K., et al., *Decreased SPTLC1 expression predicts worse outcomes in ccRCC patients.* J Cell Biochem, 2020. **121**(2): p. 1552-1562.

156. Clarke, B.A., et al., *The Ormdl genes regulate the sphingolipid synthesis pathway to ensure proper myelination and neurologic function in mice.* Elife, 2019. **8**: p. e51067.

157. Maceyka, M. and S. Spiegel, *Sphingolipid metabolites in inflammatory disease.* Nature, 2014. **510**(7503): p. 58-67.

158. Levine, B., N. Mizushima, and H.W. Virgin, *Autophagy in immunity and inflammation.* Nature, 2011. **469**(7330): p. 323-35.

159. Harvald, E.B., A.S. Olsen, and N.J. Faergeman, *Autophagy in the light of sphingolipid metabolism.* Apoptosis, 2015. **20**(5): p. 658-70.

160. Dang, J., et al., *ORMDL3 Facilitates the Survival of Splenic B Cells via an ATF6α–Endoplasmic Reticulum Stress–Beclin1 Autophagy Regulatory Pathway.* J Immunol, 2017. **199**(5): p. 1647-1659.

161. Kiefer, K., et al., *Ceramide Imbalance and Impaired TLR4-Mediated Autophagy in BMDM of an ORMDL3-Overexpressing Mouse Model.* Int J Mol Sci, 2019. **20**(6): p. 1391.

162. Stengel, S.T., *On the Role of Endoplasmic Reticulum Homeostasis and Autophagy in Intestinal Inflammation.* Dissertation, 2018.

163. Mekahli, D., et al., *Endoplasmic-reticulum calcium depletion and disease.* Cold Spring Harb Perspect Biol, 2011. **3**(6): p. a004317.

164. Berridge, M.J., P. Lipp, and M.D. Bootman, *The versatility and universality of calcium signalling.* Nat Rev Mol Cell Biol, 2000. **1**(1): p. 11-21.

165. Brini, M., et al., *The plasma membrane calcium pump in health and disease.* FEBS J. , 2013. **280**(21): p. 5385-5397.

166. Breslow, D.K., et al., *Orm family proteins mediate sphingolipid homeostasis.* Nature, 2010. **463**(7284): p. 1048-53.

167. Cai, L., et al., *ORMDL proteins regulate ceramide levels during sterile inflammation.* J. Lipid Res., 2016. **57**(8): p. 1412-1422.

168. Li, B., et al., *IL-10 modulates DSS-induced colitis through a macrophage-ROS-NO axis.* Mucosal Immunol, 2014. **7**(4): p. 869-78.

169. Biesiada, G., et al., *Expression and release of leptin and proinflammatory cytokines in patients with ulcerative colitis and infectious diarrhea.* J Physiol Pharmacol, 2012. **63**(5): p. 471-81.

170. Ren, K. and R. Torres, *Role of interleukin-1beta during pain and inflammation.* Brain Res Rev, 2009.

60(1): p. 57-64.

171. Uko, V., S. Thangada, and K. Radhakrishnan, *Liver disorders in inflammatory bowel disease.* Gastroenterol Res Pract, 2012. **2012**: p. 642923.
172. Carvalho, F.A., et al., *Crohn's disease-associated Escherichia coli LF82 aggravates colitis in injured mouse colon via signaling by flagellin.* Inflamm Bowel Dis, 2008. **14**(8): p. 1051-60.
173. Lowry, O.H., et al., *Protein measurement with the Folin phenol reagent.* J Biol Chem, 1951. **193**(1): p. 265-75.
174. Okayasu, I., et al., *A novel method in the induction of reliable experimental acute and chronic ulcerative colitis in mice.* Gastroenterology, 1990. **98**(3): p. 694-702.
175. Franken, N.A.P., et al., *Clonogenic assay of cells in vitro.* Nat. Protoc., 2006. **1**(5): p. 2315-2319.
176. Krueger, F., *TrimGalore. A wrapper tool around Cutadapt and FastQC to consistently apply quality and adapter trimming to FastQ files.* 2015.
177. Martin, M., *Cutadapt removes adapter sequences from high-throughput sequencing reads.* EMBnet.journal, 2011. **17**(1): p. 10-12.
178. Andrew, S., *FastQC. A Quality Control tool for High Throughput Sequence Data.* 2014.
179. Dobin, A., et al., *STAR: ultrafast universal RNA-seq aligner.* Bioinformatics, 2012. **29**(1): p. 15-21.
180. Liao, Y., G.K. Smyth, and W. Shi, *featureCounts: an efficient general purpose program for assigning sequence reads to genomic features.* Bioinformatics, 2014. **30**(7): p. 923-30.
181. Love, M.I., W. Huber, and S. Anders, *Moderated estimation of fold change and dispersion for RNA-seq data with DESeq2.* Genome Biology, 2014. **15**(12): p. 550.
182. Team, R.C., *R: A language and environment for statistical computing. R Foundation for Statistical Computing, Vienna, Austria.* 2012.
183. Chen, H. and P.C. Boutros, *VennDiagram: a package for the generation of highly-customizable Venn and Euler diagrams in R.* BMC Bioinform, 2011. **12**(1): p. 35.
184. Karp, N.A., et al., *Prevalence of sexual dimorphism in mammalian phenotypic traits.* Nature Communications, 2017. **8**(1): p. 15475.
185. Costa, K.M., D. Schenkel, and J. Roeper, *Sex-dependent alterations in behavior, drug responses and dopamine transporter expression in heterozygous DAT-Cre mice.* Scientific Reports, 2021. **11**(1): p. 3334.
186. Du, X.-J., *Gender modulates cardiac phenotype development in genetically modified mice.* Cardiovascular Research, 2004. **63**(3): p. 510-519.
187. Beers, C., et al., *Cathepsin S controls MHC class II-mediated antigen presentation by epithelial cells in vivo.* J Immunol, 2005. **174**(3): p. 1205-12.
188. Buning, J., et al., *Multivesicular bodies in intestinal epithelial cells: responsible for MHC class II-restricted antigen processing and origin of exosomes.* Immunology, 2008. **125**(4): p. 510-21.
189. Hundorfean, G., et al., *Luminal antigens access late endosomes of intestinal epithelial cells enriched in MHC*

I and MHC II molecules: in vivo study in Crohn's ileitis. Am J Physiol Gastrointest Liver Physiol, 2007. **293**(4): p. G798-808.

190. Van Niel, G., et al., *Intestinal epithelial exosomes carry MHC class II/peptides able to inform the immune system in mice.* Gut, 2003. **52**(12): p. 1690-7.
191. Nava, P., et al., *Interferon-gamma regulates intestinal epithelial homeostasis through converging beta-catenin signaling pathways.* Immunity, 2010. **32**(3): p. 392-402.
192. Giroux, M., M. Schmidt, and A. Descoteaux, *IFN-gamma-induced MHC class II expression: transactivation of class II transactivator promoter IV by IFN regulatory factor-1 is regulated by protein kinase C-alpha.* J Immunol, 2003. **171**(8): p. 4187-94.
193. Anderson, C.A., et al., *Meta-analysis identifies 29 additional ulcerative colitis risk loci, increasing the number of confirmed associations to 47.* Nat Genet, 2011. **43**(3): p. 246-52.
194. Gururaj, C., R.S. Federman, and A. Chang, *Orm proteins integrate multiple signals to maintain sphingolipid homeostasis.* J. Biol. Chem., 2013. **288**(28): p. 20453-20463.
195. Khongwichit, S., et al., *Cell-type specific variation in the induction of ER stress and downstream events in chikungunya virus infection.* Microb Pathog, 2016. **101**: p. 104-118.
196. Li, M., et al., *Upregulation of miR-665 promotes apoptosis and colitis in inflammatory bowel disease by repressing the endoplasmic reticulum stress components XBP1 and ORMDL3.* Cell Death Dis, 2017. **8**(3): p. e2699-e2699.
197. Löser, S., et al., *Pulmonary ORMDL3 is critical for induction of Alternaria-induced allergic airways disease.* J. Allergy Clin. Immunol., 2017. **139**(5): p. 1496-1507.e3.
198. Araki, W., et al., *A family of membrane proteins associated with presenilin expression and gamma-secretase function.* FASEB J, 2008. **22**(3): p. 819-27.
199. Siow, D., et al., *ORMDL/serine palmitoyltransferase stoichiometry determines effects of ORMDL3 expression on sphingolipid biosynthesis.* J Lipid Res, 2015. **56**(4): p. 898-908.
200. Shimada, M., et al., *Upper gastrointestinal pathophysiology due to mouse malaria Plasmodium berghei ANKA infection.* Trop Med Health, 2019. **47**: p. 18.
201. Chen, J., et al., *Orosomucoid-like 3 (ORMDL3) upregulates airway smooth muscle proliferation, contraction, and Ca(2+) oscillations in asthma.* J Allergy Clin Immunol, 2018. **142**(1): p. 207-218.e6.
202. Rennick, D.M. and M.M. Fort, *Lessons from genetically engineered animal models. XII. IL-10-deficient (IL-10(-/-) mice and intestinal inflammation.* Am J Physiol Gastrointest Liver Physiol, 2000. **278**(6): p. G829-33.
203. Hörmannsperger, G., M. Schaubeck, and D. Haller, *Intestinal Microbiota in Animal Models of Inflammatory Diseases.* ILAR Journal, 2015. **56**(2): p. 179-191.
204. Yang, I., et al., *Intestinal microbiota composition of interleukin-10 deficient C57BL/6J mice and susceptibility to Helicobacter hepaticus-induced colitis.* PLoS One, 2013. **8**(8): p. e70783.

205. Perše, M. and A. Cerar, *Dextran sodium sulphate colitis mouse model: traps and tricks.* J Biomed Biotechnol, 2012. **2012**: p. 718617.

206. Velcich, A., et al., *Colorectal cancer in mice genetically deficient in the mucin Muc2.* Science, 2002. **295**(5560): p. 1726-9.

207. Van der Sluis, M., et al., *Muc2-deficient mice spontaneously develop colitis, indicating that MUC2 is critical for colonic protection.* Gastroenterology, 2006. **131**(1): p. 117-29.

208. Zarepour, M., et al., *The mucin Muc2 limits pathogen burdens and epithelial barrier dysfunction during Salmonella enterica serovar Typhimurium colitis.* Infect Immun, 2013. **81**(10): p. 3672-83.

209. Geremia, A., et al., *Innate and adaptive immunity in inflammatory bowel disease.* Autoimmun Rev, 2014. **13**(1): p. 3-10.

210. Buisine, M.P., et al., *Abnormalities in mucin gene expression in Crohn's disease.* Inflamm Bowel Dis, 1999. **5**(1): p. 24-32.

211. Rogers, D.F., *Airway goblet cells: responsive and adaptable front-line defenders.* Eur Respir J, 1994. **7**(9): p. 1690-706.

212. Schmiedel, B.J., et al., *17q21 asthma-risk variants switch CTCF binding and regulate IL-2 production by T cells.* Nat. Commun., 2016. **7**(1): p. 13426.

213. Prelipcean, C.C., et al., *What is the impact of age on adult patients with inflammatory bowel disease?* Clujul Med, 2013. **86**(1): p. 3-9.

214. Lakatos, P.L., *Recent trends in the epidemiology of inflammatory bowel diseases: up or down?* World J Gastroenterol, 2006. **12**(38): p. 6102-8.

215. Franceschi, C. and J. Campisi, *Chronic Inflammation (Inflammaging) and Its Potential Contribution to Age-Associated Diseases.* J Gerontol A Biol Sci Med Sci, 2014. **69**(Suppl_1): p. S4-S9.

216. Eichele, D.D. and K.K. Kharbanda, *Dextran sodium sulfate colitis murine model: An indispensable tool for advancing our understanding of inflammatory bowel diseases pathogenesis.* World J Gastroenterol, 2017. **23**(33): p. 6016-6029.

217. Oyadomari, S. and M. Mori, *Roles of CHOP/GADD153 in endoplasmic reticulum stress.* Cell Death Differ, 2004. **11**(4): p. 381-9.

218. Tajiri, S., et al., *Ischemia-induced neuronal cell death is mediated by the endoplasmic reticulum stress pathway involving CHOP.* Cell Death Differ, 2004. **11**(4): p. 403-15.

219. Adegbola, S.O., et al., *Anti-TNF Therapy in Crohn's Disease.* International journal of molecular sciences, 2018. **19**(8): p. 2244.

220. Rath, P.C. and B.B. Aggarwal, *TNF-induced signaling in apoptosis.* J Clin Immunol, 1999. **19**(6): p. 350-64.

221. Qiu, W., et al., *PUMA-mediated intestinal epithelial apoptosis contributes to ulcerative colitis in humans and mice.* The Journal of Clinical Investigation, 2011. **121**(5): p. 1722-1732.

222. Treveil, A., et al., *Regulatory network analysis of Paneth cell and goblet cell enriched gut organoids using transcriptomics approaches.* Mol Omics, 2020. **16**(1): p. 39-58.

223. Xiong, Y., et al., *ATF6 knockdown decreases apoptosis, arrests the S phase of the cell cycle, and increases steroid hormone production in mouse granulosa cells.* Am J Physiol Cell Physiol, 2017. **312**(3): p. C341-C353.

8 Supplement

8.1 Buffers and solutions

Table 15: List of Buffers and solutions used in the experiments.

Buffer/Solution	Application/Experiment	Ingredients/Company
10x TAE	Agarose gel electrophoresis	Carl Roth, Karlsruhe, Germany, cat. rr. T845.2
10x TBS	Western blotting	200 mM Tris (pH 7.6), 1.37 M sodium chloride
10x TGS	SDS page	25 mM Tris (pH 8.3), 192 mM glycine, 0.1 % (w/v) SDS
5x SDS loading dye	SDS page	250 mM Tris (pH 6.8), 10 % (w/v) SDS, 50 % (v/v) glycerol, 500 mM DTT
Anode buffer 1	Western blotting	30 mM Tris, 20 % (v/v) methanol
Anode buffer 2	Western blotting	300 mM Tris, 20 % (v/v) methanol
Blocking solution	Western blotting	5 % (w/v) non-fat dry milk in TTBS
Cathode buffer	Western blotting	25 mM Tris, 20 % (v/v) methanol, 40 mM 6-amino-n-caproic acid
DNA loading dye	SDS page	50 % (v/v) glycerol, 0.1 % (w/v) bromophenol blue, 0.1 % (w/v) xylene cyanol
ECL substrate	Western blotting	GE Healthcare, Freiburg, Germany, cat. nr. RPN2109
FCS		PAA Laboratories/ GE Healthcare, Freiburg, Germany, cat. nr. PAA A15-151
Ketanest S 25mg/ml, 10ml	Mouse sacrifice	Pfizer, New York, USA
Loading gel	Western blotting	0.5 M Tris (pH 6.8), 0.4 % (w/v) SDS
Matrigel® Matrix	Small intestinal organoids	Corning Inc., Corning, USA
MOPS SDS Running Buffer (20X)	Western blotting	Novex/Life Technologies, Darmstadt, Germany, cat. nr. NP001
OPTI-MEM	Transfection	Gibco/Life Technologies, Darmstadt, Germany, cat. nr. 31985-047
PBS (pH 7.4)	various	8 g/l sodium chloride, 0.2 g/l potassium chloride, 1.56 g/l disodium phosphate, 0.24 g/l monopotassium phosphate
RIPA buffer	Protein isolation	150 mM sodium chloride, 1 % (v/v) NP40, 0.5 % (w/v) deoxycholic acid, 0.1 % (w/v) SDS, 50 mM Tris (pH 8.0)
Rompun	Mouse sacrifice	Bayer, Leverkusen, Germany
Separation buffer	SDS page	1.5 M Tris (pH 8.8), 0.4 % (w/v) SDS
Smart Ladder	SDS page	Eurogentec, Cologne, Germany, cat. nr. MW-1700-10
Stacking buffer	SDS page	0.5 M Tris (pH 8.8), 0.4 % (w/v) SDS
Stripping buffer	SDS page	62.5 mM Tris (pH 6.8), 2 % (w/v) SDS
SYBR Safe DNA gel stain	Agarose gel electrophoresis	Life Technologies, Darmstadt, Germany cat. nr. S33102
TTBS (Washing buffer)	Western blotting	1x TBS, 0.1 % (v/v) Tween20

8.2 Chemicals

Table 16: Chemicals used for the experiments.

Chemical	Application/Experiment	Company
2-Mercaptoethanol	RNA isolation	Sigma-Aldrich, Munich, Germany
6-amino-n-caproic acid	Western blotting	Sigma-Aldrich, Munich, Germany
Acrylamide Bis Sol.30 %	SDS page	Bio-Rad, Munich, Germany
Bovine serum albumin (BSA)	Protein isolation	Carl Roth, Karlsruhe, Germany
Bromophenol blue	SDS page	Sigma-Aldrich, Munich, Germany
Deoxycholic acid	SDS page	Sigma-Aldrich, Munich, Germany
DSS reagent grade, MW 36000-50000	DSS colitis	MP Biomedicals, Illkirch Cedex, France
EDTA	Crypt isolation	Sigma-Aldrich, Munich, Germany
Ethanol	DSS colitis	Merck, Darmstadt, Germany
Glycerol	SDS page	Carl Roth, Karlsruhe, Germany
Glycine	various	Carl Roth, Karlsruhe, Germany
LE Agarose	Agarose gel electrophoresis	Biozyme, Hessisch Oldendorf, Germany
Magnesium chloride	various	Merck, Darmstadt, Germany
Methanol	Western blotting	Merck, Darmstadt, Germany
Monopotassium phosphate	various	Sigma-Aldrich, Munich, Germany
Non-fat dry milk (NFDM)	Western blotting	Bio-Rad, Munich, Germany
Penicillin/Streptomycin	Organoids	Life Technologies, Darmstadt, Germany
Potassium chloride	Various	Sigma-Aldrich, Munich, Germany
Propidium iodide staining	Organoids	BD Pharmingen™, San Jose, USA (Cat. No. 51-66211E)
RNase-free water	RNA isolation	Qiagen, Hilden, Germany
Sodium chloride	various	Merck, Darmstadt, Germany
Sodium dodecyl sulfate (SDS)	SDS page	Carl Roth, Karlsruhe, Germany
SYBR safe	Agarose gel electrophoresis	Life Technologies, Carlsbad, USA
TRIS	SDS page, Western blotting	Merck, Darmstadt, Germany
Triton-X	Histology	Sigma-Aldrich, Munich, Germany
Tween20	Western blotting	Carl Roth, Karlsruhe, Germany
Xylene cyanol	SDS page	Sigma-Aldrich, Munich, Germany

8.3 Media

Table 17: Media used for the experiments.

Media	Cell line	Ingredients/Company
DPBS (1X)	ModeK cells, Organoids	Life Technologies, Carlsbad, USA (Cat. No. 14190-094)
ModeK medium	ModeK cells	DMEM GlutaMAX (Gibco, Cat. No. 61965-026), Fetal Bovine Serum (Sigma, Cat. No. F7524), HEPES (Gibco, Cat. No. 15630-056), NEAA (Gibco, Cat No. 11140-035), Penicillin/Streptomycin (Gibco, Cat. No. 15140-122)
IntestiCult™ OGM Mouse Basal Medium	Organoids	Stemcell Technologies, Vancouver, Canada (Cat. No. #06000, #06002/3)
TrypLE™ Express	Organoids	Life Technologies, Carlsbad, USA (Cat. No. 12604-021)

8.4 Small-interfering RNA and transfection reagents

Table 18: siRNA used for the experiments.

siRNA	Cell line	Ingredients/Company
AllStars Neg. Control siRNA	ModeK cells	Qiagen, Hilden, Germany (Cat. No. 1027281)
siGENOME SMARTpool Mouse Ormdl3	ModeK cells	Dharmacon, Lafayette, USA (Cat. No. M-049023-02-0005)
Viromer BLUE	ModeK cells	Biozym, Hess. Oldendorf, Germany (Cat. No. 230005)

8.5 Enzymes and inhibitors

Table 19: Enzymes and inhibitors used for the experiments.

Enzyme/Inhibitor	Application	Company
GoTaq™ Polymerase	Stimulation	Promega, Mannheim, Germany
Halt™ combined protease and phosphatase inhibitor	Protein isolation	Thermo Scientific, Bremen, Germany
Proteinase K	Protein isolation	Thermo Scientific, Bremen, Germany
RNase-free DNase Set	RNA isolation	Qiagen, Hilden, Germany
Tunicamycin	Stimulation	Calbiochem, Darmstadt, Germany

8.6 Kits

Table 20: Kits used for the experiments.

Enzyme/Inhibitor	Application	Company
Dual-luciferase® reporter assay system	Dual-Luciferase assay	Promega, Mannheim, Germany
Maxima H Minus First Strand cDNA Synthesis Kit	cDNA synthesis	Thermo Scientific, Bremen, Germany
QIAshredder	RNA isolation	Qiagen, Hilden, Germany
RNeasy Mini Kit	RNA isolation	Qiagen, Hilden, Germany
Roti Histokit	Histology	Carl Roth, Karlsruhe, Germany
SYBR® Select Master Mix	RT-PCR	Life Technologies, Darmstadt, Germany

8.7 Plasmids

Table 21: Plasmids used for the experiments.

Plasmid	Application	Company
pGL3-UPRE	Dual-luciferase assay	Wu *et al.*, 2007 [87]; purchased from Addgene, Cambridge, USA, cat. nr. 11976
pRL-TK	Dual-luciferase assay	purchased from Promega, Mannheim, Germany, cat. nr. E2241

8.8 Antibodies

Table 22: Primary antibodies used for the experiments.

Antibody	Application	Source	Company	Catalog number
GAPDH	WB	mouse	Santa Cruz, Heidelberg, Germany	sc-365062
HSPA5	WB	rabbit	Abcam, Cambridge, United Kingdom	ab21685
HSP90B1	WB	rabbit	Cell Signaling, Leiden, The Netherlands	20292
Lysozyme	IHC	goat	Santa Cruz, Heidelberg, Germany	sc-27958
MHCII-PE	FACS	rat IgG2b	eBioScience, Frankfurt, Germany	12-5322
MHCII-PE (isotype)	FACS	rat IgG2b	eBioScience, Frankfurt, Germany	12-4031
Olfm4	IHC	rabbit	Cell Signaling, Leiden, The Netherlands	39141
ORMDL1/2/3	WB	goat	Santa Cruz, Heidelberg, Germany	sc-161143

Table 23: Secondary antibodies used for the experiments.

Antibody	Application	Company	Catalog number
Goat HRP	WB	Sigma-Aldrich, Munich, Germany	A5420
Mouse HRP	WB	Amersham Biosciences, Glattbrugg, Switzerland	NA931V
Rabbit HRP	WB	Amersham Biosciences, Glattbrugg, Switzerland	NA934V

8.9 Oligonucleotides (Primers)

Table 24: Oligonucleotides for genotyping PCR.

Target gene	Species	Forward primer	Reverse primer
Ormdl2 (WT 407 bp, KO 872 bp)	*M. musculus*	5'-ACACCTCCCCCTGAAC-CTGAAA	5'-AATACCATGGAACCAG CAAGGAATGC
Ormdl3 WT (194 bp)	*M. musculus*	5'-CTTCATCCGTTGTTGCTTGC	5'-TCCCCTACAGATCTCCTGAGG
Ormdl3 KO (277 bp)	*M. musculus*	5'-CTTCATCCGTTGTTGCTTGC	5'-TCACAGTGCCAGTAGGAAACC
Xbp1 (WT 170 bp, floxed 251 bp)	*M. musculus*	5'-CCTGTGGGACAGAATGG ACCCAG	5'-CGCATACACAGCTGCTTT TATCC
VillinCre	*M. musculus*	5'-CAAGACCCCCATAGGAAGCC	5'-ACATCTTCAGGTTCTGCGGG
VillinCre (internal control)	*M. musculus*	5'-TCATGGAAATCCTACAGC AGGGACC	5'-GTCATGCTGGAGAATGAG AAGC

Table 25: Oligonucleotides for RT-PCR (SYBR Green).

Target gene	Species	Forward primer	Reverse primer
Atf4	murine	ATGGCCGGCTATGGATGAT	CGAAGTCAAACTCTTTCAGATC CATT
Atf6	murine	ATGCCAGTGTCCCAGCAAAA	TCCCCCAGTGACTGCAAGAA
CIITA	murine	CACCCCCAGATGTGTATGTGCT	ACGAGGTTTCCCAGTCCAGAA
Ddit3	murine	CTGCCTTTCACCTTGGAGA	CGTTTCCTGGGGATGAGATA
Gapdh	murine	CCGGGGCTGGCATTGCTCTCA	CTTGCTCAGTGTCCTTGCTGGGG
H2-ab1	murine	GAGGTCAAATTCCACCCCAG	TCAGGTTCCCAGTGTTTCAG
Hspa5	murine	CCGAGTCTGCTTCGTGTCT	AACACACCGACGCAGGA
Hsp90b1	murine	TGGGTCAAGCAGAAAGGAGG	TCTCTGTTGCTTCCCGACTTT
Ormdl1	murine	ACTCACTGGGAACAGCTGGA	ATTCCAAAGATGCGAACACC
Ormdl2	murine	CTTTTGACACATTGGGAGCA	GGTAGCTTAGGCAGCAGCAC
Ormdl3	murine	GTGGCATCTGGCTCTCCTAC	TGAGCACAGTCATCAAGGACA
Xbp1s	murine	CTGAGTCCGAATCAGGTGCAG	CTCTGGGGAAGGACATTTGA
Xbp1u	murine	TGGCCGGGTCTGCTGAGT	ACAGGGTCCAACTTGTCCAG

Table 26: Oligonucleotides for RT-PCR (TaqMan assay).

Target gene	Species	Forward primer	Reverse primer
Atf6	murine	ATGCCAGTGTCCCAGCAAAA	TCCCCCAGTGACTGCAAGAA
Ddit3	murine	CTGCCTTTCACCTTGGAGA	CGTTTCCTGGGGATGAGATA
Gapdh	murine	CCGGGGCTGGCATTGCTCTCA	CTTGCTCAGTGTCCTTGCTGGGG
Hspa5	murine	CCGAGTCTGCTTCGTGTCT	AACACACCGACGCAGGA
Hsp90b1	murine	TGGGTCAAGCAGAAAGGAGG	TCTCTGTTGCTTCCCGACTTT
Ormdl1	murine	ACTCACTGGGAACAGCTGGA	ATTCCAAAGATGCGAACACC
Ormdl2	murine	CTTTTGACACATTGGGAGCA	GGTAGCTTAGGCAGCAGCAC
Ormdl3	murine	GTGGCATCTGGCTCTCCTAC	TGAGCACAGTCATCAAGGACA
Xbp1u	murine	TGGCCGGGTCTGCTGAGT	ACAGGGTCCAACTTGTCCAG
Xbp1s	murine	CTGAGTCCGAATCAGGTGCAG	CTCTGGGGAAGGACATTTGA

8.10 Consumables

Table 27: Consumables used for the experiments.

Consumable	Application	Company
0.5, 1 & 2ml reaction tubes	various	Sarstedt, Nürnbrecht, Germany
1 ml syringe	mouse sacrifice	B. Braun, Melsungen, Germany
15 ml and 50 ml reaction tubes	various	Sarstedt, Nürnbrecht Germany
100 ml culture flask	cell culture	Schott, Mainz, Germany
20 ml syringe	mouse sacrifice	BD Biosciences, San Jose, USA
22G braunule	mouse sacrifice	B. Braun, Melsungen, Germany
24- and 96-well plate	Organoids	Thermo Fisher Scientific, Massachusetts, USA
26G needles	mouse sacrifice	B. Braun, Melsungen, Germany
96-well 340 µl Storage Plate, V Bottom	FACS	Falcon/Corning Inc., New York, USA (Cat. No. 353263)
Battery Pipet Holder	Cell culture	Integra Biosciences, Biebertal, Germany
Blotting paper	Western blotting	Bio-Rad, Munich, Germany
Cell strainer, 40 µm and 100 µm	mouse sacrifice	VWR, Radnor, USA
Chemiluminescence hyperfilm	Western blotting	Life Technologies, Darmstadt, Germany
Falcon™ Round-Bottom Polystyrene Tubes	FACS	Fisher Scientific GmbH, Schwerte, Germany
HistoBond	Histology	Paul Marienfeld GmbH & Co. KG, Lauda-Königshofen, Germany
MicroAmp Optical 384-Well Reaction Plates	RT-PCR	Applied Biosystems, Foster City, USA
Microvette 500 (Potassium EDTA)	mouse sacrifice	Sarstedt, Nürnbrecht, USA
NuPAGE™ 4-12 % Bis-Tris Gel	SDS page	Life Technologies Corp., Carlsbad, USA
Pipette (filter) tips	various	Sarstedt, Nürnbrecht, Germany
PVDF membrane	Western blotting	Bio-Rad, Munich, Germany
Serological pipettes (5, 10 and 25 ml)	various	Sarstedt, Nürnbrecht, Germany
Sterile, disposable scapel blade	Mouse sacrifice	B. Braun, Melsungen, Germany

8.11 Devices

Table 28: Devices used for the experiments.

Consumable	Application	Company
7900 HT Fast Real-Time PCR System	RT-PCR	Applied Biosystems/Life Technologies, Darmstadt, Germany
96-well thermocycler	PCR	Applied Biosystems/Life Technologies, Darmstadt, Germany
Analytic balance 870-15	various	Kern, Balingen, Germany
Assistent Mini-Centrifuge SPROUT	various	Heathrow Scientific, Nottingham, United Kingdom
Automated developer machine	Western blotting	Agfa, Mortsel, Belgium
Axio Imager.Z1	various	Zeiss, Jena, Germany
Cellometer Auto T4 Plus	Cell culture	Thermo Scientific, Bremen, Germany
Centrifuge: Megafuge 16R	various	PeqLab Biotechnologie GmbH, Erlangen, Germany
Centrifuge: Fresco 21	various	Thermo Scientific, Bremen, Germany
ChemiDoc XRS Imaging System	Gel electrophoresis	Bio-Rad, Munich, Germany
Electric pipet filler	various	ThermoFisher Scientific Inc., Waltham, USA
Eppendorf Research® plus volume pipette	various	Eppendorf, Hamburg, Germany
FACSCalibur flow cytometer	FACS	BD Biosciences, Heidelberg, Germany
GeneAmp PCR System 9700	PCR	Applied Biosystems/Life Technologies, Darmstadt, Germany
Gentle-MACS™ Dissociator	LP kit	Miltenyi Biotec, Bergisch Gladbach, Germany
Incubator for cell lines	various	Binder, Tuttlingen, Germany
Laminar flow workbench HERASafe KS	various	Thermo Scientific, Bremen, Germany
Leica RM 2255 microtome	Histology	Leica Microsystems, Wetzlar, Germany
Magnetic stirrer C-MAG HS 7 IKAMAG	various	IKA, Staufen, Germany
Microwave R-239	Gel electrophoresis	SHARP, Hamburg, Germany
NanoDrop ND-1000 spectrophotometer	RNA isolation	PeqLab Biotechnologie GmbH, Erlangen, Germany
Power Pac 300	SDS page	Bio-Rad, Munich, Germany
SympHony Benchtop Meters	pH measurement	VWR, Darmstadt, Germany
Tecan Infinite F200 pro plate reader	Luciferase assay	Tecan, Männedorf, Switzerland
Thermomixer compact 5350	various	Eppendorf, Hamburg, Germany
Trans-Blot® Turbo™ Transfer System	Western blotting	Bio-Rad, Munich, Germany
Tube roller SRT6	Western blotting	Stuart Equipment, Staffordshire, United Kingdom
Vortex-Genie 2 Variable Speed	various	Sartorius, Göttingen, Germany
Water bath 1003	Histology	GFL, Burgwedel, Germany
Water purification system	various	TKA, Niederelbert, Germany
Wide Mini ReadySub-Cell GT	Gel electrophoresis	Bio-Rad, Munich, Germany
XCell SureLock® Mini-Cell	SDS page	Life Technologies, Darmstadt, Germany

8.12 Abbreviations

Abbreviation	Explanation
%	percent
AIEC	adherent-invasive *E. coli*
aqua bidest.	aqua bidestillata
ATF4	activating transcription factor 4
ATF6	activating transcription factor 6
ATF6 cl	cleaved activating transcription factor 6
ATG16L1	autophagy-related 16 like 1
APC	antigen-presenting cell
approx.	approximately
BECN1	Beclin-1
Bmi1	BMI1 proto-oncogene, polycomb ring finger
BrdU	5-Bromo-2´-Deoxyuridine
BSA	bovine serum albumin
°C	degree Celsius
C1P	ceramide-1-phosphate
Ca^{2+}	calcium
CAU	Christian Albrechts University Kiel
CBC	crypt base columnar cell
ccRCC	clear cell renal cell carcinoma
CD	Crohn's disease
CHOP	C/EBP homologous protein
CIITA	class II major histocompatibility complex transactivator
CO_2	carbon hydroxide
CoA	palmitoyl coenzyme A
CXCL10	C-X-C motif chemokine 10
DAI	disease activity index
DC	dendritic cell
Ddit3	DNA damage inducible transcript 3
DNA	deoxyribonucleic acid
Dnajc3	DnaJ homolog subfamily C member 3
DR5	death receptor 5
DSS	dextran sodium sulfate
EDTA	ethylenediaminetetraacetic acid
e.g.	exempli gratia (for example)
eIF2α	eukaryotic translation initiation factor 2A
eIF2α-TC	eIF2−GTP–Met-tRNA ternary complex
eQTL	expression quantitative trait loci
ER	endoplasmic reticulum
ERAD	endoplasmic reticulum-associated protein degradation
Ern1	endoplasmic reticulum to nucleus signaling 1
ER stress	endoplasmic reticulum stress
ERSE	endoplasmic reticulum stress element
FACS	fluorescence-activated cell sorting
Grp78	78 KDa Glucose-Regulated Protein
GWAS	genome-wide association study
h	hour
H2-Ab1	H-2 class II histocompatibility antigen, A beta chain
HLA	human leukocyte antigen
HRP	horseradish peroxidase
Hspa5	heat shock protein family A (Hsp70) member 5
Hsp90b1	heat shock protein 90 beta family member 1
IBD	inflammatory bowel disease
ΔIEC	gene knockout specifically in intestinal epithelial cell
IEC	intestinal epithelial cell
IFNB1	interferon beta 1
IL-	interleukin
IL23R	interleukin 23 receptor
iMEF	immortalized mouse embryonic fibroblast

IRE1	inositol-requiring enzyme 1
IRE1α	inositol-requiring enzyme 1 alpha
IRE1β	inositol-requiring enzyme 1 beta
IRGM	immunity-related GTPase M
ISC	intestinal stem cell
IVC	individually ventilated cages
Jak1	Janus kinase 1
JNK	Jun-related kinase
kDa	kilodalton
Ki67	Kiel67
Lcb1/2	serine C-palmitoyltransferase LCB1/2
Lgr5	leucine-rich repeat-containing G protein-coupled receptor 5
loxP	locus of X-over P1
LP	lamina propria
Lrig1	leucine rich repeats and immunoglobulin like domains 1
Lyz	lysozyme
mA	milliamps
Mbtps1	membrane-bound transcription factor site-1 protease
M cell	microfold cell
MHC	major histocompatibility complex
min	minute
mRNA	messenger ribonucleic acid
Muc2	mucin 2
NeoR	neomycin resistance
NF_KB	nuclear factor kappa B
nm	nanometer
NOD2	nucleotide-binding oligomerization domain-containing protein 2
Olfm4	olfactomedin 4
ON	overnight
ORMDL1/2/3	ORM1 (S. Cerevisiae)-like 1/2/3
P/p	phosphorylation/phosphorylated
PAMP	pathogen associated molecular pattern
PBS	phosphate buffered saline
PCR	polymerase chain reaction
PDI	protein disulfide isomerase
PERK	PRKR-like endoplasmic reticulum kinase
PI	propidium iodide
PuroR	puromycin resistance
PVDF	polyvinylidene difluoride
RNA	ribonucleic acid
RNase	Ribonuclease
RPAP2	RNA polymerase II associated protein 2
rpm	rounds per minute
RT	room temperature
S1P/S2P	site 1/2 protease
siRNA	small interfering RNA
SNP	single nucleotide polymorphism
SOCE	store operated calcium entry
SPF	specific pathogen-free
SPT	serine palmitoyltransferase
Stat3	signal transducer and activator of transcription 3
TBS	Tris-buffered saline
TBST	Tris-buffered saline + Tween
TF	transcription factor
TM	tunicamycin
TNBS	trinitrobenzene sulfonic acid
TNFα	tumor necrose factor alpha
TUNEL	terminal deoxynucleotidyl transferase dUTP nick end labelling
UC	ulcerative colitis
UKSH	University Medical Center Schleswig-Holstein
µl	microliter
µm	micrometer
UPR	unfolded protein response
UPRE	unfolded protein response element

UTR	untranslated region
V	Volt
Wnt11	Wnt family member 11
Wnt2b	Wnt family member 2 beta
Xbp1	X-box binding protein 1
$Xbp1^{\Delta IEC}$	Xbp1 deletion specifically in intestinal epithelial cells
$Xbp1^{fl/fl}$	Xbp1 floxed/floxed
Xbp1u	unspliced X-box binding protein 1
Xbp1s	spliced X-box binding protein 1

8.13 Acknowledgments

This thesis is a big team effort, which would not have been possible without the contribution of my research colleagues, friends, and family. I would therefore like to thank

Prof. Dr. Philip Rosenstiel for offering me the opportunity to pursue this PhD. Even though there were days that I would have loved to spend without any ORMDLs in my life, I was and still am very grateful for this opportunity to learn and grow as a researcher. Thank you for your support, your understanding and your kind support through to the end of my project.

I would also like to thank the other members of my PhD committee for kindly agreeing to evaluate my thesis and for their willingness to be part of my evaluation committee.

The funding sources that provided the financial support for this research and the possibility to participate in different kinds of advanced training: the Collaborative Research Centre 877 "Proteolysis as a Regulatory Event in Pathophysiology" and the Research Training Group "Genes, Environment, Inflammation" (RTG1743).

Dr. Philipp Arnold and Katrin Neblung-Masuhr from the institute of anatomy who have been great collaborators and provided me with a first glance into the Paneth cells of *Ormdl3 Xbp1*-deficient mice.

The whole team of VHH and ZTH – especially Ines, Andy, Tabea, Meike and Andrea. You really are the best animal caretakers anyone could ever wish for.

My fellow cellbiology/systems immunology colleagues and friends: Thank you all for supporting me and my work and providing a great working atmosphere. I really enjoyed working with you.
I am especially grateful to Dr. Marlene Jentzsch and Dr. Stephanie Stengel for providing helpful insights into the crazy ORMDL universe.
Dr. Maren Falk-Paulsen and PD Dr. Konrad Aden for their supervision, continuous support and effort to bring this project to a successful end.
Dr. Joana Pimenta Bernardes for the analysis of the RNA sequencing results and to Dr. Neha Mishra for great conversations and her support with any statistical "riddles".
A big, fat thank you goes out to Dorina, Karina, Katha, Maren R., Melanie, Myriam, Sabine and Steffi and Tatjana: Ihr habt es von Tag 1 an geschafft, dass ich mich in der Zellbio willkommen gefühlt habe. Ihr seid ein wahnsinnig tolles TA-Team und ohne eure Unterstützung (sowohl in Bezug auf Experimente als auch auf Gespräche jeglicher Art) wäre diese Arbeit nicht möglich gewesen. Danke!
To Steffi, Antonella, Dora, Helene and Anna: Thank you for your support, understanding and your friendship. I could not have made it without you and am looking forward to the day when we can all celebrate our PhD titles together.
Alexx Shumway: It was great having you for your DAAD Rise internship. I've learned a lot in our 10

weeks – and I hope you did, too!

Frauke Degenhardt for her friendship and both for keeping me company and motivating me while writing this thesis. Frauke, I sure hope that we will continue having our weekly coffee sessions and visits at the Tiergehege even when both our theses are written!

My special thanks go to my family and friends for their understanding, great patience and unyielding support. Finally, thanks to Christian, Olga and Fluff for always making me smile when I come home.

8.14 Curriculum Vitae

8.15 Eidesstattliche Erklärung

Hiermit erkläre ich, Berith Messner, an Eides statt, dass ich die vorliegende Arbeit unter der wissenschaftlichen Leitung von Prof. Dr. Philip Rosenstiel selbstständig und ohne fremde Hilfe verfasst habe. Diese Abhandlung stellt nach Form und Inhalt meine eigene Arbeit dar und ich habe außer der Beratung meiner Betreuer, Prof. Dr. Philip Rosenstiel, Dr. Maren Falk-Paulsen sowie PD Dr. Konrad Aden, keine weitere Hilfe in Anspruch genommen.

Desweiteren habe ich keine anderen als die von mir angegebenen Quellen und Hilfsmittel benutzt und die den verwendeten Werken wörtlich und inhaltlich entnommenen Passagen als solche kenntlich gemacht. Diese Arbeit wurde unter der Einhaltung der Regeln guter wissenschaftlicher Praxis der Deutschen Forschungsgemeinschaft erstellt. Auszüge meiner Dissertation wurden bereits in Posterbeiträgen veröffentlicht.

Ich versichere, dass ich weder an der Christian-Albrechts-Universität zu Kiel noch anderweitig versucht habe, eine Dissertation einzureichen oder mich einer Promotionsprüfung zu unterziehen.

Hiermit erkläre ich, dass mir kein akademischer Grad entzogen wurde.

Kiel, den _____

_____

Berith Messner